OFDM for Underwater Acoustic Communication

Arjun Thottappilly

Thesis submitted to the Faculty of the

Virginia Polytechnic Institute and State University

in partial fulfillment of the requirements for the degree of

Master of Science

in

Electrical Engineering

A. A. (Louis) Beex, Chair

Jeffrey H. Reed

Steven W. Ellingson

August 17th, 2011

Blacksburg, Virginia

Keywords: Orthogonal Frequency Division Multiplexing, Underwater Acoustic Communication, Wideband Doppler Correction, Time Warp

OFDM for Underwater Acoustic Communication

Arjun Thottappilly

ABSTRACT

Communicating wirelessly underwater has been an area of interest for researchers, engineers, and practitioners alike. One of the main reasons for the slow rate of progress in this area is that the underwater acoustic channel is in general much more hostile – in terms of multipath, frequency selectivity, noise, and the Doppler effect – than the over-the-air radio frequency channel. In this work a time warp based technique which can be used to model time-varying wideband Doppler shifts (as seen in an UWA channel) in MATLAB is proposed. A corresponding procedure to estimate the parameters from observed data, required for inverting the effect of the time warp, is also proposed. Two different Doppler correction methods are compared; both can be used to undo the Doppler effect in measured data from an experiment subject to the wideband Doppler effect.

The techniques presented correct for the wideband Doppler effect as if it changed the time scale of the received signal. The first resampling based technique corrects for the average expansion/contraction over a packet, inherently assuming the relative velocity to be constant over the duration of the packet. The second time warp based technique models time-varying Doppler shift. Sinusoids, added to the beginning and end of each packet, are used to estimate the parameters required to invert the effect of the warp.

The time warp based methods are demonstrated using Orthogonal Frequency Division Multiplexing (OFDM) signals, but will in principle work for other kinds of wideband signals

also. The presented results – using MATLAB based simulations, and over-the-air experiments performed in such a way as to introduce the Doppler effect in the received signals – emphasize the improvements that can be attained by using the time warp based Doppler modeling and correction method. The thesis concludes with suggestions for future work.

Acknowledgements

First and foremost, I would like to thank my advisor Dr. A. A. (Louis) Beex for giving me the opportunity to work under him in the DSP Research Laboratory at Virginia Tech. The time I spent working under his guidance has been most productive period of my academic life so far, and I indeed learned a lot more than just DSP from him. I would also like to thank him for all his insightful instructions at various points of this work. None of this would have been possible without his help. I would like to extend my gratitude to Drs. Steven Ellingson and Jeffrey Reed for being a part of my committee and reviewing the work.

Special thanks to my friend Gautham for all his excellent suggestions while reviewing the work. I would like to thank my lab mates Amy, Areg and Roshin. Working in the DSPRL wouldn't have been as much fun without them around. I would also like to thank Krishnan, Bharat and all my friends who made Blacksburg home away from home.

Words cannot express my love and gratitude to my parents for their unconditional love and support. Their dedication and interest towards teaching and research has always inspired me to put in my best effort into all my endeavors.

Table of Contents

List of Abbreviations

ACI – Adjacent Channel Interference

AUV – Autonomous Underwater Vehicle

BER – Bit Error Rate

BPSK – Binary Phase Shift Keying

CCDF – Complementary Cumulative Distribution Function

CDF – Cumulative Distribution Function

CFO – Carrier Frequency Offset

CIR – Channel Impulse Response

CP – Cyclic Prefix

CS – Cyclic Suffix

DFT – Discrete Fourier Transform

DMT – Discrete Multi-Tone

DSWC – Double Sliding Window Correlation

FDM – Frequency Division Multiplexing

FFT – Fast Fourier Transform

ICI – Inter Carrier Interference

IFO – Integer Frequency Offset

ISI – Inter Symbol Interference

LFM – Linear Frequency Modulated

MF – Matched Filter

OFDM – Orthogonal Frequency Division Multiplexing

PAPR – Peak to Average Power Ratio

PRC – Peak Reduction Carriers

PTS – Partial Transmit Sequence

RC – Raised Cosine

SLM – Selected Mapping

SNR – Signal to Noise Ratio

SONAR – Sound Navigation and Ranging

SS – Spherical Spreading

STO – Symbol Timing Offset

TL – Transmission Loss

TR – Tone Reservation

UWA – Underwater Acoustic

UWB – Ultra Wide Band

UWSN – Underwater Wireless Sensor Network

VC – Virtual Carriers

VLSI – Very Large Scale Integration

ZP – Zero Padded

List of Figures

List of Tables

1 Introduction

1.1 Background

Underwater wireless communication is a rapidly growing area of research and engineering. The interest in communicating underwater stems from several military and commercial applications which require transmission of data between two or more nodes located underwater. There has also been a growing interest in building distributed and scalable underwater wireless sensor networks (UWSN) that will provide performance enhancement for various underwater applications for pollution control, climate monitoring, deep sea exploration, gathering of scientific data, etc.

However, it is much more challenging to communicate in an underwater acoustic (UWA) channel than in its over-the-air radio frequency counterpart. The reverberation effect, which causes the receiver to detect multipath signals (due to signals bouncing off the surface and bottom), results in much larger delay spreads in UWA channels, leading to strong frequency selectivity. Moreover, the channel also undergoes rapid temporal and spatial variation (different temperature layers). Being both frequency and time selective, UWA channels pose a great challenge for high rate communication. Many of the techniques used at radio frequencies do not work in the hostile UWA channel. This is one of the main reasons for the slow progress made in this area.

Another prominent reason for the slow rate of progress in UWA communication is the lack of a universally applicable channel model for the UWA channel. The absence of an all-encompassing

channel model – that can be readily used in simulation – has made performing research in this area a rather expensive and cumbersome task.

Existing UWA communication relies on coherent single carrier modulation with decision feedback equalization to deal with the time-varying and highly dispersive UWA channels. Since the frequency selectivity of the channel (and therefore equalizer complexity) increases with the symbol rate, substantial rate improvement is not possible with single carrier modulation schemes. Multicarrier modulation schemes on the other hand convert a frequency selective channel into a set of flat fading channels, thus greatly simplifying the equalization process at the receiver. Successful implementation of OFDM in an UWA channel could result in significant improvements in data rate when compared to what is being achieved right now with single carrier modulation techniques.

OFDM is a multicarrier modulation technique in which orthogonal subcarriers are used to carry data in a spectrally efficient manner. The basic idea is to divide the transmitted bit stream into multiple parallel bit streams and to send these over separate overlapping sub-carriers. The orthogonality between subcarriers is achieved by placing each of the sub-carriers at a multiple of $\frac{1}{T}$, where T is the OFDM symbol period. The data rate on each of the sub-carriers is much lower than the total data rate, and hence the corresponding sub-carrier bandwidth is also lower than the total system bandwidth. The number of sub-carriers is chosen such that the bandwidth of each of the sub-carriers is lower than the coherence bandwidth of the channel. As a result, the sub-carriers experience relatively flat fading. The latter makes equalization at the receiver relatively simple in OFDM in comparison to what is required in conventional single carrier modulation. Moreover, a cyclic prefix - which is used as the guard interval - facilitates canceling

out ISI due to multipath. Hence the inherent ability of OFDM to combat multipath and frequency selective channels could prove to be beneficial in dealing with UWA channels.

However, the problems with using OFDM in an UWA channel are very different from the ones experienced at radio frequency. Acoustic communication is wideband in nature because the carrier frequency is often comparable to the bandwidth of operation. As a result, frequency offsets due to the Doppler effect (caused by unavoidable relative motion between the underwater transmitter and receiver) are significantly different for different frequencies. The narrowband Doppler correction technique, which involves correcting for Doppler as if it were a constant carrier frequency offset, will not work for acoustic communication. Since OFDM is very sensitive to carrier frequency offsets (because offsets in sub-carrier frequency can cause the orthogonality of the subcarriers to be lost), the narrowband Doppler correction technique will lead to severe Inter Carrier Interference (ICI). The Doppler effect experienced in acoustic communication is more accurately modeled as a change in the time scale of the received waveform.

This work first discusses a resampling based Doppler correction technique which corrects for the average Doppler expansion/contraction over a packet. The resampling method inherently assumes that the relative velocity between the transceivers is constant within a packet. In order to expand the realm of Doppler correction, a linear time-varying time scaling model is proposed and analyzed. The needed parameters are estimated based on observable variables. This time-warping based technique is expected to correct for Doppler rates which vary (almost linearly) within a packet. The work also proposes a way to simulate the wideband Doppler effect in MATLAB.

1.2 The Experiment

The experiment that was used to evaluate the Doppler correction techniques was performed, over the air, in the Digital Signal Processing Research Laboratory at Virginia Tech. The experiment involved using two computers which acted as the transmitter and receiver respectively. OFDM generated in the acoustic band (using MATLAB) was played out using a speaker connected to the sound card of the first computer. A microphone connected to the second computer was used to record the sound waves transmitted by the speaker. These recorded sound waves were sampled using the sound card of the second computer and processed in MATLAB. The wideband Doppler effect was introduced in the received signal by moving the microphone, either along a semi-circle or directly towards and/or away from the speaker, while the packet transmission was in progress.

The lower speed of sound in air (relative to that in water) results in larger propagation delays and a more pronounced Doppler effect at slower speeds when compared to its underwater counterpart. Moreover, the reverberation time of an office-size room is on the order of 100 ms, which is comparable to the delay spread experienced in an UWA channel. Hence, the over-the-air channel is in many ways less conducive to acoustic transmission than the UWA channel. As a result, it can be deduced that the over-the-air experiment is a very good indicator of how effective a Doppler correction technique can be underwater. An important advantage is that conducting over-the-air experiments is much simpler than underwater experiments.

This thesis consists of six chapters. The second chapter discusses the concepts and working principles of OFDM in detail. The third chapter provides a background of the features, problems, and history of communication in an UWA channel. The fourth chapter describes the over-the-air experiment (for the case of constant velocity within a packet) and discusses the results that were

obtained. The fifth chapter explains the proposed wideband Doppler model, and also proposes a solution to the problem of within-packet variation of Doppler shift. Chapter six concludes the thesis.

2 Orthogonal Frequency Division Multiplexing

2.1 Introduction

Orthogonal Frequency Division Multiplexing (OFDM) is a type of multicarrier modulation scheme in which the data bits are divided into several different bit streams in parallel, which are then transmitted using overlapping sub-carriers. OFDM is different from Frequency Division Multiplexing as the subcarriers in OFDM overlap each other in such a way that no interference is created, i.e. the subcarriers are made orthogonal to each other. This is achieved by placing each of the sub-carriers at a multiple of $\frac{1}{T}$, where T refers to the duration of the OFDM symbol. As a result OFDM does not require guard bands between subcarriers in the frequency domain, which results in savings in useful spectrum as shown in Figure 2.1.

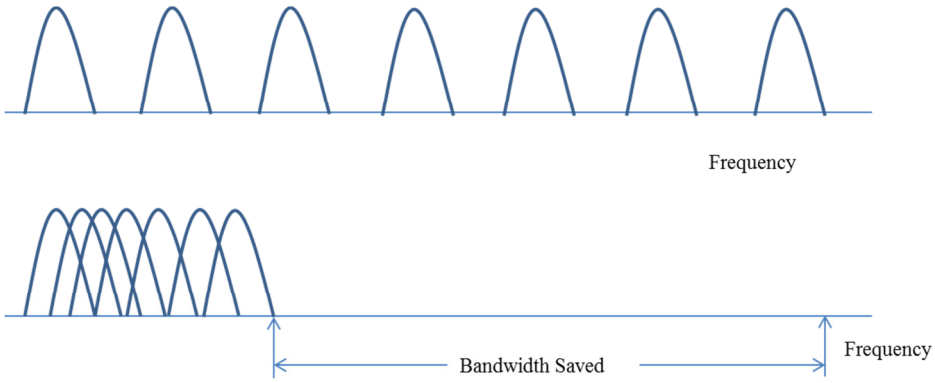

Figure 2.1. Spectral efficiency of OFDM compared to FDM.

The data rate on each of the sub-carriers is much lower than the total data rate, and hence the corresponding subcarrier bandwidth is also lower than the total system bandwidth. The number of sub-carriers is chosen such that the bandwidth of each sub-carrier is lower than the coherence bandwidth of the channel. In other words the number of subcarriers is chosen in such a way that the symbol duration in each subcarrier is greater than the delay spread of the channel. As a result, the subcarriers experience relatively flat fading as depicted in Figure 2.2.

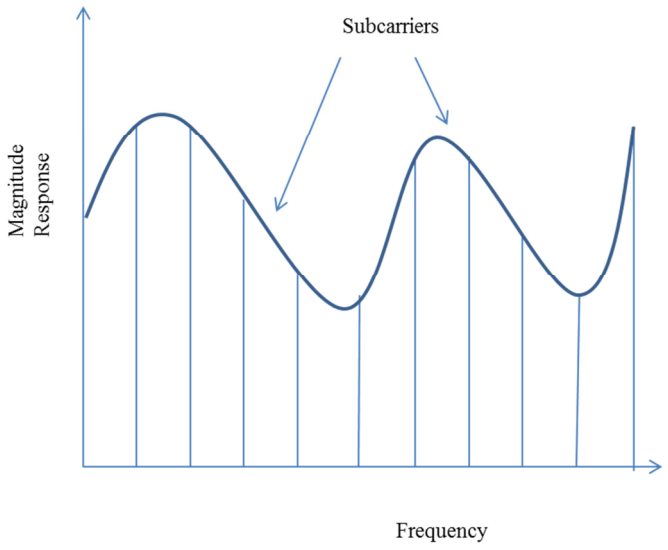

Figure 2.2. Each subcarrier experiences a relatively flat fade.

This makes equalization at the receiver far simpler in OFDM in comparison to conventional single-carrier modulation. The equalizer only has to multiply each detected sub-carrier (each Fourier coefficient) by a constant complex number. In a single carrier system, a single fade or interferer can cause the entire link to fail, but in a multicarrier system, only a small percentage of the subcarriers will be affected. Error correction coding can then be used to correct for the few

erroneous subcarriers. Moreover, ISI can be completely eliminated through the use of a (time-domain) guard interval, as will be explained in Section 2.3.

2.2 Generation of Orthogonal Subcarriers

Figure 2.3 illustrates the basic structure and concept of a multicarrier transceiver [2].

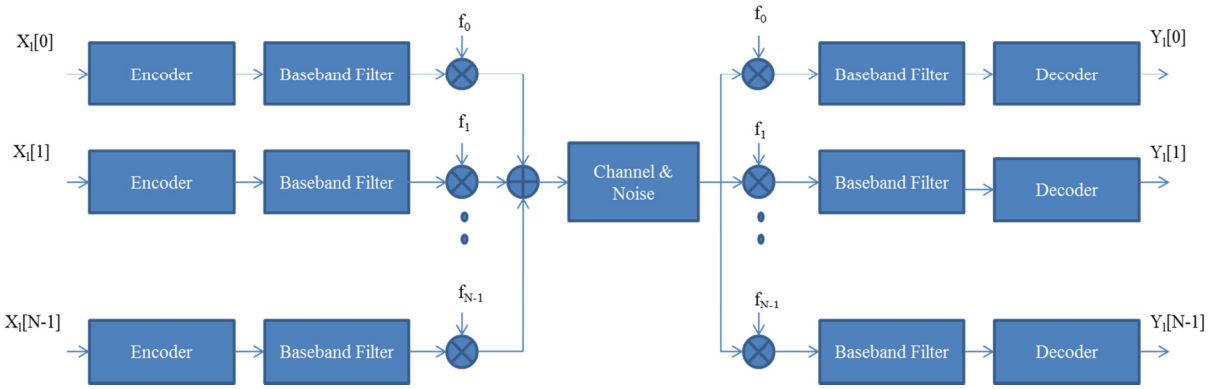

Figure 2.3. Basic structure of a Multicarrier Transceiver.

This transceiver requires a bank of *N* oscillators and filters at both transmit and receive sides. This type of a transceiver could prove to be expensive as well as difficult to implement, as the filters and oscillators have to be really accurate to prevent Inter Carrier Interference (ICI).

In 1971, Weinstein and Ebert applied the Discrete Fourier Transform (DFT) to parallel data transmission systems as part of the modulation and demodulation process [3]. To prove that an OFDM symbol can be generated using IDFT let us consider each subcarrier to be of the form:

$$\phi_k(t) = e^{j2\pi f_k t} \quad ; \; 0 < t < NT \tag{2.1}$$

where N refers to the number of subcarriers and $f_k = \frac{k}{NT}$ refers to the k^{th} subcarrier frequency. Since one OFDM symbol multiplexes *N* orthogonal subcarriers, the time domain OFDM symbol can be written as:

$$s(t) = \frac{1}{\sqrt{N}} \sum_{k=0}^{N-1} I_k \phi_k(t) \quad ; \; 0 < t < NT \tag{2.2}$$

where I_k refers to the data symbol to be modulated onto the k^{th} subcarrier. Substituting (2.1) into (2.2), and sampling (2.2) with period T, we find:

$$s(nT) = s_n = \frac{1}{\sqrt{N}} \sum_{k=0}^{N-1} I_k e^{\frac{j2\pi nk}{N}} \tag{2.3}$$

Equation (2.3) suggests that s_n can be obtained by taking the *N*-point IDFT of I_k. Similarly, I_k can be extracted by taking the *N*-point DFT of s_n.

Recent advances in very-large-scale integration (VLSI) technology have made high-speed, large-size FFT chips commercially affordable. Using this method, both transmitter and receiver can be implemented using efficient FFT techniques that reduce the number of operations from N^2 in a direct DFT implementation to $N\log_2 N$ in an FFT implementation.

2.3 Guard Interval

If the signal passes through a multipath channel this could cause Inter Symbol Interference (ISI). In an OFDM system, this means that the orthogonality of the subcarriers is lost, which results in Inter Carrier Interference (ICI). To overcome these problems, guard intervals have to be

introduced in the time domain. The guard intervals can be of three different types, namely (a) Cyclic Prefix [4], (b) Cyclic Suffix, and (c) Zero Pad [5]. A cyclic prefix is a copy of the last part of the OFDM symbol that is prepended to the transmitted symbol as shown in Figure 2.4.

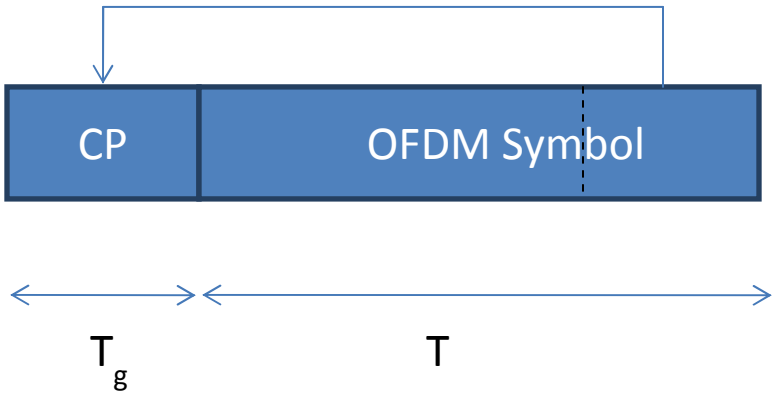

Figure 2.4. Cyclic Prefix.

The cyclic prefix (CP) should be at least as long as the delay spread of the channel. The benefit of using the cyclic prefix is two-fold. First, it avoids ISI because it acts as a guard interval between successive OFDM symbols and second, the linear convolution between the OFDM symbol and the Channel Impulse Response (CIR) can be modeled as a circular convolution since the presence of the CP makes the received symbol look periodic. As the cyclic convolution in the time domain translates into multiplication in the DFT frequency domain, the subcarriers remain orthogonal and ICI will not be experienced. However, use of a cyclic prefix involves transmitting redundant information, which results in a reduction of the data rate as well as an increase in the transmitted power.

The cyclic suffix (CS) is also a cyclic extension of the OFDM symbol. It is however different from CP in that the CS is a copy of the beginning of the OFDM symbol which is appended at the end of the symbol. The pros and cons of using CS are the same as that of CP.

Instead of creating the guard interval by cyclically extending the OFDM symbol, we can pad each OFDM symbol with zeros, and use this as the guard interval. However, the corresponding padded samples at the receiver have to be added to the beginning of the same OFDM symbol to model the linear convolution, between the OFDM symbol and the CIR, as circular convolution. The main advantage of using zero padding is that no extra power is required for transmission. Using zero padding as the guard interval could result in significant savings in power, especially if the delay spread of the channel is very long. As a result, zero padding is generally adopted in multiband OFDM in an Ultra Wide-band (UWB) system and in Acoustic OFDM for underwater communication.

Each subcarrier of an OFDM symbol with duration NT can be regarded as a single frequency signal multiplied by a rectangular window of duration NT, whose spectrum is a sinc function with zero crossings at multiples of $\frac{1}{NT}$. Therefore the spectrum of an OFDM symbol is the sum of many frequency shifted sinc functions, which has a large out of band power such that Adjacent Channel Interference (ACI) is incurred. Two ways to solve this problem is to either use a band pass filter, to filter out the out of band radiation, or use a time domain window like the raised cosine (RC) [6]. Another more commonly used method to solve this problem is to use Virtual Carriers (VC) [7], which are the unused subcarriers at both ends of the transmission band. However, this method can result in a reduction of spectral efficiency.

2.4 Choice of OFDM Parameters

The choice of OFDM parameters is a tradeoff between several requirements. The three main requirements are bandwidth, bit rate, and delay spread. The guard time should be selected such that it is greater than the delay spread of the channel. In order to reduce the amount of overhead per OFDM symbol, it is desirable to make the symbol length much larger than the guard time. However, the symbol duration cannot be arbitrarily large, as larger symbol duration means a larger number of subcarriers with smaller subcarrier spacing, more sensitivity to phase noise and frequency offsets, as well as an increase in the peak to average power ratio. Hence a practical design choice is to make the symbol duration about five times the guard time [6]. The number of subcarriers can be found directly by dividing the total bandwidth by the subcarrier spacing, which is the inverse of the symbol duration less the guard time.

Hence a simplified OFDM transceiver is shown in Figure 2.5. The data bits are first mapped to symbols. An IFFT is performed on these symbols after converting them to parallel. This is followed by adding the guard time (cyclic extension) to each symbol and up-conversion. The received symbols are first down-converted to baseband. This is followed by receiver operations that reverse the transmitter operations.

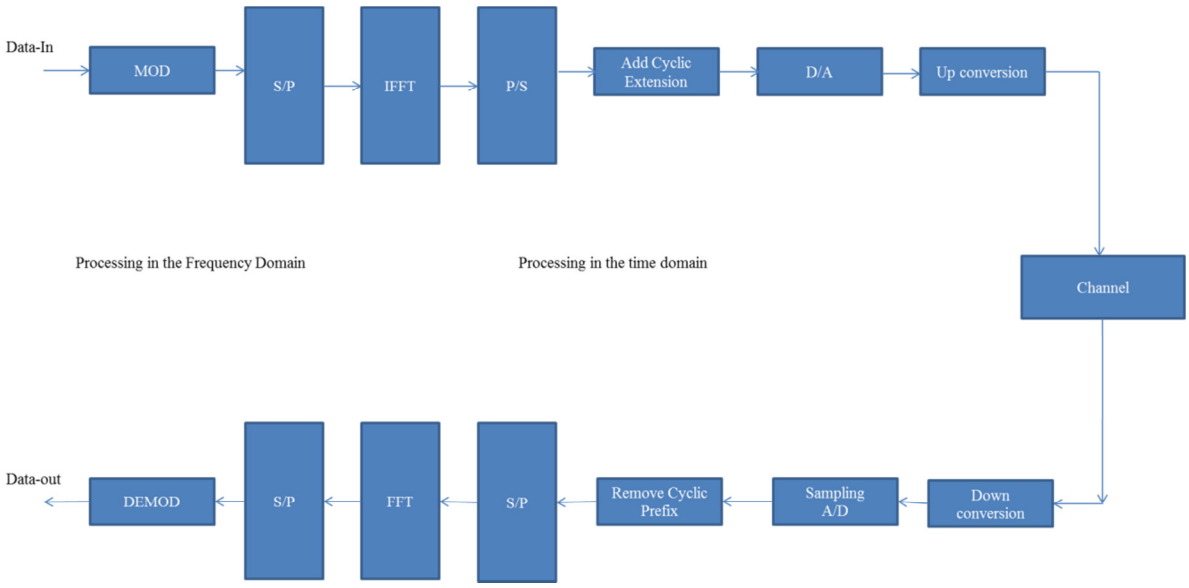

Figure 2.5. OFDM Transceiver Diagram.

2.5 Synchronization in OFDM Systems

Synchronization is one of the most important design constraints that have to be considered while designing any communication system. Earlier in this chapter we discussed how OFDM carries data on subcarriers which are orthogonal to each other, combating a frequency selective channel or equivalently the Inter Symbol Interference (ISI) in a multi-path fading channel. However, the advantages of OFDM – in combating the frequency selectivity of the channel – can only be fully realized if the transmitter and the receiver are synchronized in both time and frequency. Poor synchronization in either the time or frequency domain can result in ISI and ICI, which in turn can result in a severe degradation of performance. The methodology adopted for achieving synchronization varies with the type of application. At present, OFDM is used both for broadcast and packet switched applications. Broadcast systems typically transmit data continuously. Hence, the receiver in such systems can afford to spend a longer duration of time, in the beginning, to synchronize itself with the transmitter and later switch to tracking mode. Packet

switched networks, on the other hand, typically use random access techniques for data transmission. This would require synchronization to be performed once the packet is received. In such cases the receiver cannot afford to spend too much time on synchronization. This type of synchronization is called "single-shot" synchronization.

This section is divided into two parts. The first part describes and analyzes the effect of a symbol timing offset (STO) and a carrier frequency offset (CFO), while the second part describes some of the widely used synchronization techniques. Let ε and δ refer to the normalized CFO and STO respectively. Then the received baseband signal $y[n]$, in the presence of CFO and STO, can be written as [2]:

$$\begin{aligned} y[n] &= IDFT\{Y(k)\} = IDFT\{H(k)X(k) + Z(k)\} \\ &= \frac{1}{N}\sum_{k=0}^{N-1} H(k)X(k)e^{j2\pi(n+\delta)(k+\varepsilon)/N} + z[n] \end{aligned} \tag{2.4}$$

where $X(k)$ and $H(k)$ refer to the Fourier transform of the input and the frequency response of the channel respectively, and $z[n]$ refers to the $IDFT\{Z(k)\}$.

2.5.1 Effects of STO

In order to maximize the performance of the OFDM transceiver, the receiver should ideally be able to take a DFT over the exact same window used for calculating the IDFT at the transmitter. In other words, the receiver must be able to detect the beginning of each OFDM symbol quite accurately before performing the demodulation. Note that a symbol timing offset of δ results in a phase offset of $2\pi k\,\delta/N$ in the frequency domain.

The effect of STO can be quite different depending on the location of the estimated starting point. The various cases illustrated in Figure 2.6 describe the effect that different symbol timing estimates have on the performance of the transceiver:

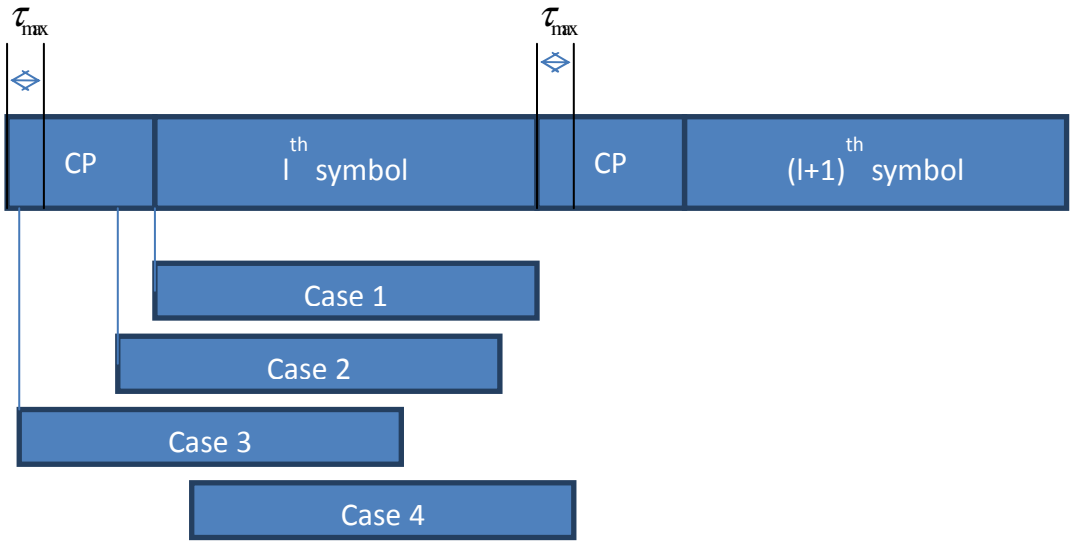

Figure 2.6. Four different possible symbol timing estimates.

Here we assume that the multipath delay spread of the channel is τ_{max} as shown in Figure 2.6.

a. Case 1: In this case the estimated starting point of the OFDM symbol coincides with the exact timing, thereby preserving the orthogonality of the subcarriers. Hence the data can be recovered without any kind of interference.
b. Case 2: In this case the starting point is estimated to be before the exact point, but after the end of the channel response to the previous OFDM symbol. In order to see the effects of the STO, consider the received signal in the frequency domain by taking the FFT of the time domain received samples $x[n+\delta]$:

$$
\begin{aligned}
Y[k] &= \frac{1}{N}\sum_{n=0}^{N-1} x[n+\delta]e^{-j2\pi nk/N} \\
&= \frac{1}{N}\sum_{n=0}^{N-1}\left\{\sum_{p=0}^{N-1} X[p]e^{j2\pi(n+\delta)p/N}\right\}e^{-j2\pi nk/N} \\
&= \frac{1}{N}\sum_{p=0}^{N-1} X[p]e^{j2\pi p\delta/N}\sum_{n=0}^{N-1} e^{\frac{j2\pi(p-k)n}{N}} \\
&= X[k]e^{j2\pi k\delta/N}
\end{aligned}
\tag{2.5}
$$

From (2.5), it is clear that the orthogonality of the subcarriers is preserved. However, there exists a phase offset that is proportional to the subcarrier index k and STO δ. This is compensated for by using a single tap frequency domain equalizer.

c. Case 3: In this case the starting point is estimated to be before the end of the channel response to the previous OFDM symbol. Thus the symbol timing estimate is too early to avoid ISI. In this case the orthogonality of the subcarriers is destroyed by the ISI, thereby causing ICI as well.

d. Case 4: In this case the starting point is estimated to be after the exact timing point. The DFT window therefore consists of a part of the cyclic prefix of the next OFDM symbol. This breaks the orthogonality of the subcarriers, hence resulting in ICI. This is easily the worst of all four cases and should be avoided under all circumstances.

2.5.2 Effects of CFO

The baseband OFDM symbols are converted to passband by a carrier modulation at the transmitter, and the received symbols are converted down to baseband using a local oscillator at the receiver. There are two types of distortions that could result from this. One is the phase noise which occurs due to instability in the local oscillators at the transmitter and the receiver, which

can be modeled as a zero mean Wiener random process [8]. The other is the CFO caused by Doppler frequency shift due to relative motion between the transmitter and the receiver. The parameter ε mentioned before refers to the normalized CFO, i.e. the difference in carrier frequencies at the transmitter and the receiver divided by the subcarrier spacing. We can rewrite ε as the sum of ε_i and ε_f, which refer to the integer and fractional part of the normalized CFO respectively. Note that for a time domain signal $x[n]$ a CFO of ε causes a phase offset of $2\pi n\varepsilon$. This is equivalent to a frequency shift of $-\varepsilon$ on the frequency domain signal $X[k]$. If the carrier frequency offset is an integer (IFO), the transmit signal $X[k]$ is cyclically shifted by ε_i in the receiver, thus producing $X[k-\varepsilon_i]$ in the k^{th} subcarrier. Even though the orthogonality of the subcarriers is not lost, the receiver incurs a significant degradation in bit error rate (BER) if the IFO is not compensated for. On the other hand, a fractional frequency offset would destroy the orthogonality of the subcarriers, causing ICI which again results in a significant degradation of BER performance.

2.5.3 Methods for Achieving Timing Synchronization

Synchronization in the time domain is achieved in two steps at the receiver, namely packet detection and symbol synchronization. Packet detection refers to the techniques used to get a rough idea of the beginning and end of the symbols. The performance of a packet detection algorithm can be analyzed using the probability of detection P_D and probability of false alarm P_{FA} [9]. P_D is the probability of detecting a packet when it is actually present and P_{FA} is the probability of incorrectly detecting the presence of a packet. In general increasing P_D also increases P_{FA} and vice versa. However, false alarm is less severe an error than not detecting a

packet at all because the latter always results in loss of information. On the other hand there are several ways for the receiver to discard a falsely detected packet.

There are several techniques that can be used to perform packet detection, some of which are discussed below:

a. Energy Detection

The simplest technique that can be used, in the absence of appreciable noise, to get a rough estimate of the start and end of a packet is energy detection. The received signal is divided into windows of length L, and the energy in the window forms the decision metric m_n. In the absence of a packet the window contains just noise. However in the presence of a packet the energy in the window will be much higher. Thus the packet can be detected as a change in the received energy level. The decision metric can be written as:

$$E = \sum_{k=0}^{L-1} \left| y[n-k] \right|^2 \tag{2.6}$$

The main drawback with this method is that the decision threshold depends on the energy in the received signal. This makes the task of setting a threshold more difficult and unpredictable.

b. Double Sliding Window

This technique involves calculating the energy in two consecutive windows. The basic idea is to form a decision metric which is a ratio of the total energy contained in the two windows. Figure 2.7 provides a schematic representation of the technique. The windows

A and B are considered to be stationary relative to the packet that slides from the left to the right. The decision metric first increases, when the packet is present only in window A, and then decreases, when the packet enters window B.

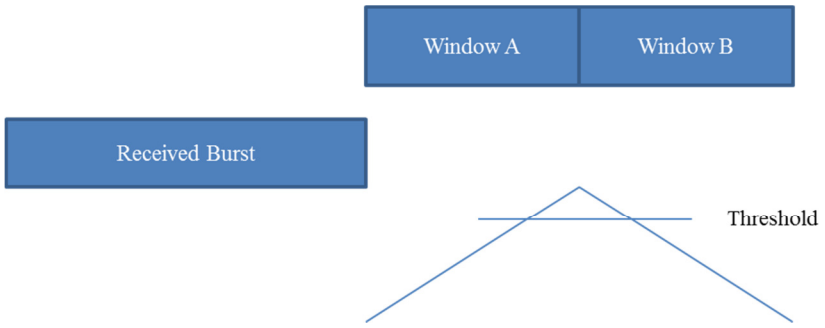

Figure 2.7. Double sliding window packet detection.

Let E_a and E_b refer to the energy in windows A and B respectively.

$$E_a = \sum_{m=0}^{M-1} |y[n-m]|^2$$
$$E_b = \sum_{m=M}^{2M-1} |y[n-m]|^2 \qquad (2.7)$$
$$E_{sw} = \frac{E_a}{E_b}$$

The main benefit of using this method is that the decision metric is no longer dependent on the energy of the received signal. However, if the receiver has additional information about the received data more accurate techniques can be devised as described next.

c. Double Sliding Window Correlation

This technique is similar to the one that Schmidl and Cox [10] proposed for estimating symbol timing and CFO. The technique involves using a pre-amble with a repetitive

structure. More specifically, the pre-amble consists of two identical OFDM training symbols, or a single OFDM symbol with a repetitive structure. The repetitive structure can be obtained by inserting zeros between subcarriers. However, a guard time will still have to be used to prevent the occurrence of ISI. The receiver uses two consecutive sliding windows which are correlated with each other. The correlator produces a high output when the two windows contain the exact same repetitive parts of the pre-amble. The correlation technique can be mathematically written as:

$$\begin{aligned} c_n &= \sum_{k=0}^{L-1} y[n+k]\, y^*[n+k+D] \\ p_n &= \sum_{k=0}^{L-1} \left| y[n+k+D] \right|^2 \\ m_n &= \frac{c_n}{p_n} \end{aligned} \tag{2.8}$$

The correlation output does not have a single peak; instead it has a flat interval (equal to the length of the cyclic prefix).

Symbol synchronization follows packet detection and is the process used to obtain estimates of the beginning and end of the symbols at a sample level precision. There are several methods that can be used to attain symbol synchronization in OFDM, some of which are described below.

a. Matched Filter

The simplest way to attain symbol synchronization is to use a pre-amble which is known both to the transmitter and the receiver. This enables the receiver to calculate the cross correlation of the received signal with the known pre-amble $t[n]$. Equation (2.9) shows

how to calculate the cross correlation. The value of n that maximizes the absolute value of the cross correlation is the symbol timing estimate.

$$\hat{t}_s = \arg\max_n \left| \sum_{k=0}^{L-1} y[n+k] t_k^* \right| \tag{2.9}$$

A drawback of this technique is that it increases the overhead required for correct reception. Moreover the technique will fail when the received signal has undergone a lot of distortion or when there is a CFO between transmitter and receiver.

The double sliding window correlation technique described earlier can also be used for the purpose of symbol synchronization. The accuracy of the method can be improved by using more repetitions of the same symbol in the pre-amble. A problem is that this method does not produce a distinct peak in the correlation output. The flat region that the correlation output produces does not help in finding precise symbol time. This problem can be solved to some extent, however, by taking the average of correlation values over the length of the CP [11].

The performance of the matched filter correlator is in general considered to be better than the double sliding window correlator when there is no CFO between the transmitter and the receiver.

b. Using Cyclic Prefix

Consider an OFDM symbol with a cyclic prefix of N_G samples and data of N_{sub} samples. Recall that the CP is a copy of the last N_G samples of the OFDM symbol. This feature can be used to estimate the STO. Consider two sliding windows W1 and W2 which are spaced N_{sub} samples apart. The similarity between W1 and W2 is maximized

when the CP of an OFDM symbol falls into W1. The similarity between W1 and W2 can be found by either finding the point where the difference between the two windows is minimized or the correlation between the windows is maximized [12] as shown next.

$$\hat{\delta} = \arg\min_{\delta} \left\{ \sum_{i=\delta}^{N_G-1-\delta} \left| y[n+i] - y[n+N_{sub}+i] \right| \right\}$$
$$\hat{\delta} = \arg\max_{\delta} \left\{ \sum_{i=\delta}^{N_G-1-\delta} \left| y[n+i]\, y^{*}[n+N_{sub}+i] \right| \right\} \quad (2.10)$$

This technique may not work when the delay spread of the channel is comparable to the length of the CP, as the cyclic prefix would have undergone too much distortion for the correlator to produce a distinct peak.

In the area of timing synchronization techniques for OFDM a lot of research has been done to date. There exist several alternate techniques which can be used to achieve timing synchronization. There also exist several frequency domain approaches to attain timing synchronization [13]. However, the techniques discussed here are the ones most commonly used in practice.

2.5.4 Techniques to Estimate and Correct for CFO

One of the main drawbacks of OFDM is its sensitivity to CFO. CFO can cause the subcarriers to lose their orthogonality, which in turn causes ICI and a severe degradation of BER performance. Hence it is of paramount importance to synchronize the OFDM symbols in the frequency domain. The various algorithms that have been proposed to estimate and correct for CFO have been broadly divided into three categories [14]:

a. Data aided algorithms

These methods are based on training symbols that are embedded into the transmitted OFDM symbols. The training symbol required is at least two consecutive repeated symbols. To explain the method let us neglect the presence of a channel between the transmitter and the receiver. The received signal is different from the transmitted signal in that it is demodulated using a slightly different carrier frequency. Let $s[n]$ and $x[n]$ refer to the transmitted signal in baseband and passband respectively and let f_{tx} and f_{rx} refer to the carrier frequencies generated locally at the transmitter and receiver respectively. Then,

$$x[n] = s[n]e^{j2\pi f_{tx} nT_s} \tag{2.11}$$

The received signal at baseband is given by:

$$\begin{aligned} y[n] &= s[n]e^{j2\pi f_{tx} nT_s} e^{-j2\pi f_{rx} nT_s} \\ &= s[n]e^{j2\pi (f_{tx} - f_{rx})nT_s} \\ &= s[n]e^{j2\pi \Delta f nT_s} \end{aligned} \tag{2.12}$$

where $\Delta f = f_{tx} - f_{rx}$. Let D be the length of each repeated half of the training symbol. The frequency offset estimator is obtained as follows:

$$\begin{aligned} m_n &= \sum_{n=0}^{L-1} y[n]y^*[n+D] \\ &= \sum_{n=0}^{L-1} s[n]s^*[n+D]e^{j2\pi \Delta f nT_s} e^{-j2\pi \Delta f (n+D)T_s} \\ &= e^{-j2\pi \Delta f DT_s} \sum_{n=0}^{L-1} \left| s_n \right|^2 \end{aligned} \tag{2.13}$$

The CFO estimate can thus be obtained as:

$$\hat{\Delta f} = \frac{-1}{2\pi DT_s} \angle m_n \tag{2.14}$$

It should be noted that the range of values of CFO which this type of estimator can estimate is given by:

$$|\Delta f| \leq \frac{1}{2DT_s} \tag{2.15}$$

This type of estimator cannot estimate CFOs outside this range.

b. Using the CP

Recall that the CP is just a replica of the last portion of the OFDM symbol. Hence the CFO can be estimated using the CP in a manner similar to that in the previous case. As before let N_G refer to the number of samples in the CP and N_{sub} refer to the effective data length in each OFDM symbol. Then the CFO estimate is given as:

$$\Delta f = \frac{1}{2\pi N_{sub} T_s} \arg\left\{ \sum_{n=0}^{N_G - 1} y[n] y^*[n + N_{sub}] \right\} \tag{2.16}$$

This method has all the disadvantages that the previous method has. However this method will also not work when the delay spread of the channel is comparable to the length of the CP, because the CP would have undergone too much distortion to produce a good estimate.

c. Non data aided algorithms

There are several passive algorithms, which use the inherent structure of the OFDM symbol post-FFT, to get an estimate of the CFO. These techniques involve the usage of

known information such as pilot subcarriers or null subcarriers to derive estimates. One of these techniques will be discussed in Section 3.4.

2.6 Peak to Average Power Ratio in Multicarrier Transmission

High Peak to Average Power Ratio (PAPR) is a major drawback of multicarrier systems like Orthogonal Frequency Division Multiplexing (OFDM) or Discrete Multi-Tone (DMT). This section gives an introduction to the problem of high PAPR in multicarrier systems, and also provides an overview of several techniques available to alleviate this problem.

In spite of all the advantages that OFDM has in combating frequency selective fading, it suffers from the problem of high PAPR of the transmit signal. This occurs when a number of independently modulated subcarriers are added with the same phase. The high PAPR could cause a fatal degradation in the BER performance due to the inter-modulation noise in the non-linear power amplifier. The easiest solution to this problem is to operate the non-linear amplifier in its linear region by using sufficient input back-off. This method however degrades the efficiency of the amplifier and also increases battery consumption. Moreover, high PAPR can also increase the burden on Analog to Digital (A/D) and Digital to Analog (D/A) converters, as the same resolution has to be maintained over a wider dynamic range to prevent the Signal to Quantization Noise Ratio (SQNR) from varying too much. Therefore, an OFDM signal may require expensive A/D and D/A converters, compared to many other modulation formats, and for some applications suitable A/D and D/A converters may not be available at all. Hence in many low cost applications, the problem of high PAPR may outweigh all the potential benefits that OFDM has.

The PAPR of the transmit signal can be defined as:

$$PAPR = \frac{\max_{0<t<NT} |s(t)|^2}{\frac{1}{NT}\int_0^{NT} |s(t)|^2 \, dt} \tag{2.17}$$

Since $s_n = s(nT)$, PAPR can also be written as:

$$PAPR = \frac{\max_{0\le n<N} |s_n|^2}{E\left[|s_n|^2\right]} \tag{2.18}$$

The cumulative distribution function (CDF) of the PAPR is one of the most frequently used performance measures for PAPR reduction techniques. In the literature, the complementary CDF (CCDF) is commonly used instead of the CDF itself. The CCDF of the PAPR denotes the probability that the PAPR of a data block exceeds a given threshold. From the central limit theorem, the real and imaginary parts of the time domain signal samples follow Gaussian distributions. Hence, the amplitude of a multicarrier signal has a Rayleigh distribution, while the power distribution becomes a central chi-square distribution with two degrees of freedom. The CDF of the amplitude of a signal sample is given by:

$$F(z) = \left(1 - e^{-z}\right) u(z) \tag{2.19}$$

where $u(z)$ refers to the unit step function. The CCDF of the PAPR of a data block with Nyquist rate sampling is derived as:

$$P(PAPR > z) = \left(1 - (1 - e^{-z})^N\right) u(z) \tag{2.20}$$

However, it is well known that the PAPR of the continuous-time signal cannot be obtained precisely by the use of Nyquist rate sampling. It was shown that oversampling by a factor of 4 can provide sufficiently accurate PAPR results [15].

The result in (2.20) assumes that the N time domain signal samples are mutually independent and uncorrelated. This assumption is not valid, however, when oversampling is applied. Also, the expression is not accurate for a small number of subcarriers since the Gaussian assumption does not hold in this case.

2.6.1 PAPR Reduction Techniques for Multicarrier Transmission

The PAPR reduction techniques can be broadly divided into four categories:

a) Signal Distortion Techniques: This category includes techniques such as clipping and filtering, peak windowing, and peak cancellation. Amplitude clipping is by far the easiest method to reduce PAPR. This method passes the signal unchanged or saturates the peak envelope of the signal to a pre-determined value.

$$B(s) = \begin{cases} s & |s| \le A \\ Ae^{j\phi(s)} & |s| > A \end{cases} \tag{2.21}$$

where $\phi(s)$ is the phase of s. The distortion caused by amplitude clipping falls both in-band and out-of-band. The in-band noise results in a degradation of the BER performance, while the out-of-band radiation reduces the spectral efficiency. Filtering can be used to reduce the out-of-band radiation, but may result in peak re-growth. To reduce overall peak re-growth, a repeated clipping and filtering technique [16] can be used. However, this method requires several iterations for the peak to reach a desired amplitude level.

An alternate approach is to multiply large signal peaks with a window [17]. This would be equivalent to the convolution of the spectrum of the OFDM signal with that of the window. This process is called Peak Windowing. Hence the spectrum of the window

should be as narrowband as possible. Moreover, the window should not be too long in the time domain either, so as to keep the bit error rate degradation to a minimum. Some of the commonly used window functions are cosine, Kaiser, and Hamming window.

b) Coding Techniques: Block coding can be used to reduce PAPR [18]. The method involves block coding a sequence of data bits so as to eliminate those bit sequences which result in high PAPR. However, this approach suffers from the need to perform an exhaustive search to find the best codes and to store large lookup tables for encoding and decoding, especially for a large number of subcarriers. Moreover, this approach does not address the problem of error correction. A better method [19] is to select a linear code for its error correction capabilities and use specific offsets of this chosen code word for the purpose of reducing PAPR. This method enjoys the benefit of error correction as well as PAPR reduction. However, the technique is computationally intensive and a considerable PAPR reduction is not guaranteed in all cases. Considering that the usefulness of these techniques is limited to multicarrier systems with a small number of subcarriers, and the required exhaustive search for a good code is expensive, the actual benefits of coding for PAPR reduction for practical multicarrier systems are limited.

c) Scrambling Sequence Techniques: These techniques involve scrambling an OFDM symbol with different scrambling sequences and selecting the sequence with the lowest PAPR. Two of the most popular techniques which utilize this concept are Partial Transmit Sequence (PTS) [20] and Selected Mapping (SLM) [21].

PTS involves dividing a block of data sets into multiple sub blocks (called partial transmit sequences) and multiplying all the subcarriers in each sub block by a phase factor. The phase factor is selected in such a way as to reduce the PAPR to a minimum.

However, the complexity of finding an optimum set of phase factors increases exponentially with the number of sub blocks. A block diagram of the PTS technique is shown below:

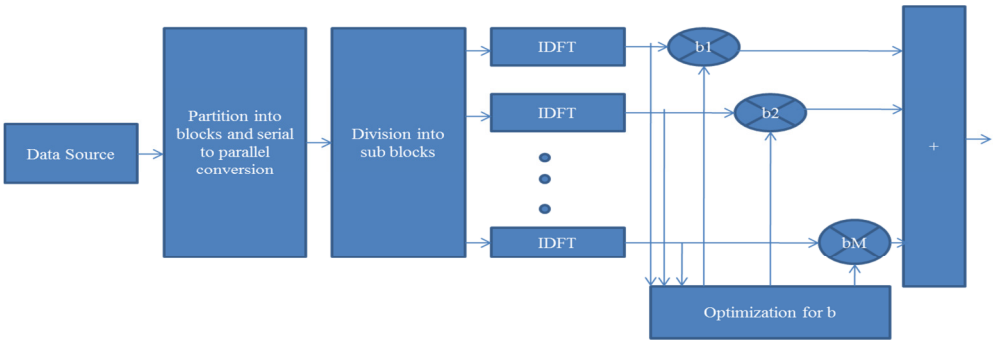

Figure 2.8. Block diagram of the PTS technique.

In the SLM technique each data block is multiplied by different phase vectors, thereby generating different candidate data blocks each representing the same information. The transmitter then selects the data block with the lowest PAPR from the candidate data blocks. The block diagram of the technique is given below:

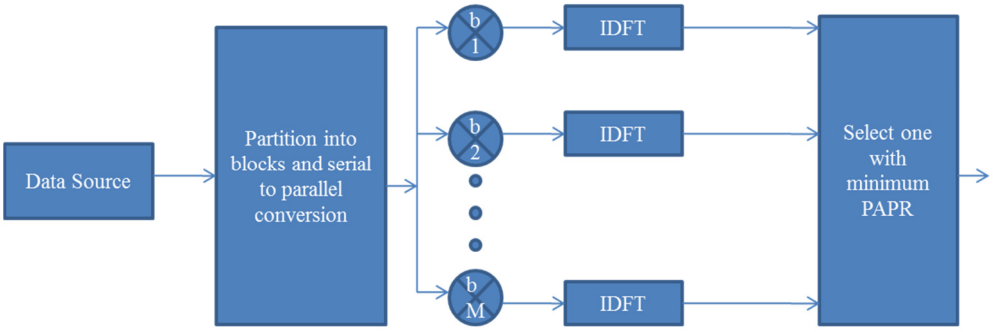

Figure 2.9. Block diagram of the SLM technique.

Both of these techniques require information about the phase sequences used at the transmitter to be transmitted to the receiver. Transmitting the phase sequences can result in incorrect reception, which in turn may degrade the bit error rate performance of the system.

d) Tone Reservation (TR): The main idea behind the tone reservation method proposed by Tellado and Cioffi [22] is to find a time domain signal that can be used to cancel out the peaks in the time domain OFDM symbol. More specifically, this method involves the optimization of a small portion of the available subcarriers for the purpose of reducing PAPR.

Let $S = [S_0, S_1, ...S_{N-1}]^T$ denote the collection of data symbols in the frequency domain and $s = [s_0, s_1, ...s_{N-1}]^T$ denote the time domain samples. If we add a frequency domain vector $C = [C_0, C_1, ...C_{L-1}]^T$ to S, the new time domain signal can be represented as $s + c = IDFT\{S + C\}$, where c is the time domain signal due to C. The TR technique restricts the data block S and peak reduction vector C to lie in disjoint frequency subspaces. The *L* nonzero positions in C are called peak reduction carriers (PRCs). Since the subcarriers are orthogonal, these additional signals cause no distortion on the data bearing subcarriers. To find the value of C a convex optimization problem, which is cast as linear programming, has to be solved.

Selecting the most suitable PAPR technique is a tradeoff decision left to the discretion of the designer. Some of the factors to be considered while selecting the most suitable PAPR reduction technique include the amount of PAPR reduction required, BER increase at the receiver, data rate loss, computational complexity, and power increase in the transmitted signal. In practice,

PAPR reduction techniques can be used only after careful performance and cost analyses for realistic environments.

3 Underwater Acoustic Communication

3.1 Introduction

Two thirds of the earth surface is covered by water and still remains vastly unexplored. Apart from playing a key role in international commerce and fishing, oceans contain a lot of information about the history of the planet, climate, as well as yet to be explored energy resources and forms of life. Hence observation of the oceans is of a lot of interest to several people(s) around the world. One of the key technologies which enable extensive ocean exploration is transmission of information wirelessly underwater. Wireless signal transmission can be used for gathering scientific data, pollution control, climate monitoring, detection of objects on the ocean floor, transmission of images to remote sites on land, etc. Wireless information transmission is also useful for surveillance and other military applications, as well as Autonomous Underwater Vehicles (AUVs) which could serve as mobile nodes in future Underwater Wireless Sensor Networks (UWSNs).

Although radio and optical techniques can be used for very short range applications, acoustic signals are generally used for communicating underwater (UW). Radio waves that propagate underwater are the extra low frequency ones (30 Hz – 300 Hz), but these require very large antennas and extremely high transmission power [23]. Optical techniques do not suffer from the problem of attenuation as much; however, they are affected by scattering. Moreover, optical communication requires very high precision in pointing a narrow laser beam in the right direction, which is still being perfected for practical use. Hence acoustic transmission looks like

the best possible option for UW transmission for now. A comparison of the three transmission techniques in sea water is given in Table 3-1 [31].

Table 3-1. Comparison of Acoustic, Radio wave, and Optical communication in seawater.

	Acoustic	Radio	Optical
Speed of Propagation	~1500 m/s	~33,333,333 m/s	~33,333,333 m/s
Power Loss	>0.1dB/m/Hz	~28 dB/km/100MHz	Depends on Turbidity of water
Bandwidth	~kHz	~MHz	~10-150 MHz
Antenna Size	~0.1 m	~0.5 m	~0.1 m
Frequency band	~kHz	~MHz	~10^{14}-10^{15} Hz
Effective Range	~km	~10 m	10-100 m

Underwater Acoustic (UWA) communication is governed by three major factors, namely limited bandwidth because of signal attenuation which increases as a function of distance and frequency, time varying multipath propagation, and the slow speed of sound underwater [24]. These factors combine to produce a channel of very poor quality and high latency. Finding efficient techniques to communicate in such a channel has been an area of active research over the past several decades. Because of the challenging environment and limited understanding of the phenomena involved, several problems still remain to be solved before efficient communication with predictable performance can take place.

3.2 Channel Model

The underwater acoustic channel combines the worst properties of a radio channel, i.e. poor physical link quality of a mobile terrestrial radio channel and the high latency of a satellite channel. These channels are considered to be the most difficult to communicate on due to the limited bandwidth and the wideband (bandwidth comparable to the carrier frequency) nature of the signals used. Delay spreads of over tens and up to hundreds of milliseconds result in frequency selective distortion, and the almost unavoidable relative motion between the transmitter and the receiver creates Doppler effects as well. The background noise is neither Gaussian nor white, and in many cases has a power spectral density decaying with frequency [25]. Moreover, surface waves, internal turbulence, the variation of the speed of sound due to variation in density, and several other small scale phenomena create random signal variations. As a result of these factors, there is no standard channel model which fully describes the effect of the UWA channel.

Several researchers have tried to develop an all-encompassing model for the UWA channel [26-28]. Salinity, temperature, depth, environmental noise, transmission loss, spreading loss, frequency used, etc., are some of the factors that have been considered, in varying levels of detail, for modeling the channel. We next discuss some of the properties of the UWA channel in more detail.

3.2.1 Propagation Delay

The speed of sound in water increases with the salinity, temperature, and pressure (or depth) of the water. Near the surface of the water the temperature and pressure are almost constant, thus

leading to a constant speed of sound. In temperate climates the temperature decreases with depth, while the increase in pressure is not significant enough to offset the effect of the decrease in temperature. Hence the speed of sound decreases in the region called the main thermocline. After some depth the temperature reaches a constant level of 4 °C, and from there on the speed of sound increases with depth.

Let T be the temperature in degrees Celsius, S the salinity in parts per thousand, and D the depth in meters. Then the speed of sound in water can be estimated using any of the following empirically derived formulae [29]:

$$
\begin{aligned}
c_1 &= 1492.9 + 3(T-10) - 6\times10^{-3}(T-10)^2 - 4\times10^{-2}(T-18)^2 + 1.2(S-35) - 10^{-2}(T-18)(S-35) + \frac{D}{61} \\
c_2 &= 1449.2 + 4.6T - .055T^2 + .00029T^3 + (1.34 - 10^{-2}T)(S-35) + 1.6\times10^{-2}D \\
c_3 &= 1448.96 + 4.591T - .05304T^2 + .0002374T^3 + 1.34(S-35) + .0163D + 1.675\times10^{-7}D^2 - .0102T(S-35) - 7.139\times10^{-13}TD^3 \\
c_4 &= 1449 + 4.6T + .055T^2 + .003T^3 + (1.39 - .012T)(S-35) + .017D \\
c_5 &= 1449.2 + 4.6T + .055T^2 + .00209T^3 + (1.34 - .01T)(S-35) + .06D
\end{aligned}
\tag{3.1}
$$

The propagation delay can then be calculated as:

$$\tau = \frac{d}{c} \tag{3.2}$$

where τ is time in seconds and d is distance in meters.

3.2.2 Transmission Loss

The distinguishing property of acoustic channels is that the path loss depends on the signal frequency. This is a direct consequence of absorption, i.e. the transfer of acoustic energy to heat.

Path loss in the ocean can be categorized into attenuation loss and spreading loss. Attenuation loss includes losses incurred due to absorption, leakage out of ducts, scattering, and diffraction. In the low frequency range (100 Hz - 3 kHz) the absorption coefficient can be calculated as [30]:

$$\alpha(f) = \frac{0.11 f^2}{1+f^2} + \frac{44 f^2}{4100+f^2} + 2.75\times10^{-4} f^2 + 0.003 \tag{3.3}$$

where f is frequency in kHz and α is the absorption coefficient. The absorption coefficient increases rapidly with frequency. The spherical spreading factor (*SS*) is given by:

$$SS = 20\log_{10} r \tag{3.4}$$

where r is the distance in meters between the transmitter and the receiver. Note that the spreading loss increases with distance. The spreading loss consists of spherical spreading (seen in a deep water environment) and cylindrical spreading (seen in shallow water). Finally, the transmission loss (*TL*) is given by [31]:

$$TL = SS + \alpha(f) r \times 10^{-3} \tag{3.5}$$

Urick defines TL as [32]:

$$TL(f,d) = \chi \log_{10}(d) + \alpha(f) d + A \tag{3.6}$$

where χ is the path loss exponent, d the distance, f the frequency, and A the transmission anomaly which accounts for the degradation of the acoustic intensity due to multipath propagation, refraction, diffraction, and scattering of sound. However, Stojanovic and Preisig [25] define overall path loss as:

$$A(l,f) = \left(\frac{l}{l_r}\right)^k \alpha(f)^{l-l_r} \tag{3.7}$$

where l is the transmission distance taken in reference to some l_r. The path loss exponent k models the spreading loss and its values are usually 1 or 2 for cylindrical and spherical spreading respectively.

3.2.3 Noise

Noise in an acoustic channel consists of ambient noise and site specific noise. Ambient noise is always present in the background, while the site specific noise is unique to the location. Examples of site specific noise include breaking of ice in Polar Regions and snapping of shrimp in warmer waters. These types of noises are non-Gaussian and generally modeled using a Gaussian mixture, generalized Gaussian, Gaussian double exponential [33], or stable distributions [34].

The ambient noise in an underwater environment can be divided into four categories [25], namely turbulence (N_t), shipping (N_s), wind (N_w), and thermal (N_{th}):

$$\begin{aligned}
10\log N_t(f) &= 17 - 30\log_{10} f \\
10\log N_s(f) &= 40 + 20(s-.5) + 26\log_{10} f - 60\log_{10}(f+0.03) \\
10\log N_w(f) &= 50 + 7.5\sqrt{w} + 20\log_{10} f - 40\log_{10}(f+0.4) \\
10\log N_{th}(f) &= -15 + 20\log_{10} f
\end{aligned} \tag{3.8}$$

where *w* and *s* refer to the speed of wind and ship in m/s, and *f* refers to the frequency of operation. While this noise is often modeled as Gaussian, it is not white. The power spectral density of the ambient noise decays at a rate of approximately 18 dB/decade [25]. Hence the

attenuation which increases with frequency (3.7) and the noise whose spectrum decays with frequency result in a signal to noise ratio (SNR) that varies over the signal bandwidth. Let Δf refer to a narrow band of frequencies around some frequency f. Then the SNR in this band can be expressed as [25]:

$$SNR(l, f) = \frac{S_l(f)}{A(l, f)N(f)} \tag{3.9}$$

where $S_l(f)$ is the power spectral density of the transmitted signal. For any given distance the SNR is a function of frequency. Hence it is apparent that the acoustic bandwidth depends on the transmission distance. The bandwidth is severely limited for very large distances. This calls for the use of bandwidth efficient modulation schemes. Another important observation to be made here is that the acoustic bandwidth is on the order of the carrier frequency. The latter fact creates a lot of differences in the signal processing techniques that can be used, as the narrow band assumption, on which many radio communication principles are based, is not valid.

3.2.4 Multipath

Multipath is caused by the presence of multiple paths that sound waves can take to travel from the transmitter to the receiver. Multipath is created underwater by two different effects: sound reflection at the surface, bottom, and any objects, and refraction of sound. The latter is caused by the spatial variation of the speed of sound. The impulse response of the acoustic channel depends on the nature of the channel and its reflection and refraction properties, which in turn determines the number of propagation paths that contribute significant energy components at the receiver.

Each path of an acoustic channel can be assumed to act like a low pass filter, and hence the overall impulse response can be written as [25]:

$$h(t) = \sum_{p} h_p(t - \tau_p) \tag{3.10}$$

where $h_p(t)$ refers to the time varying path gain and τ_p refers to the path delay of the p^{th} path. The delay spread of the channel depends on the longest path delay, which is typically on the order of tens or even hundreds of milliseconds.

Another property of the UWA channel is that it varies with time. This is caused by two factors: inherent changes in the transmission medium and changes caused by the relative motion between the transmitter and receiver. Inherent changes would range from changes which occur over a long period of time (e.g. changes in weather) to changes which occur relatively quickly (e.g. surface waves, storms, etc.). Unlike for the radio channel, where a number of models have been accepted universally for both the probability distribution (e.g. Rayleigh, Rice) and power spectral density (e.g. Jakes's model) of fading, there is no consensus on the statistical characterization of acoustic communication channels.

3.2.5 Doppler Effect

Non-negligible Doppler shift/spread is another factor that distinguishes an acoustic channel from the radio channel. The magnitude of the Doppler effect (a shift) is measured by the ratio $a = \frac{v}{c}$, where v is the relative velocity between transmitter and receiver, c is the speed of sound, and a is called the relative Doppler shift. Since the speed of sound is very low when compared to

electromagnetic waves, the distortion due to Doppler can be quite severe for acoustic signals. Even when there is no intentional movement, the transducers tend to drift with waves and tides with a non-negligible velocity. There is always some amount of movement present in the system and this has to be considered while designing a communication system. The Doppler Effect can have a significant impact on multicarrier signals as will be explained in Section 3.4.

For a single frequency component, at say ω_n, the Doppler effect can be modeled as a scaling of frequency:

$$\tilde{\omega}_n = \omega_n(1+a) \tag{3.11}$$

This assumption often works for narrow band signals in which the whole spectrum is assumed to be shifted by the same frequency as the carrier. In such cases the Doppler shift can be negated by carrier synchronization, which is equivalent to adjusting the local carrier frequency.

In wideband signals, the Doppler effect is more accurately modeled as a time scaling (expansion or contraction) of the signal waveform. Hence each frequency component is shifted by an amount which is significantly different from that at other frequencies.

$$r(t) = s((1+a)t) \tag{3.12}$$

where $s(t)$ and $r(t)$ refer to the transmitted and Doppler shifted received signals respectively. This wideband model of the Doppler effect is used for UWA communication. We now discretize (3.12) by sampling the signals with period T_s:

$$r(nT_s) = s((1+a)nT_s) \tag{3.13}$$

If the relative Doppler shift is known, the Doppler effect can be negated by inverse time scaling the received signal. In a multirate DSP system this is equivalent to resampling the received signal by the factor $1+a$.

$$s(nT_s) = r\left(\left(\frac{n}{1+a}\right)T_s\right) \tag{3.14}$$

Hence, correcting the received signal for Doppler involves scaling the sampling frequency.

$$\tilde{f}_s = (1+a) f_s \tag{3.15}$$

3.3 Advances in Underwater Acoustic Communication

The past three decades have seen growing interest in underwater communication. As a result significant improvements in performance have been achieved when compared to the initial efforts, so much so that research has come a long way from just point to point communication to building fully scalable underwater networks. This section provides a historic background to the area of UWA communications and also provides an overview of the developments over the past two decades.

3.3.1 Initial Efforts

The initial efforts made in communicating underwater dates back to the time when manned submarines were developed, and the need arose to communicate between them. The “Gertrude,” or the underwater telephone, was developed for audio communication using analog modulation

at carrier frequencies between 2 and 15 kHz [24]. This analog system uses analog filters for the voice band, combined with spectral shaping and single sideband modulation of the carrier. In the receiver, the signals are demodulated and filtered with relatively poor fidelity. This method is still being used in both military and commercial systems, and works satisfactorily because of the ability of the human brain and ear to put together distorted speech.

The development of digital communication techniques for UWA communication dates back to the time when simple ping-based SONARS, operating in the audible band, were used for communication. The advent of digital communication in the 1960s proved that the data rate that can be achieved in a multipath channel is limited to $\frac{1}{T_d}$, where T_d refers to the delay spread of the channel. Thus in the highly reverberant underwater channel, the data rate can be very low unless some technique is devised to specifically increase the data rate.

3.3.2 Incoherent and Coherent Modulation

Most of the early UWA digital communication systems used incoherent modulation schemes as they were much simpler and more reliable. Coherent modulation schemes were initially used only in vertical links in deep-water, as the delay spread experienced in these cases was very small. As a result, the biggest challenge in the latter cases was to track the carrier phase change with respect to distance. It was not until the early 1990s that the use of phase coherent modulations in a multipath channel began to attract attention. The increased interest stemmed from the fact that coherent modulation schemes are much more bandwidth efficient than incoherent modulation schemes. The desire to achieve higher throughput in a band-limited channel led to research in using adaptive equalizers to combat the effects of multipath. Coherent

modulation schemes such as phase shift keying (PSK) along with adaptive decision feedback equalizers have been proven to be an effective but computationally expensive way of communicating in such channels [35]. Although the channel has a large delay spread, the multipath arrivals at the receiver are often discrete. This fact has motivated the use of sparse equalizers [36-38] and sparse Partial Response Equalizers [39]. Several blind equalization techniques that use only the statistical properties of the signal have also been tried but with limited success [40]. The use of equalization techniques for UWA channels is a large area of research in itself, and beyond the scope of this work.

Although less bandwidth efficient, incoherent modulation techniques are still being used because of their simplicity, requiring modest processors which in turn reduce cost and power consumption. Hence these techniques would work satisfactorily if the required data rate for communication is not a concern. The incoherent methods used include frequency hopping and *M*-ary frequency shift keying, using a symbol time that is longer than the delay spread of the channel.

3.4 OFDM for an Underwater Acoustic Channel

Existing coherent underwater communication techniques rely on single carrier modulation with adaptive decision feedback equalization to deal with the highly dispersive UWA channel. Since the frequency selectivity of the channel increases with the symbol rate, equalization complexity restricts the data rate that can be achieved. Another, more elegant, way of communicating over a multipath channel would be to use a multicarrier modulation scheme such as OFDM. Recall that

OFDM converts a frequency selective channel into a set of flat fading channels. As a result the complexity of the equalizer to be used is significantly reduced.

While OFDM does look like a good solution to the multipath problem, it requires the receiver to be very accurately synchronized to the transmitter. OFDM can only tolerate a CFO that is a small fraction of the subcarrier spacing, as any residual CFO causes ICI. Several techniques can be used to achieve carrier synchronization in OFDM (as discussed in Chapter 2). Most of these techniques are based on the assumption that the signals under consideration are narrowband. However, this assumption is not valid for an acoustic channel. In a wideband system the motion induced Doppler distortion results in frequency shifts that are non-uniform across the entire band. As a result the Doppler shift that the lowest subcarrier experiences is quite different from the Doppler shift that the highest subcarrier experiences. In other words it is not correct to assume that the Doppler shift is equal across all subcarriers. Hence most of the synchronization algorithms used for radio communication do not work for UWA communication.

There has been a lot of interest recently in building OFDM transceivers for UWA communication. Different types of receiver designs have been proposed, which includes a low complexity adaptive OFDM receiver [41], a pilot tone based block by block receiver [42], and a non-coherent OFDM receiver based on on-off keying [43]. In this work zero-padded OFDM with a pilot tone based block by block receiver has been used. The details of the receiver will be explained in Chapter 4.

3.4.1 Non Uniform Doppler Compensation Technique

A two-step approach has been adopted, at the receiver, to mitigate the frequency dependent Doppler shift [44]. To explain this process, let us first consider a ZP-OFDM symbol generated at the transmitter. Let T and T_g denote the OFDM symbol duration and the guard interval respectively. The subcarrier frequency spacing is $\Delta f = \frac{1}{T}$. Hence the k^{th} subcarrier is at a frequency:

$$f_k = f_c + k\Delta f \ , \ k = \frac{-K}{2},...,\frac{K}{2}-1 \tag{3.16}$$

where f_c refers to the carrier frequency and K refers to the total number of subcarriers used. Let $d[k]$ denote the data symbol to be transmitted on the k^{th} subcarrier. The total number of subcarriers is divided into mutually exclusive sets of active carriers and null carriers denoted by S_A and S_N respectively. The transmitted signal in passband can be written as:

$$s(t) = \mathrm{Re}\left\{\left[\sum_{k\in S_A} d[k]e^{j2\pi k\Delta ft} g(t)\right] e^{j2\pi f_c t}\right\}, \ t \in [0, T+T_g] \tag{3.17}$$

where the zero padding operation is reflected by

$$g(t) = \begin{cases} 1 & t \in [0,T] \\ 0 & t \in [T, T+T_g] \end{cases} \tag{3.18}$$

We assume the multipath underwater channel to have an impulse response of the form:

$$c(t,\tau) = \sum_p A_p(t)\delta(\tau - \tau_p(t)) \tag{3.19}$$

where $A_p(t)$ and $\tau_p(t)$ refer to the time varying path gain and path delay respectively. We assume that the path gains and relative Doppler shifts are constant over an OFDM symbol. Moreover, we also assume that all paths have the same relative Doppler shift a:

$$\tau_p(t) = \tau_p - at \tag{3.20}$$

The received signal in passband can be written as the following convolution:

$$\begin{aligned}\tilde{y}(t,\tau) &= s(t) * c(t,\tau) \\ &= \mathrm{Re}\left\{\sum_p A_p \left[\sum_{k\in S_A} d[k] e^{j2\pi k\Delta f(t+at-\tau_p)} g(t+at-\tau_p)\right] e^{j2\pi f_c(t+at-\tau_p)}\right\} + \tilde{n}(t)\end{aligned} \tag{3.21}$$

where $\tilde{n}(t)$ is the additive noise. The received signal in baseband can hence be written as:

$$y(t) = \sum_{k\in S_A}\left\{d[k] e^{j2\pi k\Delta ft} e^{j2\pi a f_k t}\left[\sum_p A_p e^{-j2\pi f_k \tau_p} g(t+at-\tau_p)\right]\right\} + n(t) \tag{3.22}$$

where $n(t)$ refers to the additive noise at baseband. Looking at (3.22) we observe that:

a) The signal from each path has been scaled in duration from T to $\frac{T}{1+a}$. This is seen from the argument of $g(\ )$.

b) Each subcarrier experiences a Doppler shift of $e^{j2\pi a f_k t}$. Note that this shift depends on the frequency of each subcarrier. Since the OFDM under consideration is wideband in nature, each subcarrier experiences a shift which is considerably different from the others. This shows that the narrowband assumption does not hold.

A two-step approach has been adopted to negate these problems:

a) Compensation of the non-uniform Doppler shift by resampling.

b) High resolution uniform compensation on residual Doppler by modeling it as a Carrier Frequency Offset.

Let us now look at these steps more closely. First, we resample the received baseband signal $y(t)$ with a resampling parameter b.

$$\begin{aligned} z(t) &= y\left(\frac{t}{1+b}\right) \\ &= e^{j2\pi f_c t\frac{a}{1+b}} \sum_{k\in S_A} \left\{ d[k] e^{j2\pi k\Delta f \frac{1+a}{1+b} t} \left[\sum_p A_p e^{-j2\pi f_k \tau_p} g\left(\frac{1+a}{1+b} t - \tau_p\right)\right]\right\} \end{aligned} \tag{3.23}$$

The resampling parameter b should be selected such that

$$\frac{1+a}{1+b} = 1 \tag{3.24}$$

In other words, the resampling parameter should be an estimate of the relative Doppler shift. After resampling we see that:

$$z(t) = e^{j2\pi f_c t\frac{a}{1+b}} \sum_k d[k] e^{j2\pi k\Delta f t} \left[\sum_p A_p e^{-j2\pi f_k \tau_p} g(t-\tau_p)\right] \tag{3.25}$$

From (3.25) we observe that the Doppler shift has become equal for all subcarriers. The residual Doppler shift can thus be compensated for using a single Carrier Frequency Offset:

$$\varepsilon = \frac{a}{1+b} f_c \tag{3.26}$$

Compensating for this CFO in (3.25) gives us:

$$e^{-j2\pi\varepsilon t} z(t) = \sum_{k \in S_A} d[k] e^{j2\pi k \Delta f t} \left[\sum_p A_p e^{-j2\pi f_k \tau_p} g(t - \tau_p) \right] \tag{3.27}$$

De-scaling and de-rotation of the received symbol (by equalization) restores the orthogonality of the subcarriers of the ZP-OFDM.

3.4.2 Practical Implementation

In practice the resampling parameter, which in this case equals the relative Doppler shift, and the CFO ε must be estimated from the received signal. The relative Doppler shift can be estimated using the pre-amble and post-amble [45] of a data packet. After performing time domain synchronization with the pre-amble and post-amble (as will be explained in Chapter 4), the time duration of a received packet can be estimated as T_{rx}. The latter can be compared to T_{tx}, the time duration of the data packet at the transmitter, to get an idea of the expansion or contraction that the data packet has undergone. This expansion or contraction can be used to get an estimate of the relative Doppler shift:

$$\begin{aligned} T_{rx} &= (1 - \hat{a}) T_{tx} \\ \hat{a} &= 1 - \frac{T_{rx}}{T_{tx}} \end{aligned} \tag{3.28}$$

The receiver can then perform the resampling operation, as in (3.23) using $\hat{a}$ as the resampling factor.

The residual CFO is estimated using the null subcarriers used in each OFDM symbol [46]. The method involves performing a 1D search over frequency, to find that frequency which minimizes the energy spilled into the null subcarriers. To explain this technique in detail let us consider the

k^{th} discrete baseband OFDM symbol at the transmitter denoted by $\mathbf{s}(k) = \left[s_1(k), s_2(k), ...s_A(k)\right]^T$. As assumed before, the OFDM symbol consists of A active carriers and N null subcarriers out of a total of K subcarriers. Let $\mathbf{W}_A$ be a sub matrix, of dimension $A \times A$, of the $K \times K$ IDFT matrix $\mathbf{W}$. Without loss of generality we assume that carriers 1 to A are used for data transmission so that $\mathbf{W}_A = \left[\mathbf{w}_1, \mathbf{w}_2, ...\mathbf{w}_A\right]$ where $\mathbf{w}_i$ is the i^{th} column of $\mathbf{W}$. The input to the receiver for the k^{th} block is given as:

$$\begin{aligned} \mathbf{y}(k) &= \mathbf{W}_A \mathbf{H} \mathbf{s}(k) \\ &= \mathbf{W}_A diag\left[H(1), H(2), ...H(A)\right] \mathbf{s}(k) \end{aligned} \tag{3.29}$$

where $H(i), i = 1, 2, ..., A$ is the frequency response of the channel estimated using pilots uniformly inserted over the bandwidth of operation. Each subcarrier can be recovered by performing the DFT of $\boldsymbol{y}(k)$

$$\mathbf{W}_A^H \boldsymbol{y}(k) = \mathbf{H}[\mathbf{s}_1(k), ..., \mathbf{s}_A(k)] \tag{3.30}$$

However in the presence of a CFO $e^{j\phi}$, the receiver input is modulated by $\boldsymbol{E} = diag[1, e^{j\phi}, ...e^{j(A-1)\phi}]$, and becomes $\boldsymbol{y}(k) = \boldsymbol{E}\boldsymbol{W}_A \boldsymbol{H}\boldsymbol{s}(k) e^{j\phi(k-1)(K+K_g)}$, where K_g is the length of the guard interval. Since $\boldsymbol{W}_A^H \boldsymbol{E} \boldsymbol{W}_A \neq \boldsymbol{I}$, the $\boldsymbol{E}$ matrix destroys the orthogonality of the subcarriers and creates ICI.

The orthogonal complement of $\boldsymbol{W}_A$, denoted by $\boldsymbol{W}^{\perp} = [\boldsymbol{w}_{A+1}, ...\boldsymbol{w}_K]$ is known a priori. Hence in the absence of CFO,

$$\boldsymbol{w}_{A+i}^H \boldsymbol{y}(k) = \boldsymbol{w}_{A+i}^H \boldsymbol{W}_A \boldsymbol{s}(k) = 0, \; i = 1, ...K - A \tag{3.31}$$

However, this condition does not hold when $\phi \neq 0$. If we let $\boldsymbol{Z} = diag\left[1, z, z^2, ...z^{A-1}\right]$, it can be shown that when $\boldsymbol{Z} = \boldsymbol{E}$,

$$\boldsymbol{w}_{A+i}^H \boldsymbol{Z}^{-1} \boldsymbol{y}(k) = \boldsymbol{w}_{A+i}^H \boldsymbol{Z}^{-1} \boldsymbol{E} \boldsymbol{W}_A \boldsymbol{s}(k) = 0,\ i = 1,...K - A \tag{3.32}$$

This fact allows us to define a cost function,

$$\boldsymbol{P}(z) = \sum_{i=1}^{N} \sum_{k=1}^{K} \left\| \boldsymbol{w}_{A+i}^H \boldsymbol{Z}^{-1} \boldsymbol{y}(k) \right\|^2 \tag{3.33}$$

Clearly $\boldsymbol{P}(z)$ is equal to zero when $z = e^{j\phi}$. Hence one can estimate the CFO by evaluating $\boldsymbol{P}(z)$ along the unit circle, as in the MUSIC algorithm in array signal processing.

4 Acoustic OFDM – Over the Air Experiment

4.1 Introduction

This chapter describes the design and implementation of an OFDM communication system over an acoustic channel. The communication system was designed so as to estimate and correct for the Doppler effect resulting from relative motion between transmitter and receiver. The corresponding experiment was conducted, over the air, in the Digital Signal Processing Research Laboratory at Virginia Tech. Figure 4.1 describes the experiment setup.

Figure 4.1. The over-the-air experiment setup.

The OFDM burst, which was generated in the 3-5 kHz band using MATLAB, was transmitted via soundcard using a speaker connected to the computer. The acoustic transmission impinged on a microphone connected to the sound card in a second computer. This second computer acted as the OFDM receiver (implemented in MATLAB) and estimated the received bits. Hence the channel in effect consisted of a combination of two sound cards, speaker, air, and microphone. Several issues such as timing synchronization, carrier frequency offset estimation and correction, and channel equalization had to be taken into account for the system to be operational at usable bit error rates.

Since the experiment was conducted in an indoor environment which contained tables, chairs, computers, and shelves, the received signal was subject to multipath. Moreover, the Doppler effect was introduced by moving the microphone either semi-circularly or to and fro with respect to the pivot (the shoulder of the person performing the experiment). Recall that sound travels about five times slower over air when compared to underwater. This results in a larger propagation delay as well as a more pronounced Doppler effect at much slower speeds. Hence the over-the-air channel is in some ways less conducive for acoustic transmission when compared to its underwater counterpart. This chapter explains the methodologies adopted for designing an OFDM symbol and the transceiver. The chapter also discusses the results obtained from an over-the-air experiment and some of the problems with the current receiver design.

4.2 OFDM Transmitter

The OFDM transmitter generates a ZP-OFDM burst in the 3-5 kHz band. ZP-OFDM was preferred to CP/CS-OFDM because of reasons discussed in Section 2.3. The bandwidth of operation was selected to be the 3-5 kHz range because of restrictions imposed by the speaker cross-over network. The low-end speaker used at the transmitter did not transmit signals with frequency content above 7 kHz.

The OFDM burst consists of packets which in turn each consist of five OFDM symbols, a pre-amble and a post-amble. Figure 4.2 describes the burst structure.

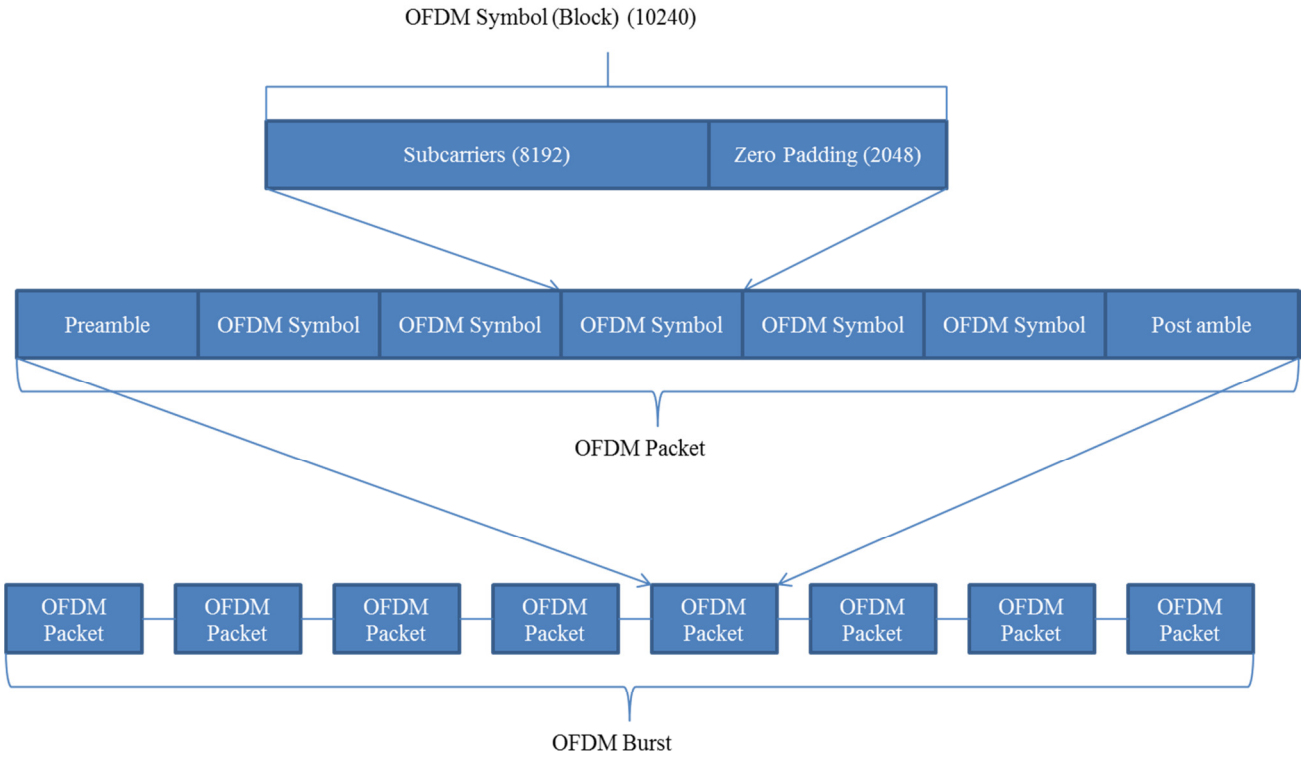

Figure 4.2. OFDM Burst structure.

It is a well-known fact that the FFT/IFFT produces real output when the input is made up of conjugate symmetric halves. This property of the IFFT was made use of to produce real OFDM samples in the specified band of operation. More specifically, each OFDM symbol was generated using an 8192 point IFFT at 44.1 kHz sampling frequency. This corresponds to a subcarrier spacing of about 5 Hz. A total of 372 active sub-carriers was used, corresponding to the bins in the 3-5 kHz range, of which 279 were used for transmitting data and 93 were used as pilots. BPSK modulation was used to modulate both the data and pilot subcarriers. The pilot subcarriers are meant for use at the receiver to estimate the frequency response of the channel, as will be explained in the next section. There are two ways in which pilots can be inserted into an OFDM symbol, namely the comb type and block type insertion [47].

Comb type pilot insertion involves using a part of the total number of subcarriers, in each of the OFDM symbols transmitted, as pilots. On the other hand, block type pilot insertion involves periodically using a whole OFDM symbol as a pilot. In other words comb type pilot insertion corresponds to periodic insertion of pilots in the frequency domain, while block type pilot insertion corresponds to periodic insertion of pilots in the time domain as shown in Figures 4.3 and 4.4.

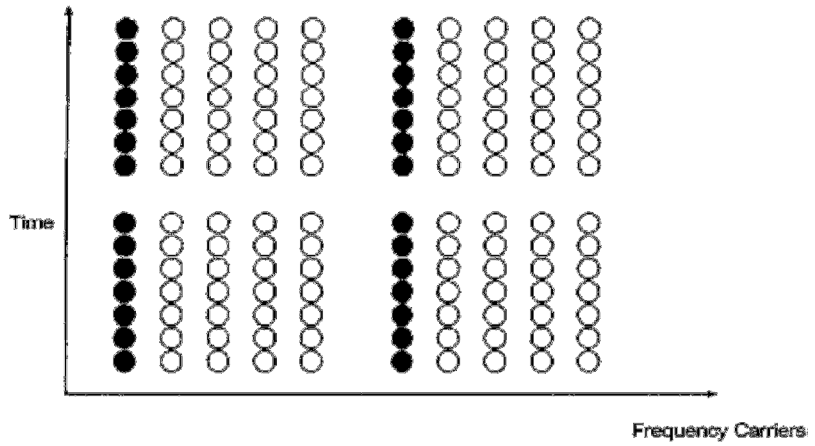

Figure 4.3. Comb type pilot insertion.

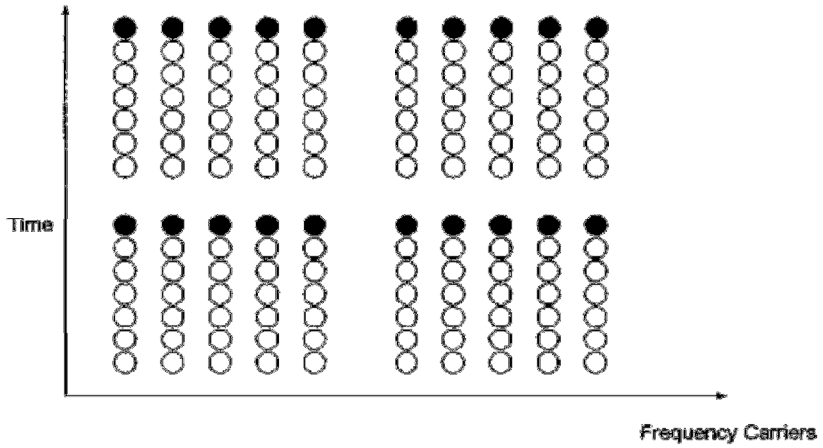

Figure 4.4. Block type pilot insertion.

In comb type pilot insertion N_p pilot symbols are inserted into $X(k)$ by the formula:

$$\begin{aligned} X(k) &= X(mL+l) \\ &= \begin{cases} x_p(m) & l=0 \\ data & l=1,...,L-1 \end{cases} \end{aligned} \tag{4.1}$$

where $X(k)$ is the OFDM symbol in the frequency domain, $L=\left\lfloor \frac{N}{N_p} \right\rfloor$ (where N refers to the total number of active subcarriers) and $x_p(m)$ is the m^{th} pilot carrier value.

Both techniques have pros and cons. Comb type pilot insertion tends to work well in a channel which does not vary too much across different frequencies while block type pilot insertion tends to yield good results in a channel which does not vary rapidly with time. However, if the channel varies rapidly in both time and across frequency the best option would be to use block type pilot insertion with an increased number of pilot OFDM symbols. Comb type pilot insertion was used in this work because the channel varied significantly from one symbol to another due to relative motion between the transmitter and receiver. The overall structure of the transmitter is shown in Figure 4.5.

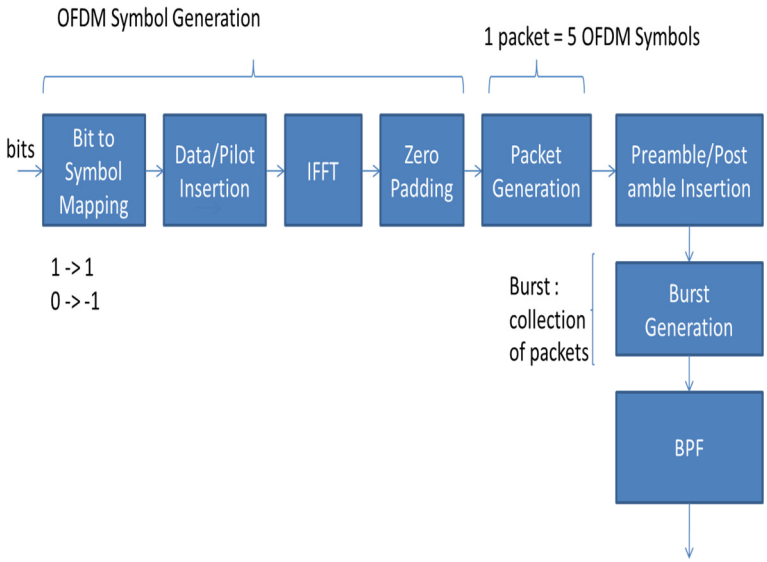

Figure 4.5. OFDM Transmitter Structure.

The input bits were first mapped to BPSK symbols. Pilot BPSK symbols were inserted periodically (with a period of four samples) in between these data symbols. The symbol stream thus created was used to generate the conjugate symmetric input to the IFFT block. The real output that the IFFT produced was sufficiently zero padded to a length greater than the delay spread of the channel. Each OFDM symbol thus generated was used to create packets. A Linear Frequency Modulated (LFM) signal or a chirp signal, with frequency varying linearly over the entire band of operation, was attached to the beginning and end of each packet for the purpose of performing timing synchronization (using a matched filter) at the receiver. The chirp signal can be expressed as:

$$s(t) = \cos\left(2\pi f_0 t + \pi k t^2\right) \tag{4.2}$$

The instantaneous frequency of the signal can be obtained by differentiation:

$$f(t) = \frac{1}{2\pi}\frac{d}{dt}\left(2\pi f_0 t + \pi k t^2\right) = f_0 + kt \tag{4.3}$$

Hence the chirp signal is characterized by its start frequency (f_0), stop frequency (f_1), and time duration (T) as:

$$k = \frac{f_1 - f_0}{T} = \frac{B}{T} \tag{4.4}$$

The pre-amble/post-amble was designed to have a repetitive structure as shown in Figure 4.6. The reason for selecting this type of a correlation waveform and pre-amble/post-amble structure will be explained in Section 4.3.3.

Figure 4.6. Pre-amble/Post-amble Structure.

The entire OFDM burst, which consisted of multiple such OFDM packets, was passed through a band pass filter to limit the out of band power. The band pass filtered signal was then played out through the speaker connected to the soundcard of the computer. Figures 4.7 and 4.8 show the OFDM burst, after band pass filtering, in the time and frequency domain respectively. The OFDM burst used in this example consists of four packets.

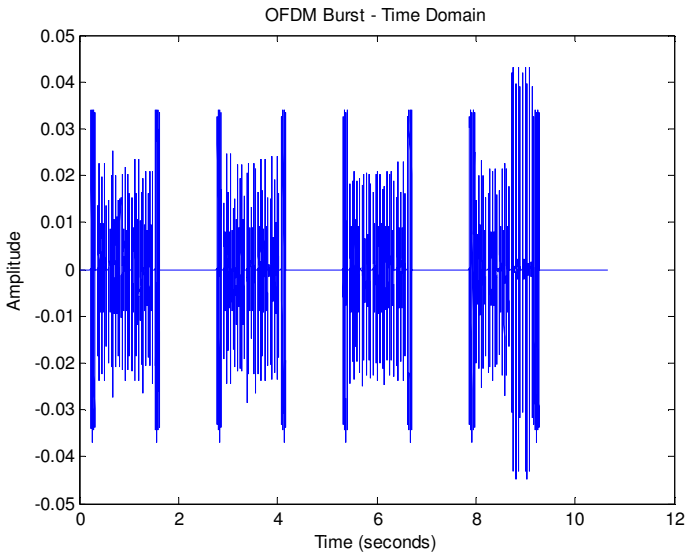

Figure 4.7. OFDM Burst.

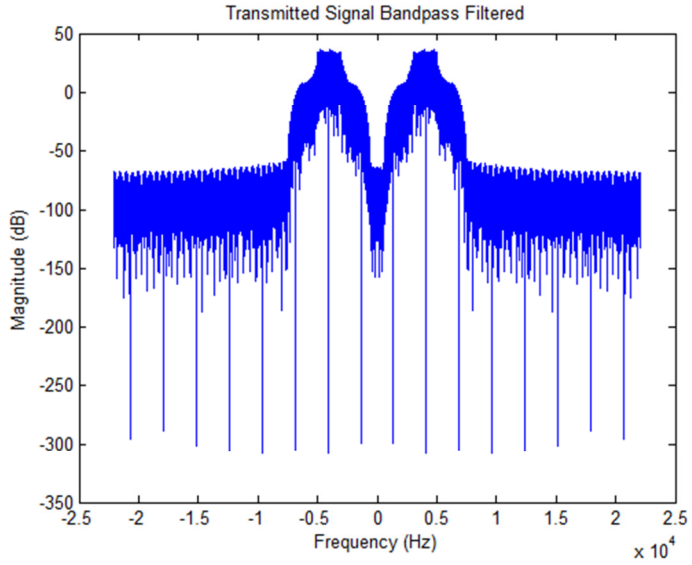

Figure 4.8. Spectrum of the transmitted OFDM Burst.

Table 4-1. Summary of the parameters used for generating the OFDM burst.

Parameter	Value
FFT/IFFT Size	8192
Active Carriers	372
Pilot Carriers	93
Data Carriers	279
Null Carriers	20
Sampling rate	44.1 kHz
ZP length	2048 samples (= 46.4 ms)
Number of OFDM symbols per packet	5
Modulation	BPSK
Pre-amble/Post-amble	Linear Chirp

4.3 OFDM Receiver

The transmitted OFDM burst was recorded using a microphone connected to another computer. The sound wave recorded by the microphone was sampled using the sound card of the computer, and was input into the OFDM receiver which was implemented in MATLAB.

The experiment had to be performed in such a way that the received burst was subject to the Doppler effect. In order to achieve this, the microphone was held in hand and moved either along a semi-circle, or directly towards or away from the speaker along a straight line. Moving the microphone to and fro uniformly in a straight line with respect to the speaker helped in maintaining a nearly constant relative velocity between the transceivers. Constant relative velocity within a packet is assumed for the Doppler estimation and correction technique

described in Section 3.4. On the other hand, moving the microphone along a semi-circle with respect to the pivot resulted in fast variation of relative velocity (within a packet), and degraded the performance of the receiver considerably. The results shown in this chapter were obtained when the receiver moved directly towards or away from the transmitter uniformly along a straight line. The case of semi-circular movement will be discussed in more detail in Chapter 5. Another problem of change in the direction of movement of the receiver during the transmission of a packet will also result in severe degradation in performance, and will be discussed in the next chapter.

The structure of the OFDM receiver is shown in Figure 4.9.

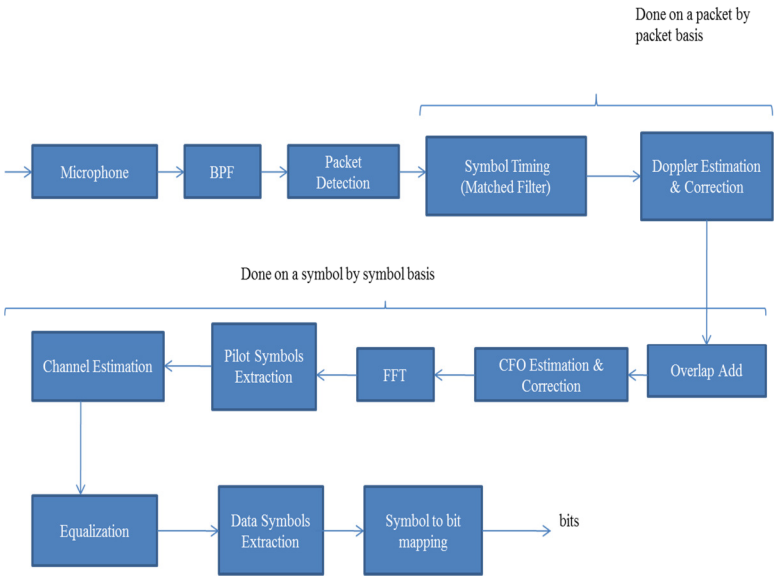

Figure 4.9. OFDM Receiver Structure.

Most of the blocks in Figure 4.9 are self-explanatory, but will be looked at in detail in this section.

4.3.1 Received Burst

Figures 4.10 and 4.11 show the received burst in the time and frequency domain respectively.

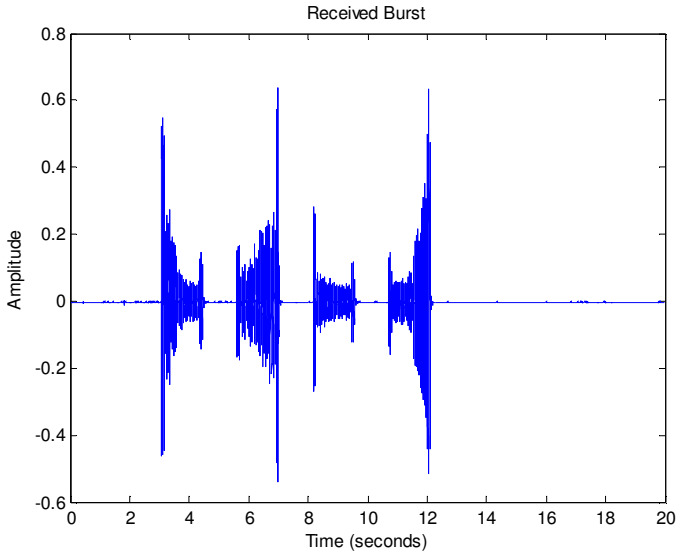

Figure 4.10. Received Burst.

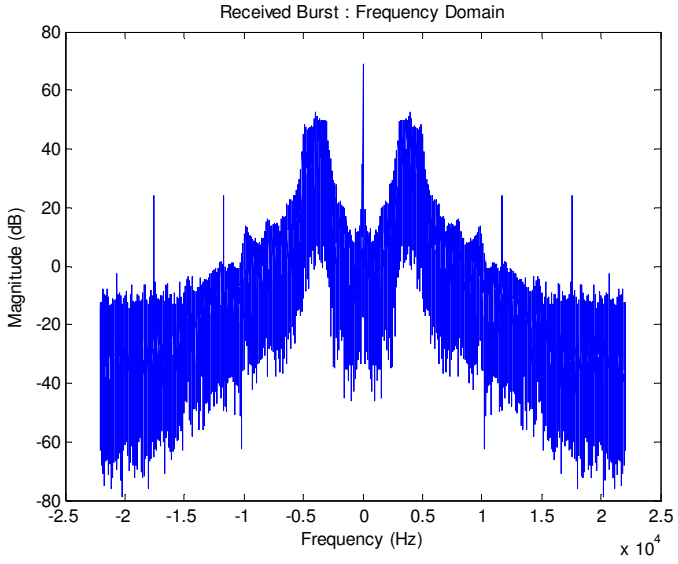

Figure 4.11. Spectrum of the received burst.

The channel was devoid of too much noise, and the SNR in the received data was on the order of 40 dB. We observe from Figure 4.11 that the received burst has a lot of out of band power, especially at DC. This was probably introduced by the soundcard of the computer. In order to reduce the out of band power, the received burst was band pass filtered using a FIR band pass filter designed using the Parks-McClellan equiripple design technique (*firpm* command in MATLAB). The frequency response of the band pass filter is shown in Figure 4.12.

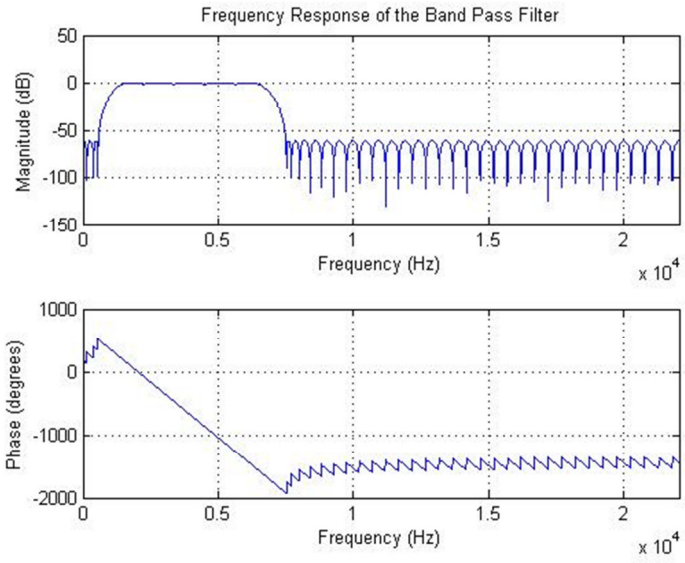

Figure 4.12. Frequency Response of the Band Pass Filter.

The spectrum of the received burst after band pass filtering is shown in Figure 4.13.

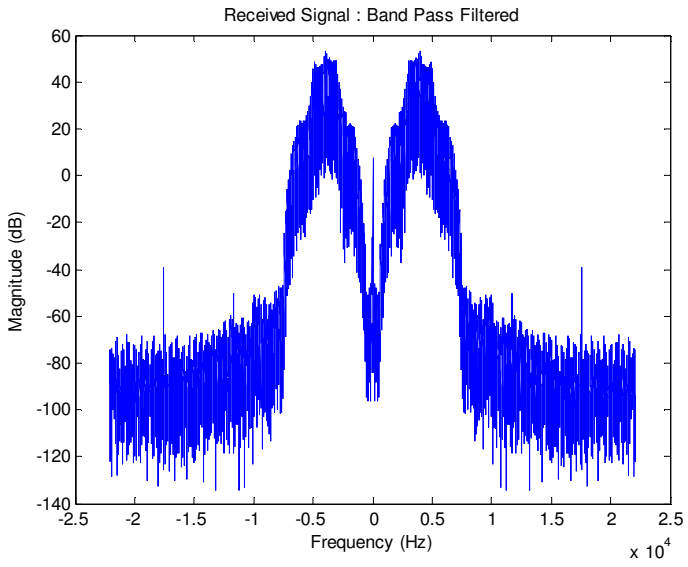

Figure 4.13. Spectrum of the burst after the band pass filter.

It is evident from Figure 4.13 that the power outside the 3-5 kHz band has been significantly reduced in comparison to Figure 4.11.

4.3.2 Packet Detection

Packet detection is the technique used to obtain a rough estimate of the beginning and end of a packet. Section 2.5.3 described three different techniques that can be used to perform packet detection in the absence of appreciable noise. Since the experiment was conducted indoors in the DSPRL, the received signal was not corrupted by a lot of noise. Hence all three techniques described earlier detected the packets satisfactorily. However, the time required by MATLAB to implement each of these three techniques was significantly different. This is evident from Table 4-2 given below:

Table 4-2. Packet detection time requirements (MATLAB code).

Method	MATLAB Simulation time (seconds)
Energy Detector	0.015765
Double Sliding Window Correlation Technique	1288.100739
Double Window Energy Detection	2402.459548

Observe that the time required by the simple energy detector, to detect the presence of a packet, is significantly less than the time required by the other two techniques. Hence the energy detector was preferred to the other techniques for performing packet detection. Figure 4.14 shows a plot of energy detected, using a window of size 4800 samples, over the entire burst.

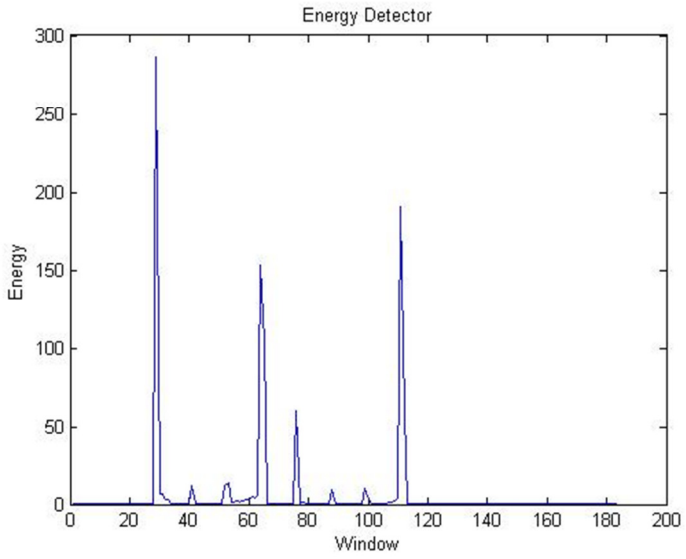

Figure 4.14. Energy Detection.

Figure 4.15 shows the part of the output of the energy detector corresponding to packet 3 (the packet with the lowest energy).

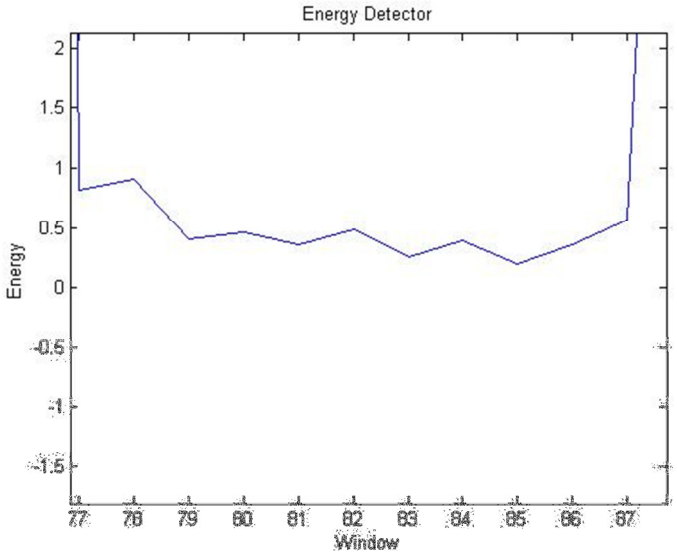

Figure 4.15. Energy detection output corresponding to packet 3.

The threshold for detection, which would depend on the energy of the received burst, had to be selected so as to maximize the probability of detection while minimizing the probability of false alarm. Falsely detecting the presence of a packet is less severe an error than not detecting a packet at all. Hence, the threshold was set at 0.01 (an order of magnitude less than the energy in packet 3). Since each packet consisted of 55200 samples, a true detection would occur only when at least 12 consecutive windows exceeded the threshold. This property was used to reduce the probability of false alarm due to noise.

4.3.3 Symbol Synchronization

Symbol synchronization is the process used to synchronize the symbols in a received burst at sample level precision. Radio frequency communication generally makes use of the repetitive structure of the pre-amble (using the double sliding window correlation technique) to attain symbol synchronization. This however will not work in the case of acoustic communication in the presence of Doppler because of the large amount of time domain expansion or contraction involved. If the pre-amble were originally periodic with a period of *N* samples, the corresponding pre-amble in the received burst which has undergone the Doppler effect, will no longer be periodic with the same period. Hence the double sliding window correlation technique will not produce a clear peak indicating the beginning or end of a packet. The loss of a distinct peak can clearly be seen in Figure 4.16 which shows the output produced by the DSWC technique for packet 1.

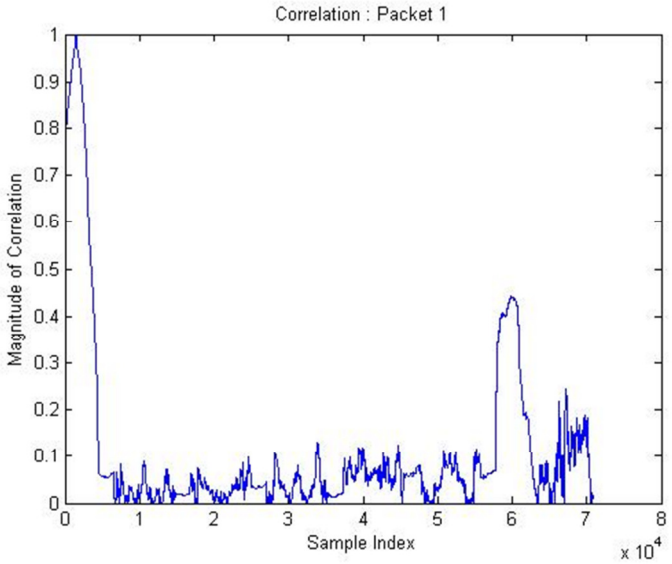

Figure 4.16. Packet detection using the Double Sliding Window Correlation technique.

The two peaks in Figure 4.16 correspond to the pre-amble and post-amble respectively. It should be observed that even though there is an increase in the magnitude of correlation near the pre-amble and post-amble, a distinct peak, which is critical for performing symbol synchronization, is absent. Hence this technique cannot be used for performing symbol synchronization when there is relative motion between the transmitter and receiver.

The technique that was finally used to perform symbol synchronization involved using a matched filter (as explained in Section 2.5.3), matched to the pre-amble/post-amble that was added to the beginning and end of each packet. The probability of errors in symbol timing using the MF can be reduced by selecting waveforms with a large bandwidth-time product ($BT \geq 100$) [45]. In order to discuss the choice of correlation waveforms, we define the ambiguity function as follows [48]:

$$\chi_{sr}(\tau, \Delta) = (1+\Delta) \int_{-\infty}^{\infty} s((1+\Delta)t) r(t-\tau) dt \tag{4.5}$$

where $s(t)$ and $r(t)$ refer to the transmitted and received signals respectively and Δ and τ refer to the relative Doppler shift and time delay respectively. The ambiguity function shows the matched filter response versus delay and relative Doppler shift variations of the received signals. The choice of correlation waveform is governed by the degree of Doppler tolerance required by the receiver. For significant Doppler shifts due to movement, a mismatch will occur between the received correlation waveform and the single correlator, with a consequent loss of a distinct peak. Therefore signals with very narrow ambiguity functions in the Doppler axis, such as PN sequences and OFDM symbols were ruled out in favor of linear or log frequency modulated FM signals. Such signals are highly Doppler tolerant due to their wide ambiguity function in the Doppler axis. Figure 4.17 shows the output of the matched filter for all four packets.

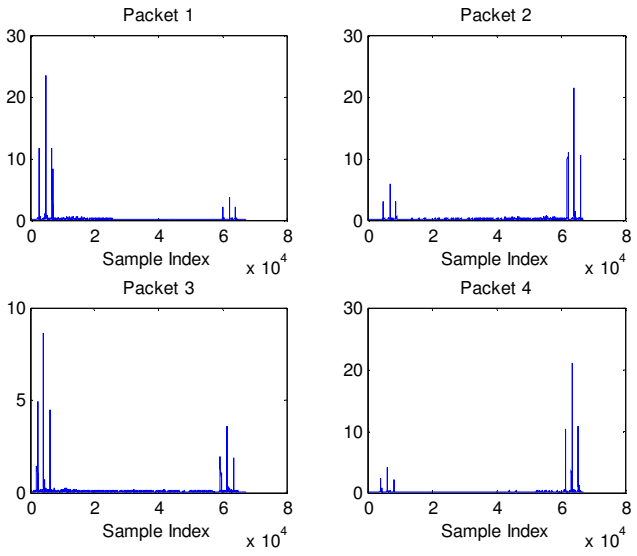

Figure 4.17. Output of the matched filter for all four packets.

Observe the two triplets of peaks in each of the four figures. This is obtained due to the repetitive structure of the pre-amble and the post-amble. The highest peak in each of the triplets in each figure indicates the detection of the pre-amble and the post-amble.

4.3.4 Doppler Estimation and Correction

Several techniques have been proposed for Doppler estimation and correction, one of which involves the usage of the ambiguity function in (4.5). Estimating the relative Doppler shift in the received signal $r(t)$ involves a search over Δ, with $\tau = 0$, to find the maximum magnitude of the cross-ambiguity function $\chi_{sr}(0,\Delta)$:

$$\chi_{sr}(0,\Delta) = (1+\Delta)\int_{-\infty}^{\infty} s((1+\Delta)t)r(t)dt \tag{4.6}$$

However, for this technique to be feasible a rough idea of the range over which Δ can vary is required. This technique is also computationally expensive when compared to the technique that has been used in this chapter.

The packet level Doppler estimation and correction technique used in this chapter was explained in Section 3.4.2. The method involved interleaving data packets with a known waveform (pre-amble/post-amble). The pre-amble and post-amble were used to measure the expansion or contraction experienced by each of the received packets. The receiver then resampled each of the received packets with a resampling parameter equal to the estimated relative Doppler shift. This technique in effect estimates and corrects for the average relative Doppler shift over a packet, and hence assumes the relative velocity between the transceivers to be constant within a packet.

Each OFDM packet generated at the transmitter consisted of 51200 samples (excluding the pre-amble/post-amble). Table 4-3 lists the number of samples in each of the received packets, and the corresponding relative Doppler shift estimated as per (3.28) in Section 3.4.2. Once the relative Doppler shift $\hat{a}$ is estimated, the relative velocity $\hat{v}$ and frequency shift $\Delta\hat{f}_k$ can be estimated using (4.7) and (4.8) respectively.

$$\hat{v} = \hat{a}c \tag{4.7}$$

$$\Delta\hat{f}_k = \hat{a}f_k \tag{4.8}$$

where f_k refers to the frequency of the k^{th} subcarrier.

Table 4-3. Effect of Doppler shift in the received burst.

Packet#	Trx (# samples)	a (x 10^{-3})	Relative velocity (m/s)	Doppler Shift Estimate (Hz) at 4 kHz
1	51250	-0.9766	-0.3320	-3.906
2	51178	0.4297	0.1461	1.719
3	51243	-0.8398	-0.2855	-3.359
4	51163	0.7227	0.2457	2.891

Observe from Table 4-3 that packets 1 and 3 have expanded while packets 2 and 4 have contracted. This corresponds to the way the experiment was performed, as the microphone was moving away from the speaker during the transmission of packets 1 and 3 while the microphone was moving towards the speaker during the transmission of packets 2 and 4. The relative velocity and relative Doppler shift estimates are positive for packets 2 and 4 and negative for packets 1 and 3. The estimates obtained for relative velocity and Doppler shift at 4 kHz also correspond to the receiver movement because the microphone moving away from the speaker is expected to both expand the packet in the time domain and reduce the frequency and vice versa.

4.3.5 Operations Performed on a Symbol by Symbol Basis

The Doppler estimation and correction was performed over a packet. The rest of the operations in the receiver were performed on a symbol by symbol basis. Each OFDM symbol generated at

the transmitter consisted of 10240 samples (8192 samples from IFFT and 2048 samples of zero padding). Hence the output of the Doppler estimation and correction block (which changed the number of samples in the received packet to be equal to what was transmitted) was divided into 5 symbols. Each symbol was then passed through the overlap adder, which added the 2048 samples at the end of each symbol to the corresponding samples at the beginning of the same symbol. As explained in Section 2.3, this helped in modeling the linear convolution between the symbol and the CIR as a circular convolution.

The Doppler correction technique described in the previous section corrects only the average relative Doppler shift over a packet. The residual CFO in each symbol is then corrected using the null subcarriers (as described in Section 3.4). The method involves performing a 1-D search over frequency to find that estimate of CFO which minimizes the energy spilled over into the null subcarriers. Figures 4.18 and 4.19 show the estimated energy in the null subcarriers, of the 15th and 17th OFDM symbol respectively, for different possible CFOs (in radians per sample).

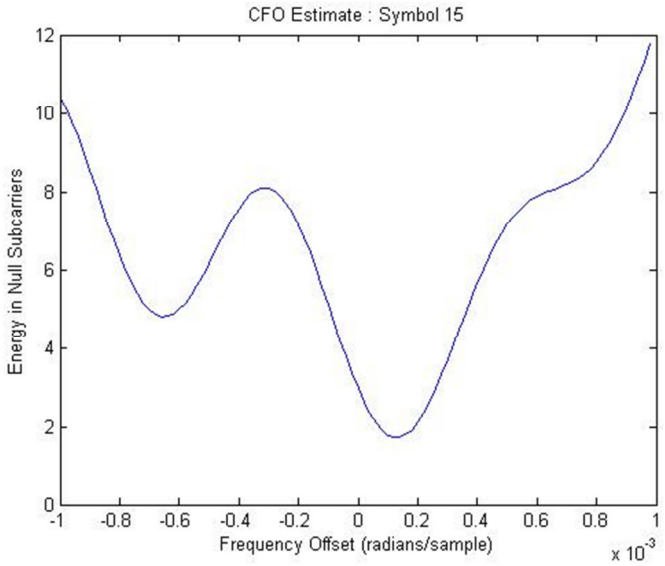

Figure 4.18. Energy in the null subcarriers for various CFOs (symbol number 15).

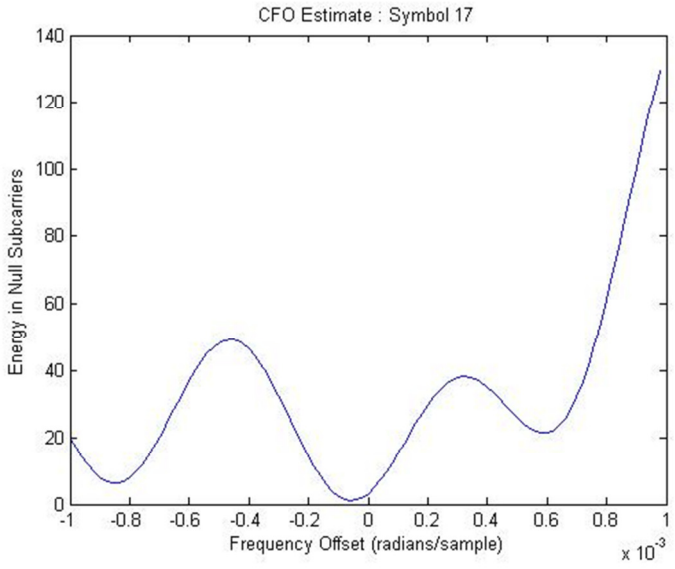

Figure 4.19. Energy in the null subcarriers for various CFOs (symbol number 17).

The CFO for the 15th and 17th symbols was estimated to be 0.8422 Hz and (-0.06 x 10^{-3} radians/sample*44100/2/π =) -0.4211 Hz respectively. The CFO estimates per OFDM symbol are shown in Figure 4.20.

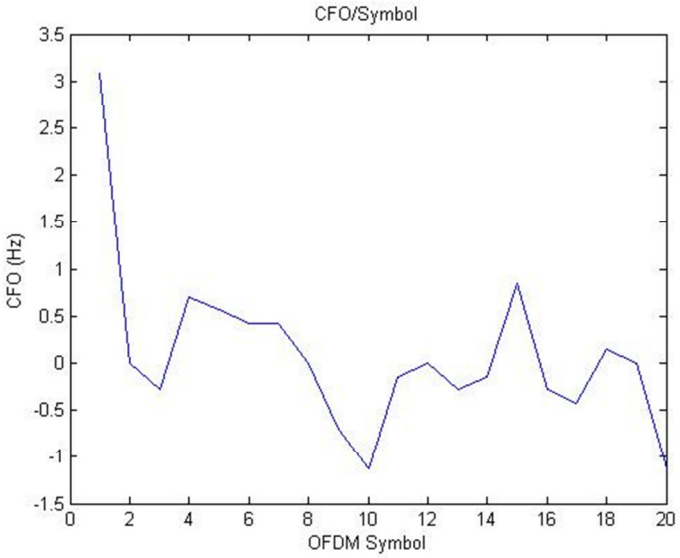

Figure 4.20. Carrier Frequency Offset estimate (Hz) per symbol.

CFO correction was followed by the FFT operation, which converted the time domain OFDM symbol into the frequency domain. This facilitated the extraction of the pilot symbols from the corresponding bins for performing channel estimation. If X_p and Y_p refer to the transmitted and received pilots at the p^{th} subcarrier, the channel impulse response (CIR) estimate corresponding to the p^{th} subcarrier is given by:

$$H_p = \frac{Y_p}{X_p} \tag{4.9}$$

The MATLAB function *interp* was used to perform cubic spline interpolation of the CIR estimates at pilot subcarriers onto the data subcarriers. Figures 4.21 and 4.22 show estimates of the frequency response of the channel obtained from symbols 3 and 4.

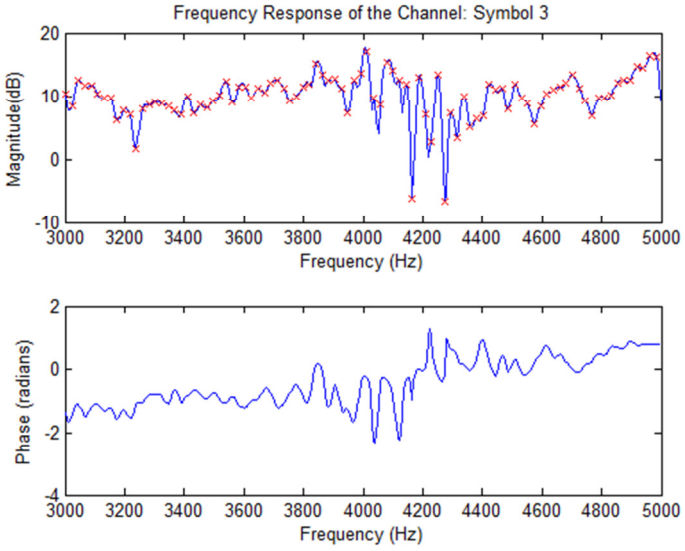

Figure 4.21. Frequency Response estimate of the channel obtained from symbol number 3.

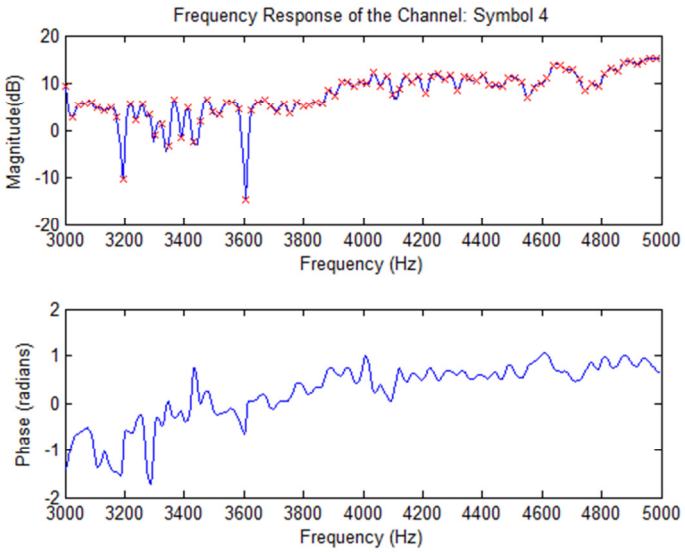

Figure 4.22. Frequency Response estimate of the channel obtained from symbol number 4.

It is evident from Figures 4.21 and 4.22 that the channel varies significantly from one symbol to another. This justifies the use of a comb type pilot insertion technique.

Once the channel estimate over the entire band of operation was obtained, frequency domain equalization was performed to negate the effect of the frequency selective channel. Let Y refer to the received OFDM symbol and H to the channel response estimate in the frequency domain. The equalized OFDM symbol in the frequency domain was obtained by:

$$X_{equalized} = \frac{Y_k}{H_k} \quad k = 1, 2, ...K_{active} \tag{4.10}$$

The data symbols were then extracted from the corresponding subcarriers of the equalized OFDM symbols. Parts of the extracted data symbols in packets 1 and 2 are shown in Figure 4.23 and 4.24.

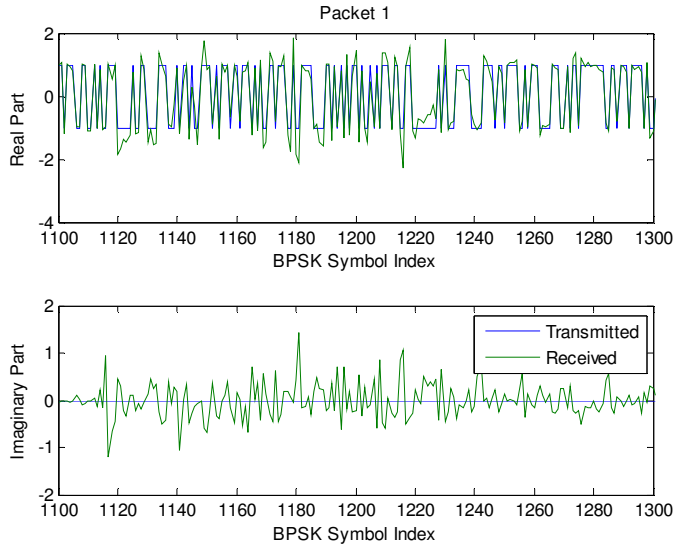

Figure 4.23. BPSK symbols extracted from packet 1.

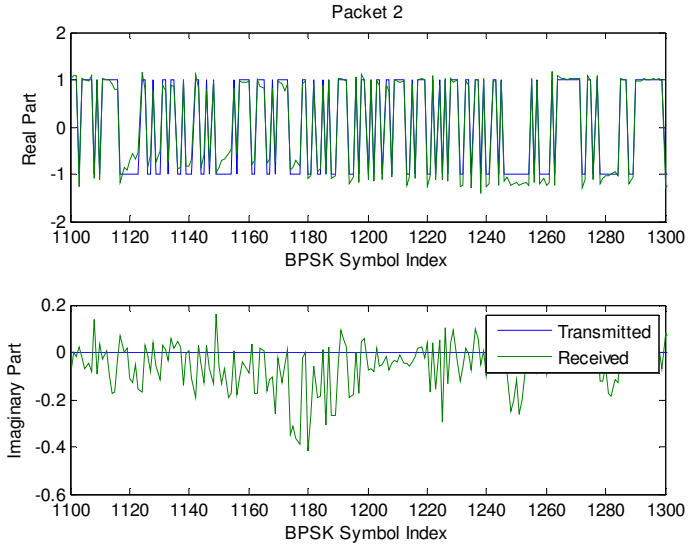

Figure 4.24. BPSK symbols extracted from packet 2.

Figures 4.23 and 4.24 indicate that the received symbols overlap quite well with the transmitted symbols. Figure 4.25 shows the scatterplot of the received BPSK symbols.

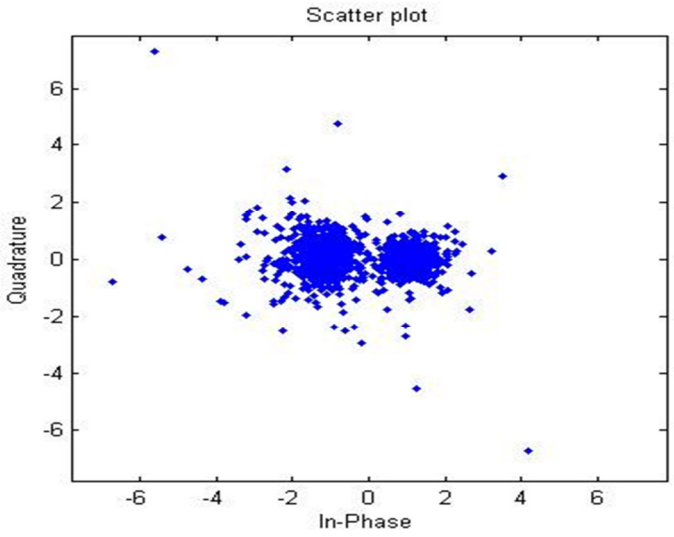

Figure 4.25. Scatterplot of the received symbols.

The data symbols were then mapped back to bits. The bit error rate (BER) experienced per OFDM symbol is shown in Figure 4.26. Figure 4.27 shows the BER incurred without performing Doppler correction on the same received burst.

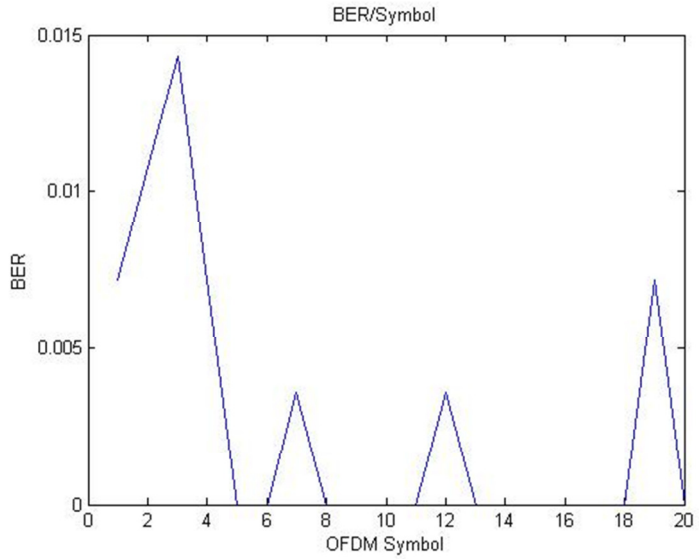

Figure 4.26. BER per OFDM symbol.

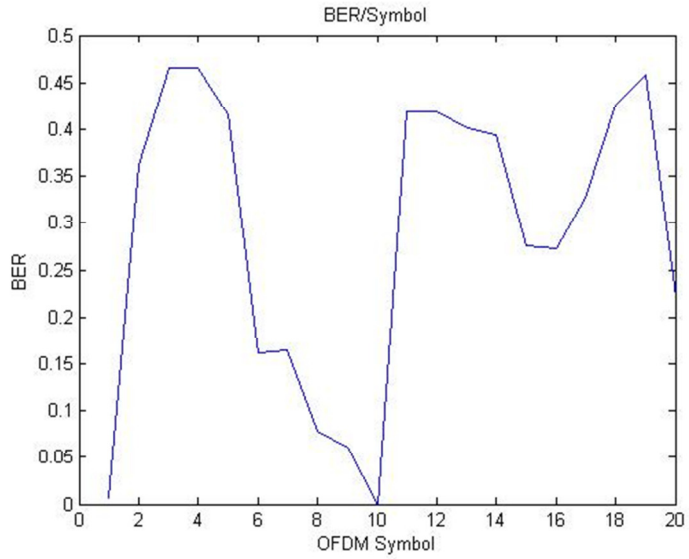

Figure 4.27. BER per OFDM symbol without Doppler correction.

Figures 4.26 and 4.27 show the improvement in the BER performance due to the Doppler correction technique used.

Recall that the results shown above were obtained when the microphone was moved directly towards or away from the speaker along a straight line in a very slow and uniform fashion. The performance of the receiver degraded significantly when the microphone was moved a little faster and in a much more non-uniform fashion (due to the non-uniform expansion/contraction that resulted from the non-uniform motion). The BER estimates (based on 3000 bits) obtained by recording the transmitted burst while moving the microphone radially in a non-uniform fashion is shown in Table 4-4. The burst used for this experiment consisted of four packets, and each packet consisted of a single OFDM symbol. The parameters estimated from each of the four packets are shown in Table 4-5.

Table 4-4. BER estimates obtained using the Doppler correction technique.

Packet #	BER Estimate
1	0.351
2	0.0471
3	0.304
4	0.341

Table 4-5. Parameters estimated for each packet.

Packet #	**T_{rx} (samples)**	**a (Relative Doppler shift) x 10^{-3}**	**Velocity (m/s)**	**Frequency shift (Hz) at 5 kHz**
1	16253	-0.8005	-0.2722	-4.003
2	16220	1.232	0.4187	6.158
3	16271	-1.909	-0.6490	-9.544
4	16227	0.8005	0.2722	4.003

The performance of the receiver also degraded significantly when the movement of the microphone was along a semi-circle with respect to the speaker. The corresponding results obtained by moving the microphone semi-circularly will be discussed in Chapter 5. The degradation resulted from the fact that the relative velocity towards the receiver varied rapidly (within a packet) due to the semi-circular movement, and the Doppler compensation technique

used in this chapter assumes the relative velocity to be constant within a packet. The aforementioned problem and the proposed solution to this problem will be explained in more detail in Chapter 5.

5 Time Warp based Doppler Correction Technique

5.1 Introduction

The previous chapter introduced a resampling based Doppler correction technique which corrects for the average Doppler shift over a packet, inherently assuming the relative velocity between transducers to be constant over the duration of the packet. The method may not yield satisfactory results when the relative velocity changes (for example, linearly) within a packet, as may be the case when the transmitter, receiver, or both are attached to platforms undergoing acceleration. In Section 4.3 it was observed that the correction technique yielded satisfactory results (in the over-the-air experiment) when the microphone was moved rather slowly and uniformly directly towards or away from the speaker, but the results degraded significantly when the microphone motion was moved either radially in a non-uniform fashion or along the arc of a circle with respect to the pivot. In order to investigate the reason for the degradation in performance in the latter case, a simulation model was developed to calculate the variation in velocity of the microphone towards the speaker with respect to angle (or time). Let l denote the distance between the microphone and the pivot (length of the arm), and d denote the distance between the microphone and the speaker. Let θ refer to the angle already traversed by the arm. The model for the case of $0 \le \theta \le 90°$ is shown in Figure 5.1. The velocity towards the speaker for motion in the counter clockwise direction can be calculated as:

$$\begin{aligned} v_{counter\_clockwise} &= v\,cos\{\phi - (90 - \theta)\} \\ &= v\,sin\{\theta + \phi\} \end{aligned} \tag{5.1}$$

where $\phi = tan^{-1}\left\{\frac{l+d-l\,sin\{\theta\}}{l\,cos\{\theta\}}\right\}$, and v is the tangential velocity in m/s. Similarly, the velocity towards the speaker for motion in the clockwise direction can be derived to be:

$$v_{clockwise} = -v\,sin\{\theta+\phi\} \tag{5.2}$$

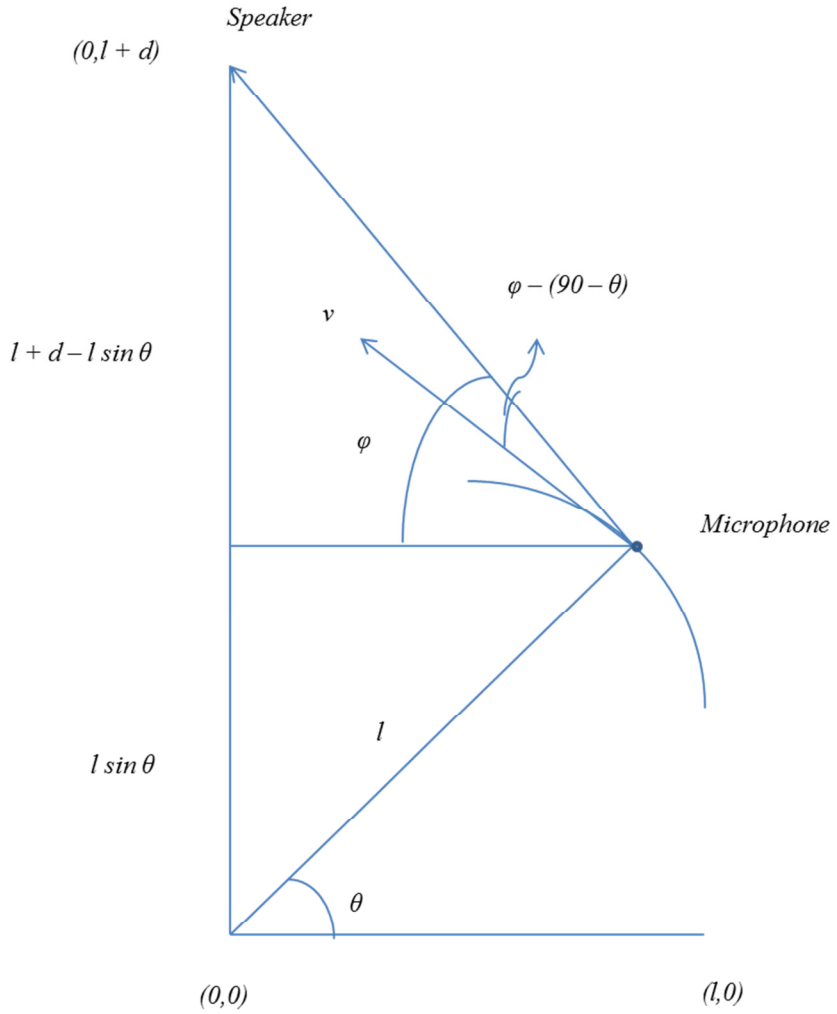

Figure 5.1. Model to calculate the relative velocity as a function of angle (or time).

The expression for relative velocity towards the speaker for $90° \leq \theta \leq 180°$ can be derived in a similar fashion, for motion in both clockwise and counter-clockwise direction. The derived expressions are shown in (5.3):

$$\begin{aligned} v_{clockwise} &= v\,sin\{\theta - \phi\} \\ v_{counter\_clockwise} &= -v\,sin\{\theta - \phi\} \end{aligned} \tag{5.3}$$

where $\phi = tan^{-1}\left\{\dfrac{l + d - l\,sin\{\theta\}}{-l\,cos\{\theta\}}\right\}$, and v is the tangential velocity in m/s.

Figures 5.2 and 5.3 show the change in velocity of the microphone and the change in the relative Doppler shift with respect to angle for $l = 1$ meters, $d =$ 0.5 meters and $v =$ 1 m/s when the movement is towards the speaker in the counter clockwise direction.

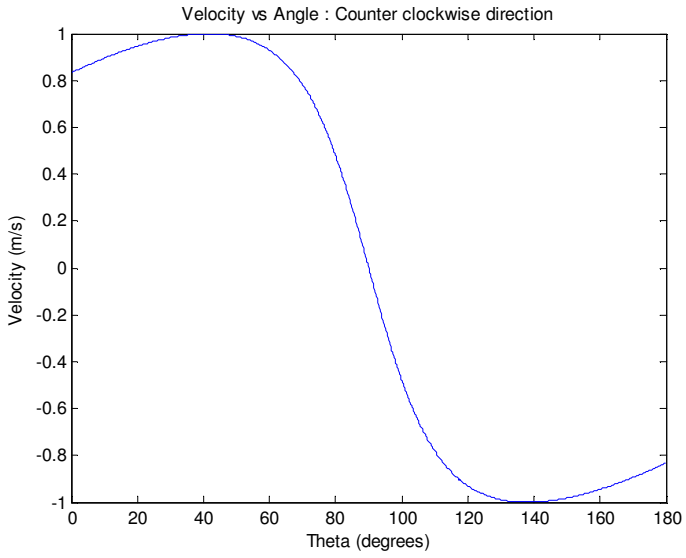

Figure 5.2. Velocity of the microphone towards the speaker for semi-circular movement in the counter clockwise direction.

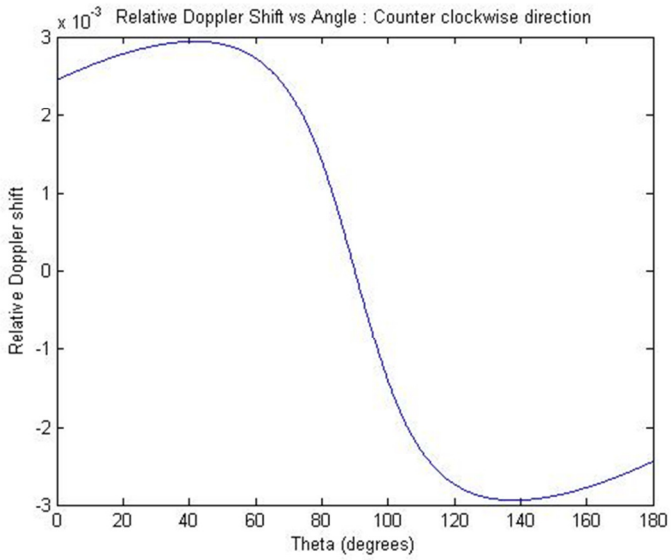

Figure 5.3. Relative Doppler shift due to semi-circular movement in the counter clockwise direction.

Observe that the velocity changes almost linearly, over any 5 to 10 degree angle, over a major portion of the arc over which the over-the-air experiment is to be performed. A linear change in velocity directly corresponds to a linear change in frequency. It was also observed that the linear change in velocity became steeper for angles near 90 degrees and even more so for when values of d are smaller. In order to verify that the outputs from the simulation closely correspond to what happens in reality, a burst containing multiple packets (each approximately 0.2 seconds long) of a sinusoid at 4 kHz was transmitted through the speaker, and received by the microphone which was undergoing motion along a circular path. Figure 5.4a shows the received packet in the time domain, and Figure 5.4b shows the spectrogram of the corresponding packet.

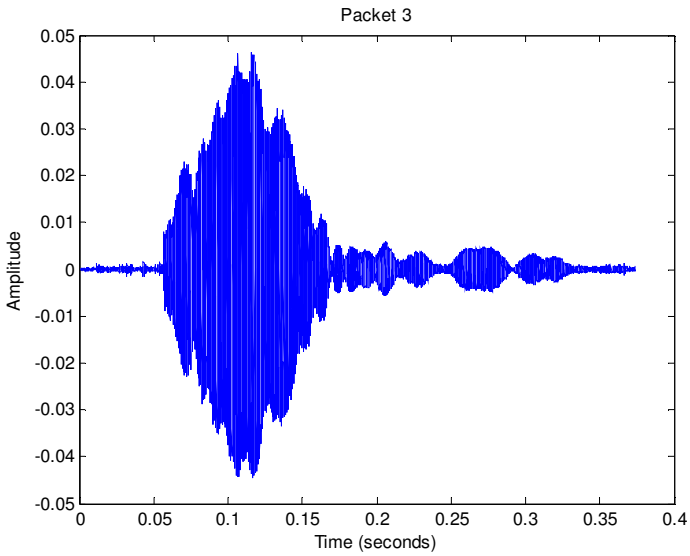

(a)

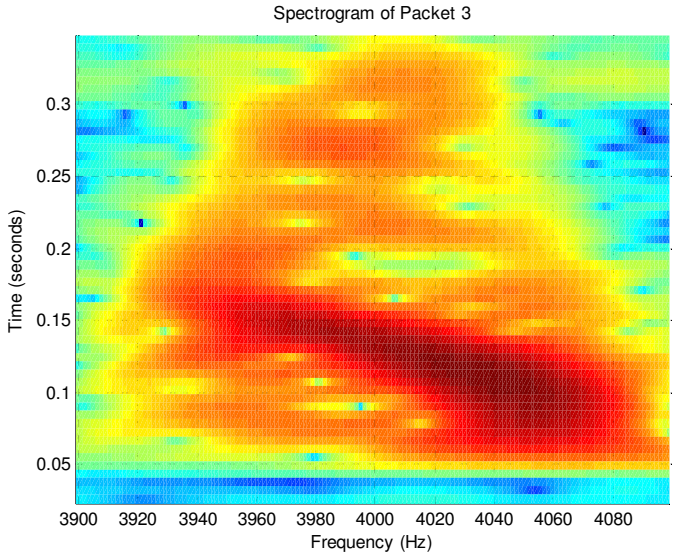

(b)

Figure 5.4. (a) Time domain version of the packet. (b) Spectrogram of the received sinusoid packet.

Even though the received packet is subject to severe multipath (as seen in Figure 5.4a), a mostly linear change in frequency is observed in the spectrogram.

As explained in Chapter 4, the uniform expansion/contraction based Doppler correction technique works well when the velocity is constant within a packet. If the velocity varies over a packet, an almost linear change over time is seen in the case currently under consideration and, the uniform expansion/contraction based Doppler correction technique may no longer work satisfactorily. Hence a different Doppler correction method, which would work even when the velocity changes within a packet, needs to be designed and implemented. In order to design and analyze a technique which may be able to correct for within-packet almost linear variation of velocity, a model which can emulate such a Doppler effect had to be created first. The next section describes such a model.

5.2 Wideband Doppler Model

This section describes a model that can be used to emulate the wideband Doppler effect in MATLAB. The technique involves using a time warp to model the Doppler effect as a change in the time scale.

5.2.1 Uniform Contraction or Expansion

Let us first consider the case of a pure contraction or expansion in time (which causes a constant Doppler shift in frequency). This can be modeled as a change in time scale by a constant factor. The relationship between the old and the new time scales is shown in Figure 5.5. The new time scale for this case can be obtained by:

$$t_{Doppler} = (1+\alpha)\, t_{original} \tag{5.4}$$

where $t_{Doppler}$ and $t_{original}$ refer to the Doppler affected time scale and the original time scale respectively, and α refers to the relative Doppler shift. Negative values of α can be used to reflect a pure contraction while positive values of α reflect a pure expansion. The Doppler effect is introduced to a uniformly sampled sequence over some time duration by uniformly resampling the output – the uniformly spaced samples that result from the Doppler inducing time warp operation in (5.4) on the original signal – over the new time duration. If $T_{Doppler}$ refers to the total time duration of the signal output from the warp, and *number of samples* refers to the number of samples in the original signal, the new sampling period can be selected to be $T_S = (T_{Doppler} /$ *number of samples*) so as to make the number of samples in the received signal the same as in the transmitted signal (while corresponding to different time durations in terms of absolute time units, such as seconds).

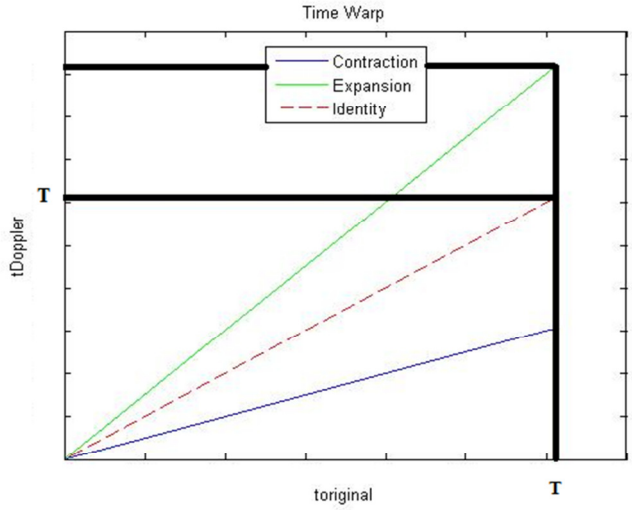

Figure 5.5. Time Warp for expansion/contraction.

To prove the effectiveness of this technique, let us analyze the effect different time warps, generated using α values of -0.5 and 0.5, have on a burst containing a 5 kHz sinusoid shown in Figure 5.6.

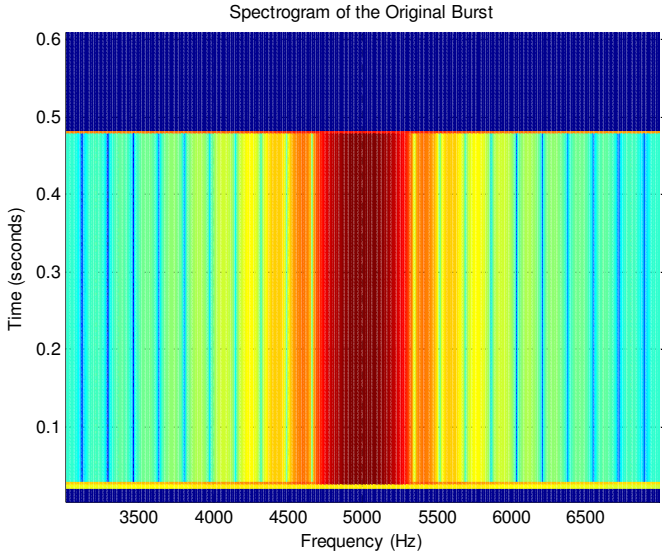

Figure 5.6. Spectrogram of the original burst.

When the value of α is -0.5, the relationship between the time scales becomes $t_{Doppler} = 0.5\,t_{original}$. This results in contraction of the signal in time, and therefore a simultaneous doubling of frequency. This change in frequency is evident in the spectrogram shown in Figure 5.7 (figure zoomed-in to show the relevant portion of the frequency axis). Similarly, when the value of α is 0.5 the relationship between the time scales becomes $t_{Doppler} = 1.5\,t_{original}$. This is equivalent to an expansion in time and a corresponding decrease in frequency (to two thirds of the actual frequency). This change in frequency is observed in the spectrogram shown in Figure 5.8. Note that the frequency of the sinusoid output from the warp is now equal to 3333.33 Hz (two thirds of 5 kHz). Also observe that the duration of the burst has been reduced to half of the

duration of the original burst in Figure 5.7, and increased to 1.5 times the duration of the original burst in Figure 5.8.

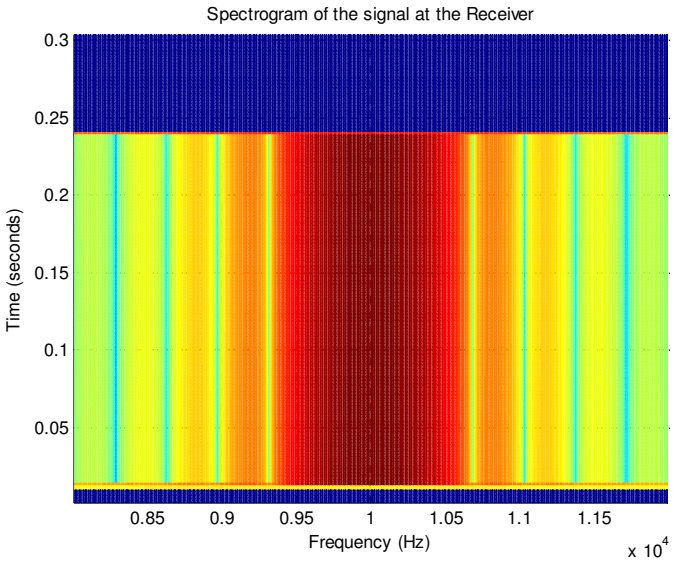

Figure 5.7. Spectrogram of the time warp generated using $\alpha = -0.5$.

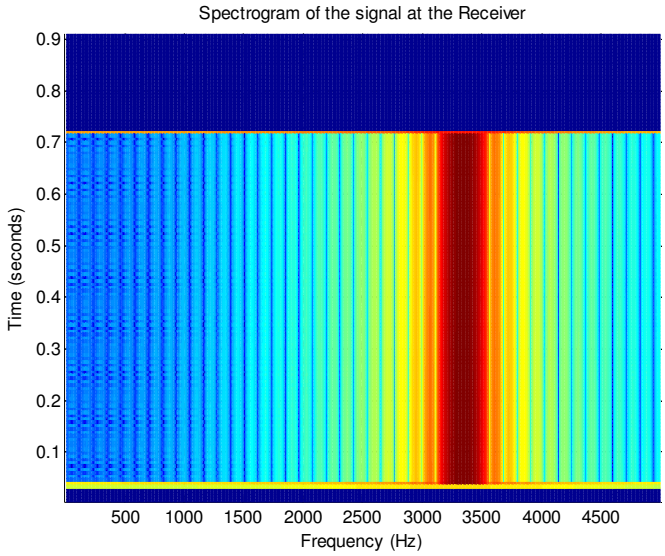

Figure 5.8. Spectrogram of the time warp generated using $\alpha = 0.5$.

The results shown above demonstrate the effectiveness of the Doppler time warp model to simulate a uniform contraction or expansion in time due to the Doppler effect. The values of α were chosen for the sole purpose of demonstrating the accuracy of the model in a rather exaggerated manner. It is not physically possible to attain such high values of α in an underwater channel. Practical values that α assumes in the UWA channel are on the order of 10^{-2} or smaller.

The Doppler effect thus generated can be undone by inverse time scaling the Doppler shifted time scale as shown in (5.5).

$$\hat{t}_{original} = \frac{t_{Doppler}}{1+\alpha} \tag{5.5}$$

For uniformly sampled sequences, this inverse time scaling is accomplished by resampling, i.e. a sampling rate change by the factor $(1+\alpha)^{-1}$.

5.2.2 Expansion/Contraction with Within-Packet Change in Doppler shift

A linear change in velocity (within a packet) results in a linear change in frequency. A linear change in frequency can in turn be obtained by changing the time scale quadratically (at least this is a good approximation as long as the linear term dominates the quadratic term). Hence the Doppler affected time scale model is written as:

$$t_{Doppler} = (1+\alpha+\beta t_{original})t_{original} \tag{5.6}$$

where $t_{original}$ and $t_{Doppler}$ refer to the original and Doppler affected time scale. Depending on the value of α and β the time warp generates a signal which has either expanded or contracted in

time, but not necessarily linearly or at a uniform rate. If the original time scale was sampled uniformly, then the corresponding time samples in the Doppler warped time scale are non-uniformly spaced. An example of a time warp is shown in Figure 5.9. In practice the input to the receiver consists of uniformly spaced samples. Hence, in simulation of a Doppler affected signal, the non-uniformly spaced output of the warp needs to be uniformly sampled over the new time duration (using linear interpolation) [49, 50].

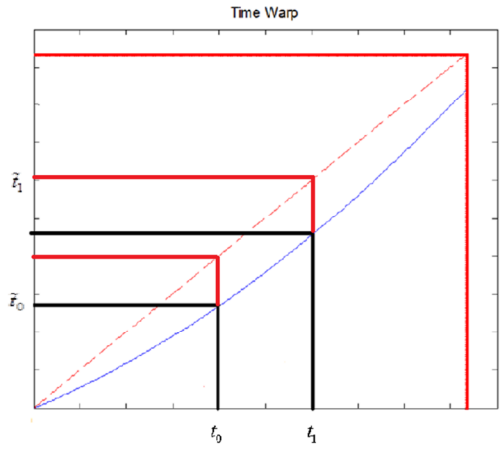

Figure 5.9. Doppler Time Warp Illustration.

If $y(t)$ refers to the received signal with the Doppler effect, the non-uniformly spaced samples of $y(t)$ that are output from the warp are converted to uniformly spaced samples spaced at T_S by performing linear interpolation of the non-uniformly spaced samples:

$$y\{t_{uniform}(n)\} = y\{t_{Doppler}(k)\} + \gamma\left[y\{t_{Doppler}(k+1)\} - y\{t_{Doppler}(k)\}\right] \tag{5.7}$$

where $t_{uniform}$ refers to the uniformly spaced Doppler affected time scale (shown in Figure 5.10), and $\gamma = \dfrac{t_{uniform}(n) - t_{Doppler}(k)}{t_{Doppler}(k+1) - t_{Doppler}(k)}$.

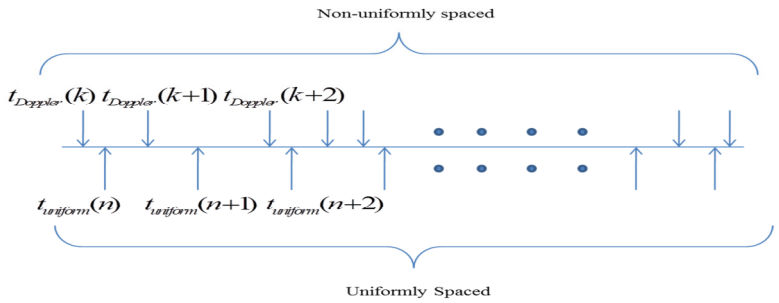

Figure 5.10. Linear interpolation to convert non-uniformly spaced samples to uniformly spaced samples.

The resulting signal $y\left(t_{uniform}(n)\right)$ is the uniformly sampled Doppler affected received signal. The above process describes how the Doppler affected received signal can be generated or simulated based on the uniformly spaced samples of the signal (to be transmitted).

In a receiver context, correcting for the Doppler effect the received signal was subject to involves reversing the above process, i.e. going through the inverse of the Doppler time warp followed by producing uniformly spaced samples based on the non-uniformly spaced samples which are the output of the inverse warp. The effect of the warp can be inverted by solving the quadratic equation for (the positive solution) $\hat{t}_{original}$ using the known $t_{Doppler}$ from (5.6). This step is followed by using the values of the received signal at the non-uniformly spaced time instants $\hat{t}_{original}$ to obtain the corresponding values at uniformly spaced time instants. The set of

operations just described will (ideally) undo the Doppler effect, and the original signal can be retrieved with considerable accuracy, as will be shown in the following example.

To demonstrate the accuracy of the model, a sinusoid at 5 kHz was passed through the time warp (generated using $\alpha = -0.01$ and $\beta = -0.1470$; based on an exaggerated arbitrary contraction of 10%) shown in Figure 5.11, and uniformly sampled. Figure 5.12 shows the Doppler affected burst in the time domain. The contraction in time experienced by the Doppler affected signal can be observed in Figure 5.13. The spectrogram of the corresponding signal (estimated using an 8192 point FFT over Hanning windows of 256 samples and an overlap of 64 samples) is shown in Figure 5.14.

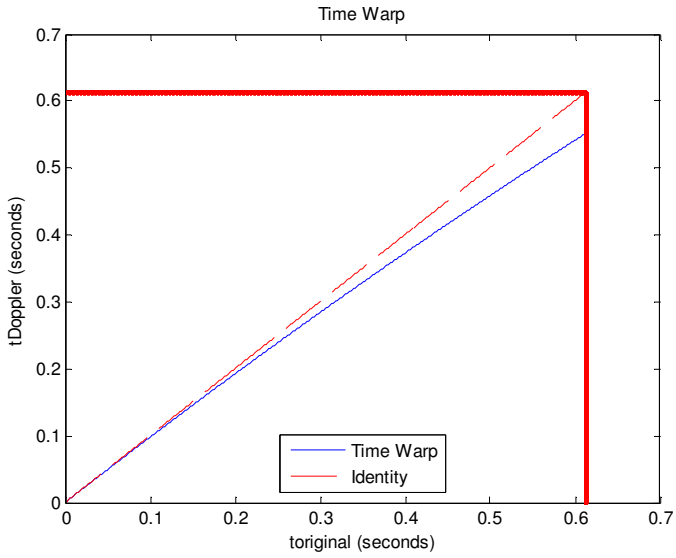

Figure 5.11. Time warp used to demonstrate the model.

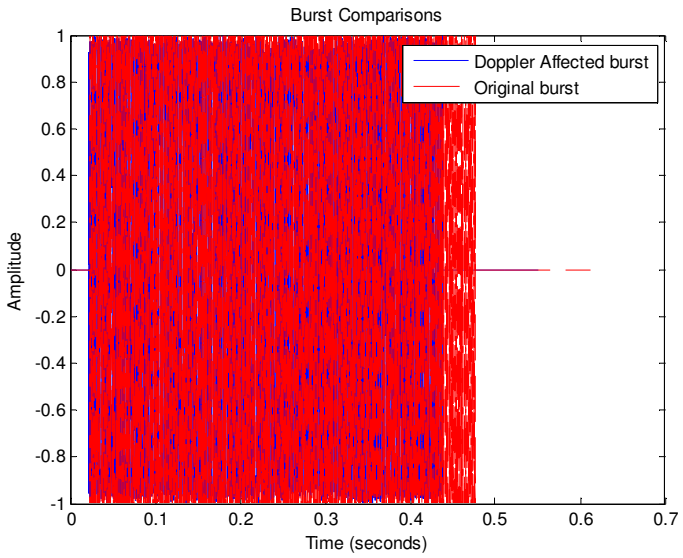

Figure 5.12. The Doppler Affected burst in the time domain.

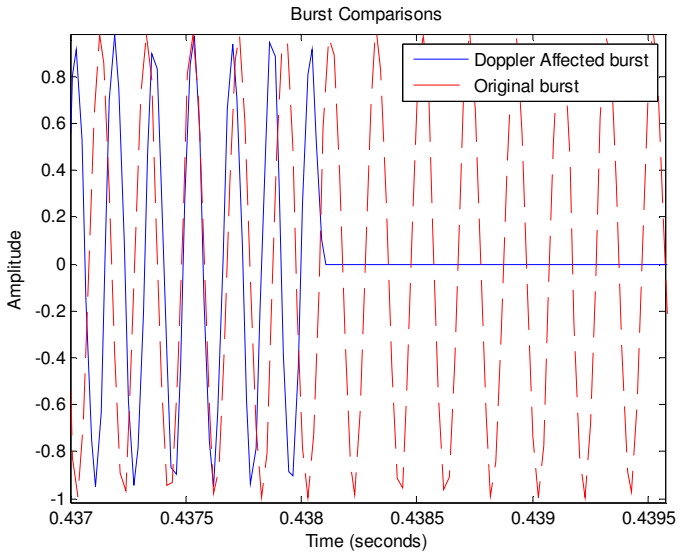

Figure 5.13. The Doppler Affected burst has contracted in time.

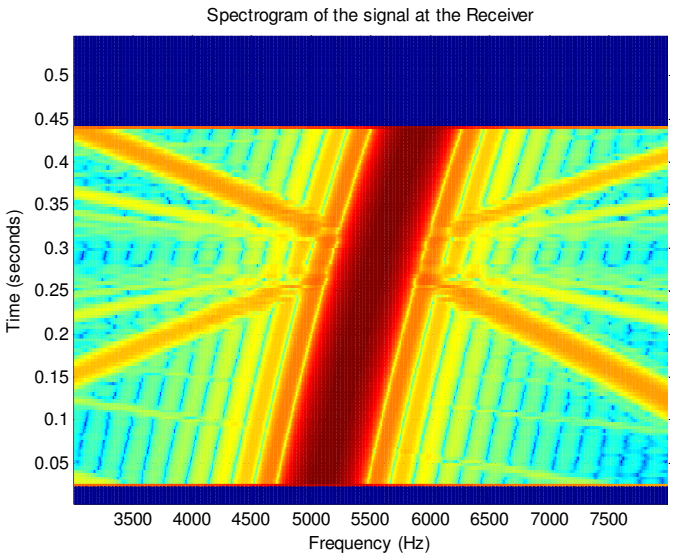

Figure 5.14. Spectrogram of the Doppler affected burst.

The more than linear change in frequency – due to β being quite large – can be observed from the spectrogram of the sinusoid at the receiver. Inverting the time warp involves mapping the Doppler time axis back to the original time axis using the same warp used to generate the Doppler effect. In the receiver context, this would mean using the estimated α and β parameters to generate an estimate of the time warp which presumably caused the observed Doppler effect (so as to facilitate the inverse mapping of the time axis). The spectrogram of the signal recovered by uniformly sampling the output of the inverse time warp is shown in Figure 5.15. Figures 5.16 and 5.17 show a comparison of the original and the recovered sinusoids in the time domain. Figure 5.16 shows a comparison of the entire burst while Figure 5.17 zooms in on the beginning and end of Figure 5.16. These illustrations show that the Doppler effect can be un-done quite efficiently if the α and β parameters can be estimated accurately based on the received burst. The next section describes the technique that can be used to estimate α and β

from the received burst. Observe that the case of pure expansion/contraction, discussed earlier in Section 5.2.1, can also be modeled using the method described in this section by setting $\beta = 0$.

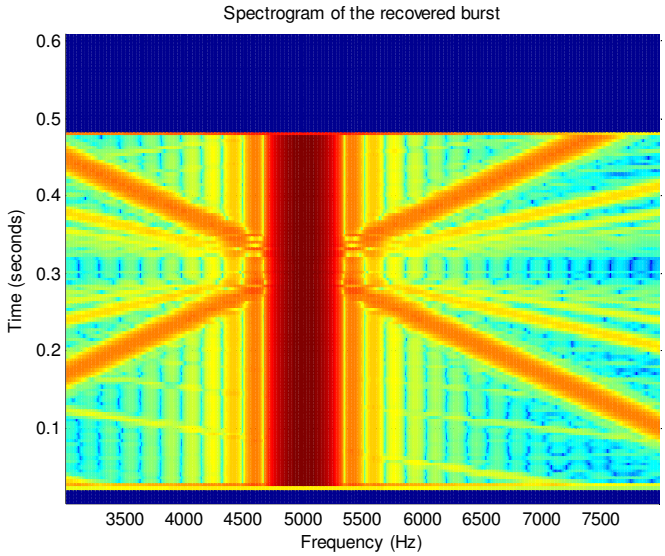

Figure 5.15. Spectrogram of the recovered sinusoid burst.

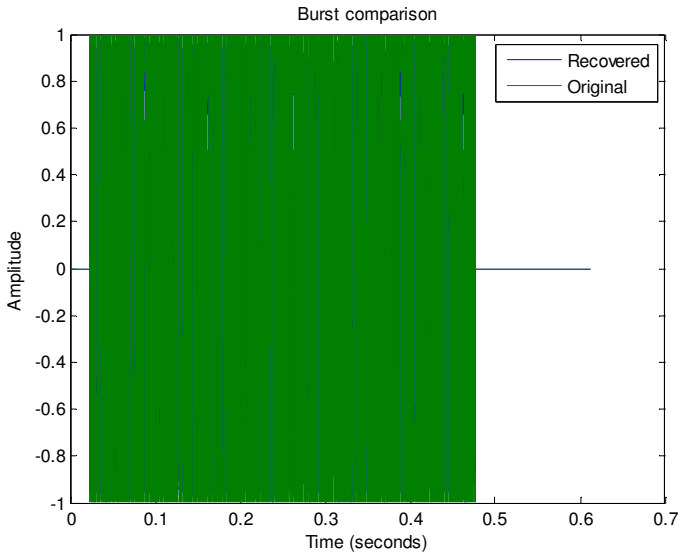

Figure 5.16. Comparison of the original and recovered burst.

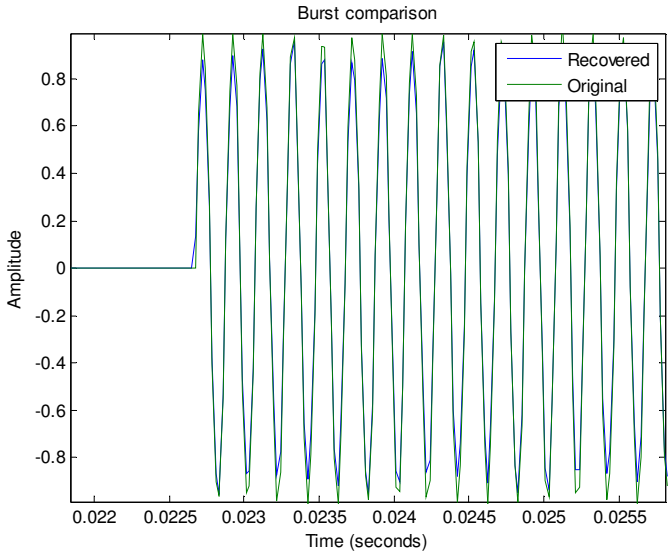

(a)

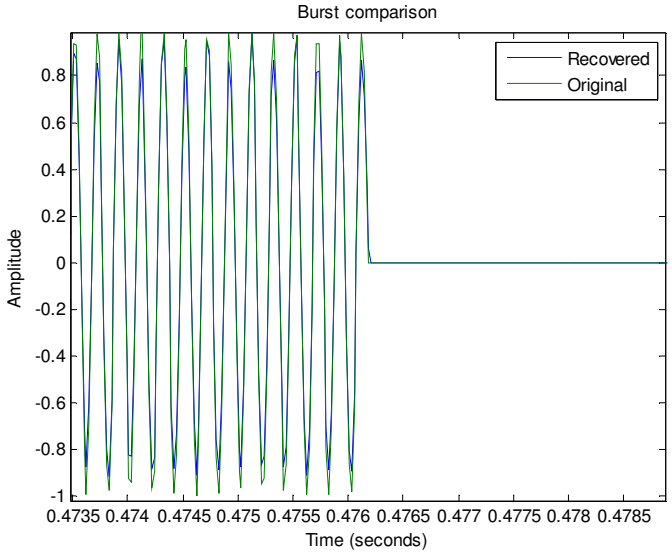

(b)

Figure 5.17 (a), (b). Comparison of the original and recovered burst (zoomed-in).

5.2.3 Estimating α and β

The Doppler correction in short involves inverting the effect of the time warp on the received burst. However, to accomplish this, a method to estimate α and β from the received burst has to be devised. Let us start by deriving a formula for how the period (and consequently frequency, being the reciprocal) of a sinusoid varies due to the time warp in (5.6), shown graphically in Figure 5.9. For the sake of simplicity let us analyze the effect the time warp has on a single period T of a sinusoid. The period of the sinusoid output from the warp can be expressed as:

$$\begin{aligned}\tilde{T} &= \{1+\alpha+\beta(t+T)\}(t+T)-(1+\alpha+\beta t)t \\ &= \{1+\alpha+\beta(t+T)\}T+\{1+\alpha+\beta(t+T)\}t-(1+\alpha+\beta t)t \\ &= (1+\alpha+\beta T)T+\beta Tt+(1+\alpha+\beta t)t+\beta Tt-(1+\alpha+\beta t)t \\ &= (1+\alpha+\beta T)T+2\beta Tt\end{aligned} \tag{5.8}$$

Equation (5.8) shows how the period of a sinusoid output from the warp varies with time. This equation can be used to solve for α and β by using two different time instants t_0 and t_1 at the beginning and end of the burst respectively. Let t_0 and t_1 map to $\tilde{t}_0$ and $\tilde{t}_1$ respectively in the Doppler affected time axis (as shown in Figure 5.9). Moreover, let us assume that $\tilde{T}_0$ and $\tilde{T}_1$ are the estimated periods of the sinusoid at $\tilde{t}_0$ and $\tilde{t}_1$ respectively. Substituting these parameters into (5.8) we find that:

$$\tilde{T}_0 = (1+\alpha+\beta T)T+2\beta Tt_0 \tag{5.9}$$

and

$$\tilde{T}_1 = (1+\alpha+\beta T)T+2\beta Tt_1 \tag{5.10}$$

We know that $t_1 = t_0 + T_b$, where T_b is the length of the transmitted packet. In practice however, T_b is the time duration from the middle of the window used for estimating the frequency of the pre-amble sinusoid, to the middle of the window used for estimating the frequency of the post-amble sinusoid. Substituting this expression for t_1 into (5.10) yields:

$$\tilde{T}_1 = (1+\alpha+\beta T)T + 2\beta T(t_0 + T_b) \tag{5.11}$$

From the equation of the warp in (5.6) an expression for t_0 can be derived as follows:

$$\begin{aligned} \tilde{t}_0 &= (1+\alpha)t_0 + \beta t_0^2 \\ t_0 &= \frac{-(1+\alpha) + \sqrt{(1+\alpha)^2 + 4\beta\tilde{t}_0}}{2\beta} \end{aligned} \tag{5.12}$$

Substituting (5.12) in (5.9) and (5.11) yields two equations:

$$\begin{aligned} \tilde{T}_0 &= (1+\alpha+\beta T)T + T\left\{\sqrt{(1+\alpha)^2 + 4\beta\tilde{t}_0} - (1+\alpha)\right\} \\ \tilde{T}_1 &= (1+\alpha+\beta T)T + T\left\{2\beta T_b + \sqrt{(1+\alpha)^2 + 4\beta\tilde{t}_0} - (1+\alpha)\right\} \end{aligned} \tag{5.13}$$

The only unknowns in the two equations in (5.13) are α and β, the other quantities can be estimated from the received burst. The two equations can be solved by using non-linear least squares optimization techniques. The MATLAB function *fsolve* was used to solve the two equations for α and β.

5.3 Wideband Doppler Model on an OFDM Burst

This section illustrates the results obtained when the wideband Doppler model described in Section 5.2.2 was used on an OFDM burst. To analyze the effect the Doppler warp can have on a

single OFDM symbol, let us first describe a single OFDM symbol (as explained earlier in Chapter 3) as:

$$s(t) = \mathrm{Re}\left\{\left[\sum_{k\in S_A} d[k]e^{j2\pi k\Delta ft} g(t)\right] e^{j2\pi f_c t}\right\} \tag{5.14}$$

The multipath UWA channel can be described (as in Chapter 3) by:

$$c(t,\tau) = \sum_p A_p(t)\delta(\tau - \tau_p(t)) \tag{5.15}$$

where $\tau_p(t) = \tau_p - (\alpha + \beta t)t$. The received signal in pass band can be written as:

$$\begin{aligned}\tilde{y}(t,\tau) &= s(t) * c(t,\tau) \\ &= \mathrm{Re}\left\{\sum_p A_p \left[\sum_{k\in S_A} d[k]e^{j2\pi k\Delta f\{(1+\alpha+\beta t)t-\tau_p\}} g\left\{(1+\alpha+\beta t)t - \tau_p\right\}\right] e^{j2\pi f_c\{(1+\alpha+\beta t)t-\tau_p\}}\right\} + \tilde{n}(t)\end{aligned} \tag{5.16}$$

We know that $t_{Doppler} = (1+\alpha+\beta t)t$. Substituting in (5.16) yields:

$$\tilde{y}(t) = \mathrm{Re}\left\{\sum_p A_p \left[\sum_{k\in S_A} d[k]e^{j2\pi k\Delta f(t_{Doppler}-\tau_p\}} g\left\{t_{Doppler} - \tau_p\right\}\right] e^{j2\pi f_c\left(t_{Doppler}-\tau_p\right)}\right\} + \tilde{n}(t) \tag{5.17}$$

Inverting the effect of the warp converts the time warp from $t_{Doppler}$ to estimates of the original time scale referred to as $\hat{t}$. Hence (5.17) becomes:

$$\tilde{s}(t) = \mathrm{Re}\left\{\sum_p A_p \left[\sum_{k\in S_A} d[k]e^{j2\pi k\Delta f(\hat{t}-\tau_p\}} g\left\{\hat{t} - \tau_p\right\}\right] e^{j2\pi f_c\left(\hat{t}-\tau_p\right)}\right\} + \tilde{n}(t) \tag{5.18}$$

The OFDM symbol thus recovered has to be de-scaled and de-rotated by equalization before the received bits can be extracted. Note that this derivation is done in the pass-band, and the result is that no CFO correction is involved.

The Doppler correction technique utilizes two sinusoids, with known period, one at the beginning and the other at the end of each OFDM symbol, to solve the non-linear simultaneous equations in (5.13) for α and β. The number of symbols to use between the sinusoids is a design trade-off which depends on the expected rate of change in Doppler rate. If the Doppler rate is not expected to change rapidly, multiple OFDM symbols can be placed between the two sinusoids. However, if the Doppler rate is expected to change rapidly (over one symbol time), the estimation facilitating sinusoids may need to be placed as often as at the front and back ends of each symbol. The new packet structure proposed for transmission is shown in Figure 5.18.

Figure 5.18. The Doppler estimation facilitating packet structure.

The chirp signals are used to perform time synchronization as explained in Chapter 4. For the sake of simplicity we analyze the effect that the time warp, generated with $\alpha = -0.001$ and $\beta = -0.0193$ shown in Figure 5.19, has on a single OFDM burst (shown in Figure 5.20). The values of α and β were selected so as to generate Doppler shifts/rate which would closely resemble the values seen in practice when the relative velocity between the transceivers is about 15 m/s.

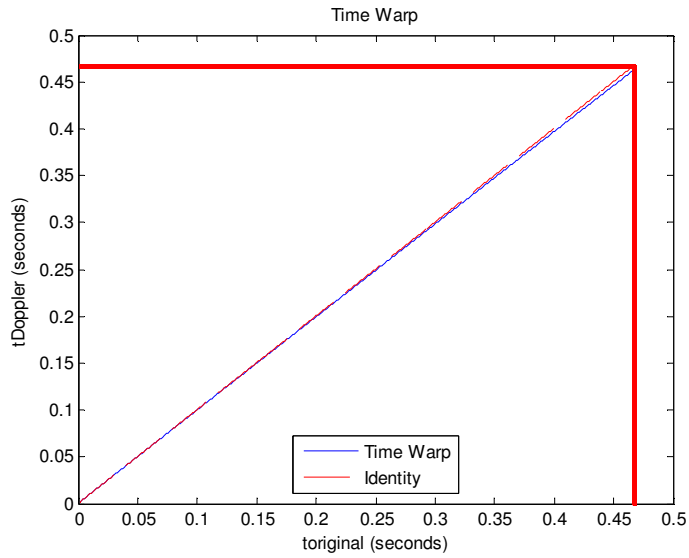

Figure 5.19. Doppler time warp generated with $\alpha = -0.001$ and $\beta = -0.0193$.

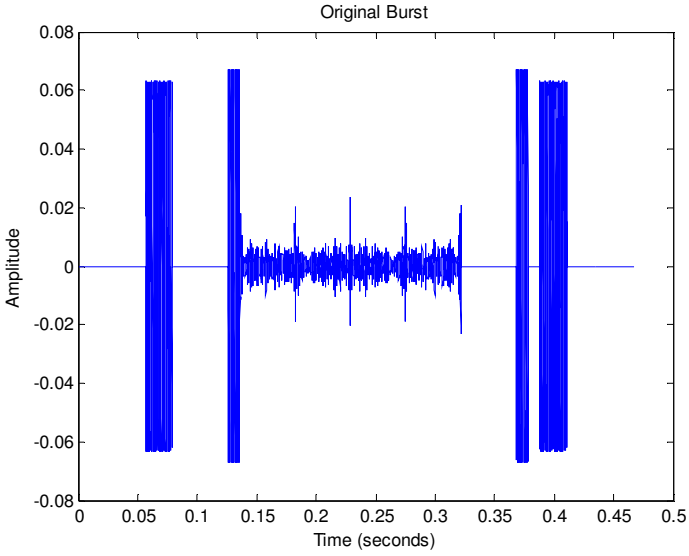

Figure 5.20. The OFDM Burst.

Figure 5.21 shows the spectrogram of the original burst. Several samples of zeros were added to the beginning and end of the burst, so as to make the actual burst occur somewhere in the middle

of the warp. The chirp signals and the 5 kHz sinusoids at each end of the OFDM symbol can be observed in the spectrogram.

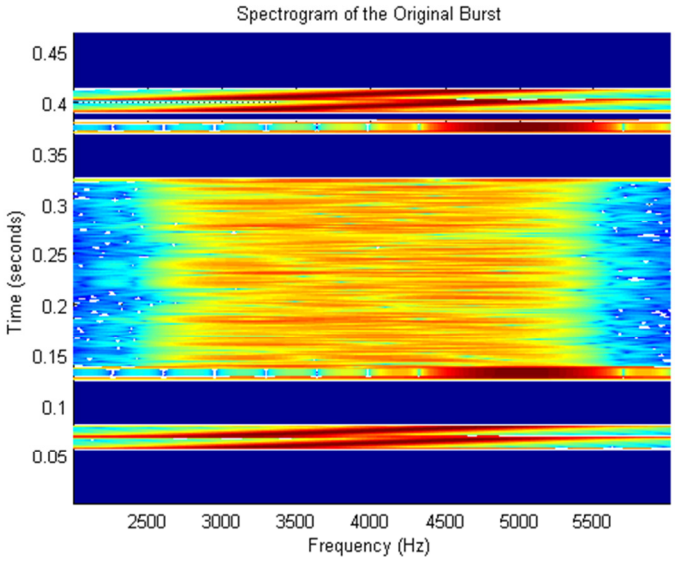

Figure 5.21. Spectrogram of the burst.

The received burst subject to the Doppler effect was obtained by passing the original burst through the time warp followed by uniformly sampling the output of the warp. The chirp signals in the received burst were used to perform time synchronization using the matched filter method. Figures 5.22 and 5.23 provide a comparison of the Doppler affected packet with the original packet. Figure 5.22 shows the sinusoid at the beginning of the packet and Figure 5.23 shows the sinusoid at the end of the packet. The Doppler affected packet seems to line up perfectly with the original packet at the beginning of the packet, but the former contracts with time as is evident from Figure 5.23. This behavior corresponds to the nature of the Doppler time warp used (Figure 5.19).

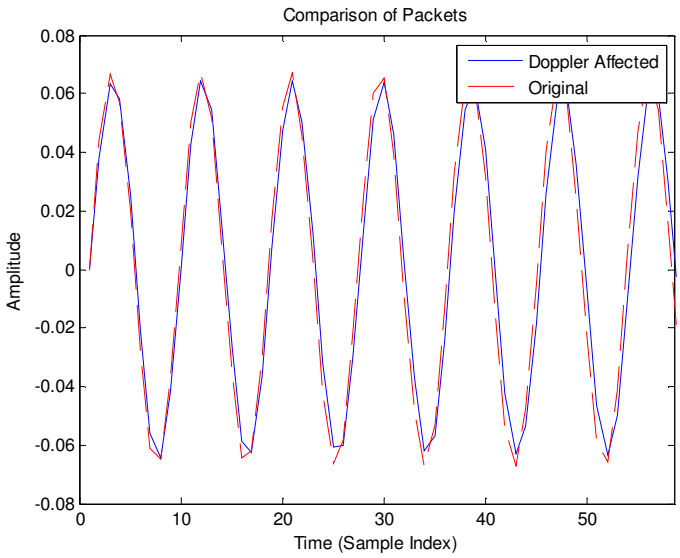

Figure 5.22. Comparison of the pre-amble sinusoids.

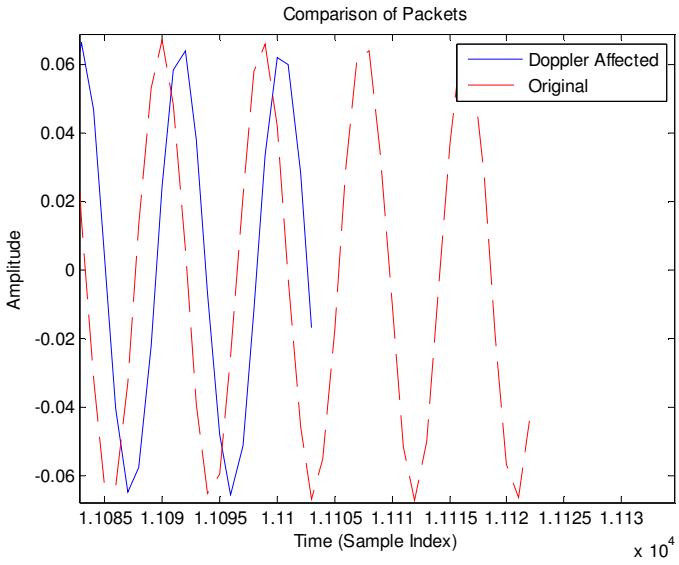

Figure 5.23. Comparison of the post-amble sinusoids.

Once synchronization in time was attained, the sinusoids were used to estimate α and β using (5.13). Figure 5.24 shows the magnitude spectrum of the pre-amble and post-amble sinusoids observed over a Hanning window of 256 samples.

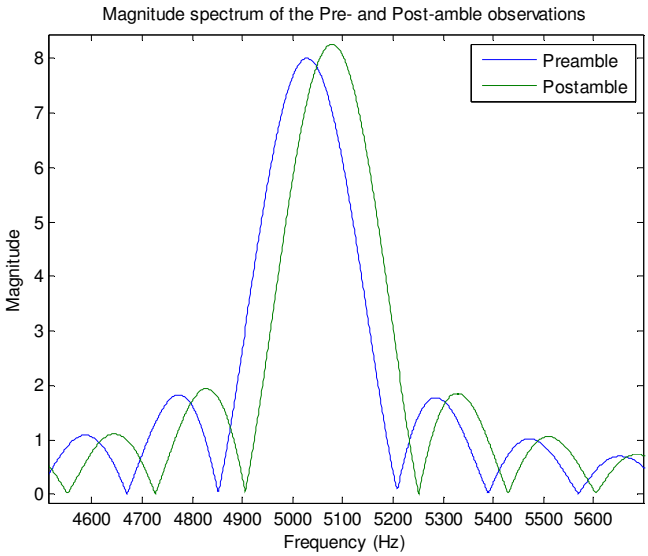

Figure 5.24. Magnitude spectrum of the pre- and post-amble observations.

The frequency of the pre-amble and post-amble sinusoids, estimated by looking for the peak in the magnitude spectrum, was equal to 5028.7 Hz and 5077.7 Hz respectively (Doppler shifts of about 29 and 78 Hz respectively). The time instant at which the frequency estimate of the pre-amble sinusoid was made, $\tilde{t}_0$, was found to be 0.1281 seconds. Using these parameters, α and β were estimated to be -7.6411 x 10^{-4} and -0.0194 respectively. Note that $\tilde{t}_1$ - which was found to be 0.3717 seconds - is not explicitly used in the estimation process; this is the result of using the assumed a priori knowledge that $t_1 = t_0 + T_b$, which connects $\tilde{t}_1$ and $\tilde{t}_0$.

The change in the frequency of the sinusoid over time can be found by substituting the estimated value of α and β in (5.8). If f_{tx} is the frequency of the sinusoid used and $\hat{f}_{rx}(t)$ the estimated frequency of the sinusoid, the relative velocity estimate can be calculated as:

$$\hat{v}(t) = \left(\frac{\hat{f}_{rx}(t) - f_{tx}}{f_{tx}} \right) c \tag{5.14}$$

where c is the speed of sound in the medium.

The change in frequency and relative velocity over the duration of the burst - according to the estimated model - is shown in Figure 5.25.

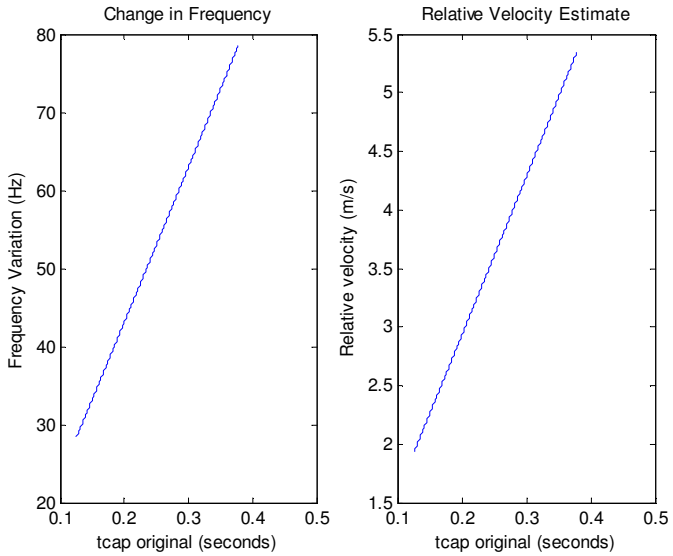

Figure 5.25. Model estimate for change in relative velocity and frequency over the duration of the burst.

The time warp generated (over the time interval during which the burst exists) at the receiver using the estimated value of α and β is shown in Figure 5.26.

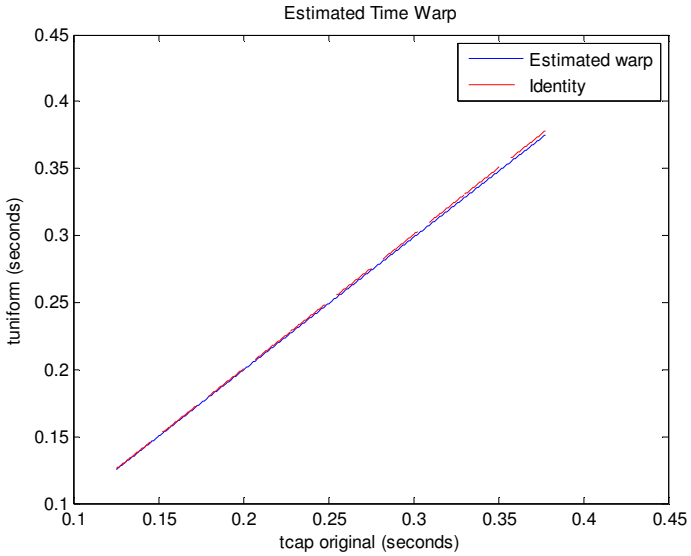

Figure 5.26. Estimated time warp.

Figures 5.27 and 5.28 compare the recovered packet (obtained by inverse mapping over the estimated warp followed by uniform sampling) to the original packet, and Figure 5.29 compares the transmitted and received BPSK symbols.

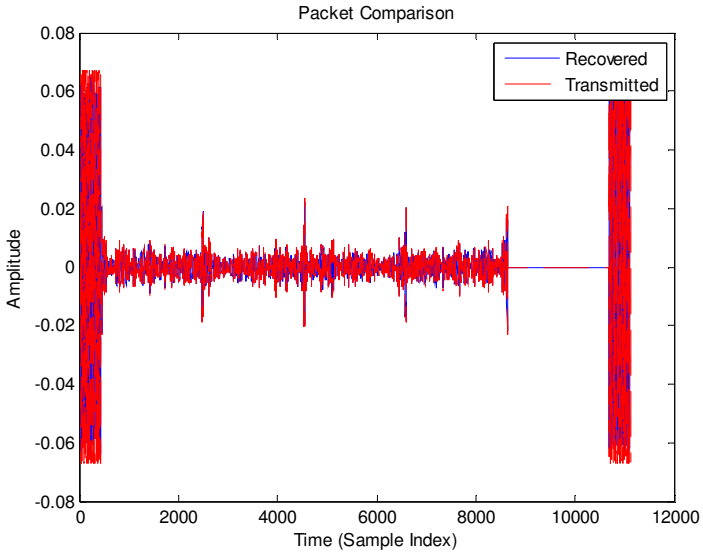

Figure 5.27. Comparison of the recovered and original packet.

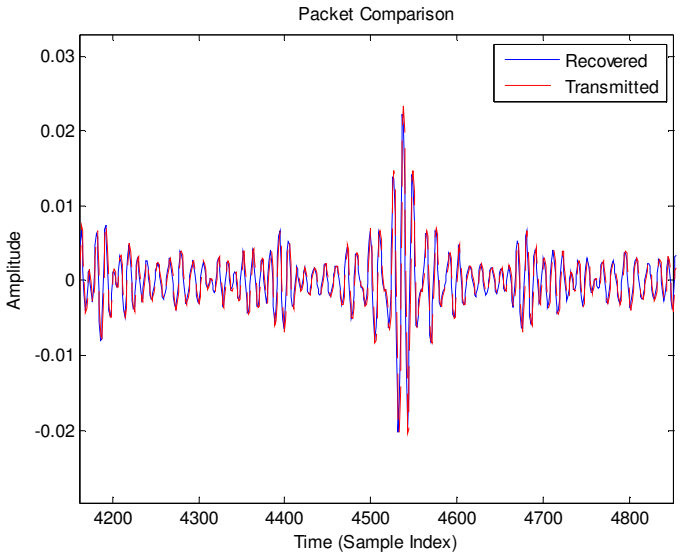

Figure 5.28. Comparison of the recovered and original packet (zoomed-in).

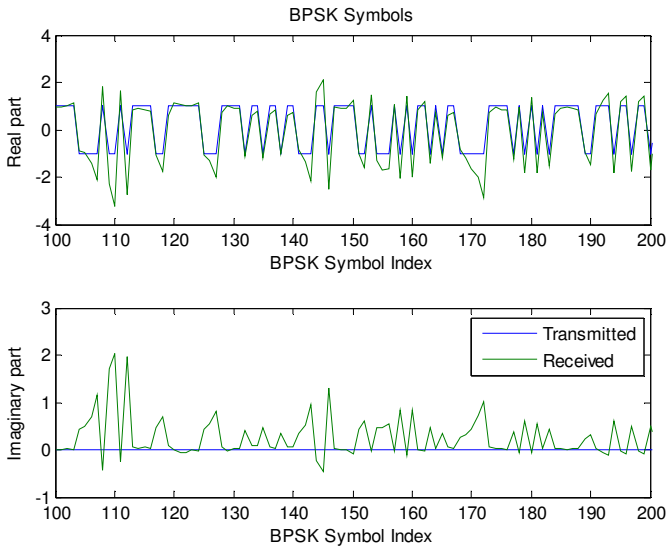

Figure 5.29. Comparison of the transmitted and received BPSK symbols.

As is evident from the results shown above, the time warp based method can effectively emulate the Doppler effect seen in wideband signals. Moreover the estimation and correction methodology used worked sufficiently well to be able to recover the transmitted bits without any error. This example illustrates that the proposed method works in principle. The next step is to apply this technique to the over-the-air experiment and analyze the results to see whether improvement is realized over the pure contraction-expansion method.

5.4 Over-the-air Experiment

The over-the-air experiment was performed using four packets, each with the structure shown in Figure 5.18. The OFDM symbols were generated using the exact same specifications used in Chapter 4. Section 5.4.1 presents the results obtained when the microphone motion was radial

and Section 5.4.2 presents the results obtained when the microphone motion was circular with respect to the pivot.

5.4.1 Radial Movement

Figure 5.30 shows the received burst (obtained by moving the microphone radially while the burst transmission was in progress) in the time domain. The four packets can be distinctly seen in the figure.

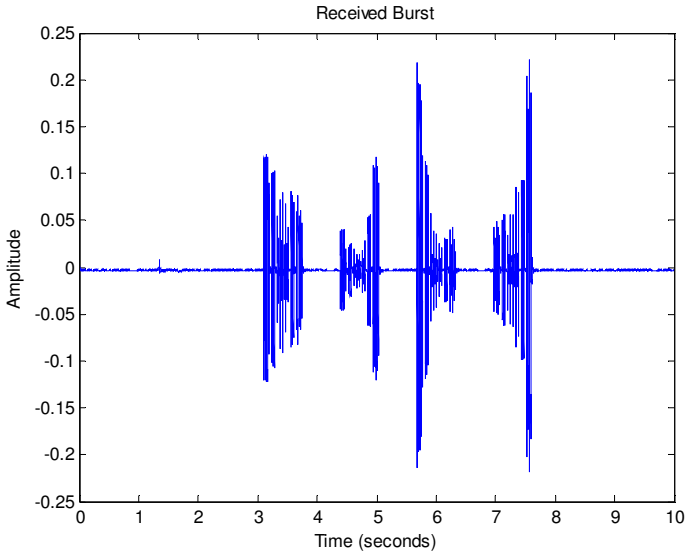

Figure 5.30. Received burst.

The received burst was synchronized in time so as to isolate each packet from the others. This was followed by estimating the frequency of the sinusoids in each packet to get estimates for α and β. Figures 5.31 and 5.32 show the magnitude spectrum of both the pre-amble and post-

amble observations of the first and third packets respectively, estimated over a Hanning window of 512 samples.

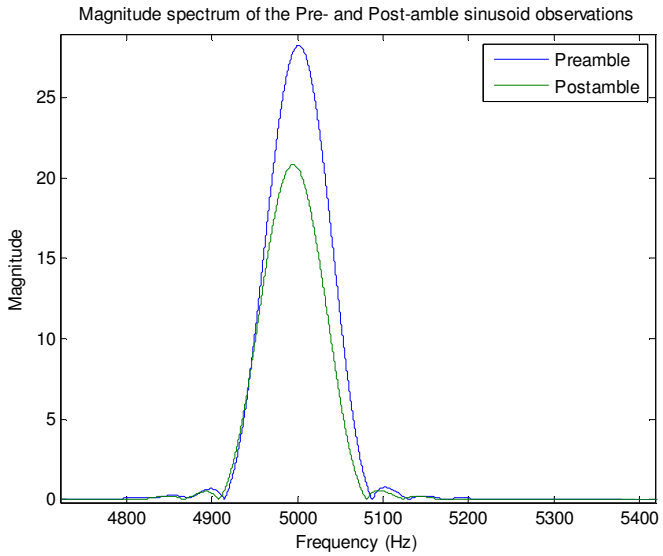

Figure 5.31. Magnitude spectrum of the pre- and post-amble observations in packet 1.

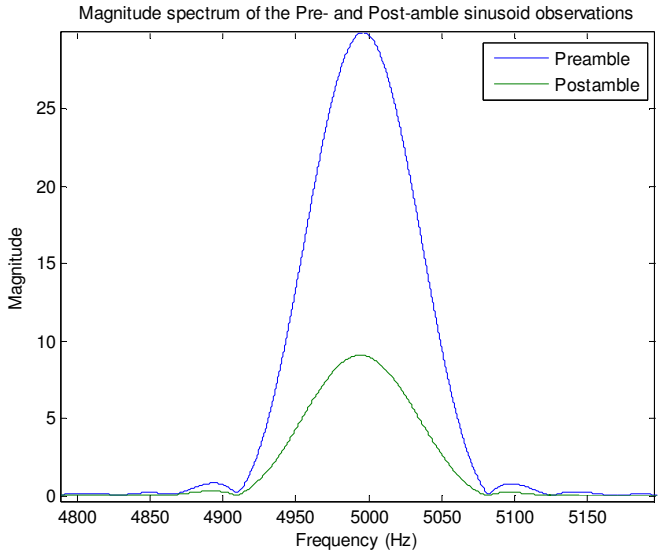

Figure 5.32. Magnitude spectrum of the pre- and post-amble observations in packet 3.

Table 5-1 provides a summary of the α and β estimated for each packet, and the values of the parameters used to solve (5.13) for α and β.

Table 5-1. Summary of Parameters.

Packet #	α	β (sec^{-1})	$\tilde{T}_0$ (msec)	$\tilde{T}_1$ (msec)	$\tilde{t}_1$ (sec)
1	-0.0125	0.00185	0.1999	0.2002	3.2607
2	-0.000431	-0.000487	0.1998	0.1998	4.5485
3	-0.00490	0.000489	0.2002	0.2002	5.8352
4	-0.00777	0.000487	0.1998	0.1999	7.1228

Figures 5.33 and 5.34 show the variation of the 5 kHz frequency sinusoid and relative velocity estimates over the duration of packets 1 and 3 respectively.

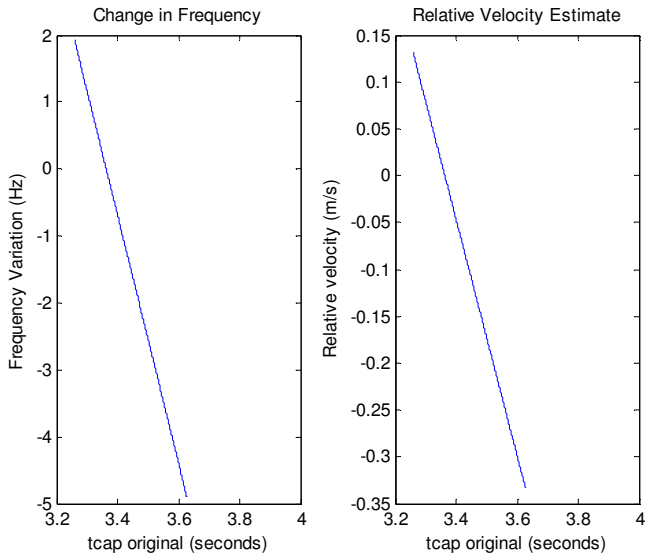

Figure 5.33. Model estimate for change in frequency and relative velocity estimate over packet 1.

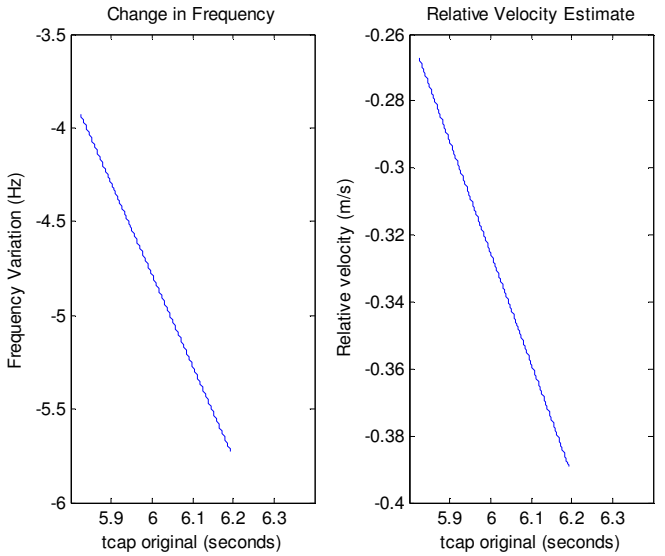

Figure 5.34. Model estimate for change in frequency and relative velocity estimate over packet 3.

Observe that the sign of the frequency shift as well as the relative velocity changed within the first packet. This suggests that the direction of the microphone motion has changed while the transmission of the first packet was in progress.

Figures 5.35 and 5.36 illustrate the time warp that were generated (estimated) over the duration of the first and third packets respectively using the estimated values of α and β.

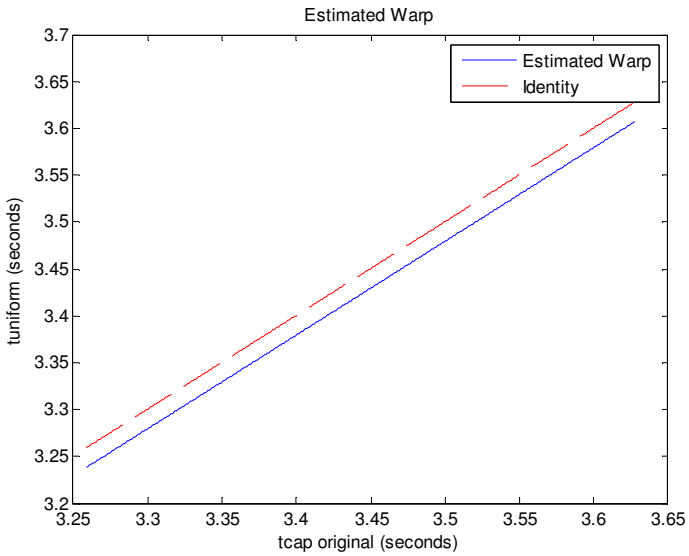

Figure 5.35. Estimated time warp for packet 1.

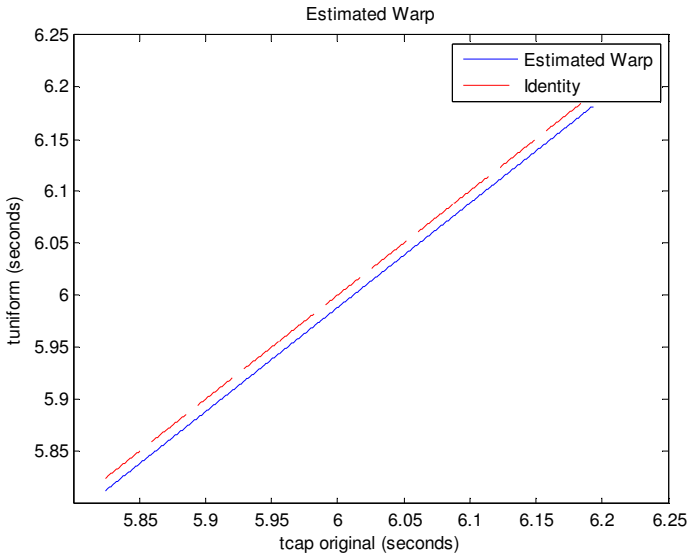

Figure 5.36. Estimated time warp for packet 3.

Figures 5.37 and 5.38 show the frequency response of the channel estimated using the symbols in packets 1 and 3 respectively.

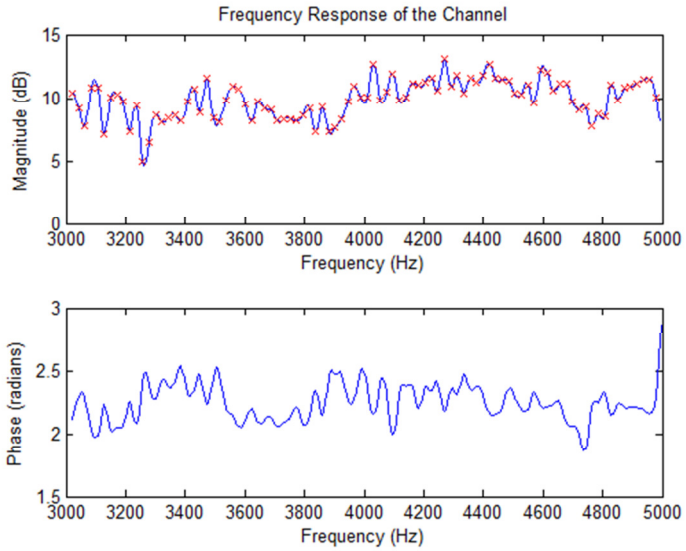

Figure 5.37. Frequency response estimate of the channel using the symbol in packet 1.

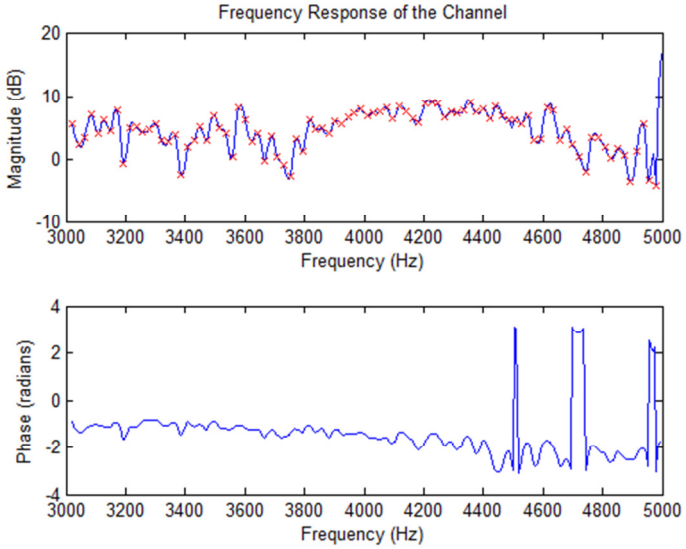

Figure 5.38. Frequency response estimate of the channel using the symbol in packet 3.

Figures 5.37 and 5.38 illustrate that the channel under consideration is frequency selective in nature and that it varies substantially from one packet to another. Figures 5.39 and 5.40 show a part of the BPSK symbols recovered from the first and third packets respectively.

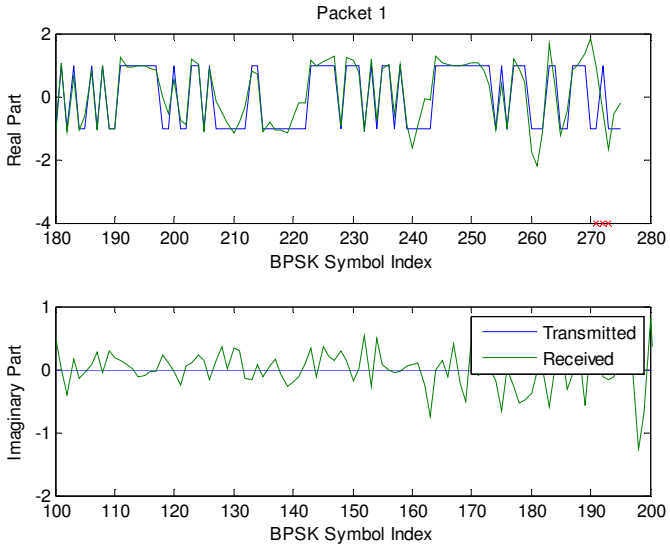

Figure 5.39. Transmitted and received BPSK symbols for Packet 1.

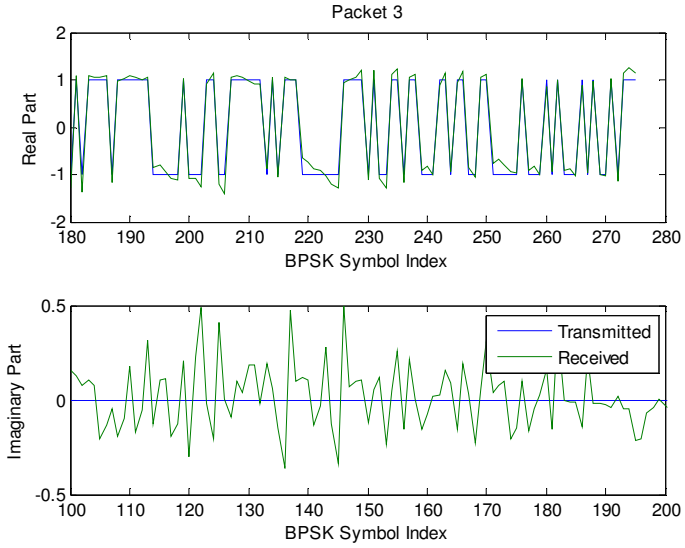

Figure 5.40. Transmitted and received BPSK symbols for Packet 3.

The 'x' in Figure 5.39 indicates that three out of the one thousand symbols recovered were in error. Figure 5.41 shows the symbols in Packet 3 detected using the expansion/contraction method discussed in Chapter 4, and Table 5-2 provides a summary of the Doppler shift, relative velocity, and frequency shift estimates obtained from the expansion/contraction method. Table 5-3 compares the BER experienced by using the two different Doppler correction techniques.

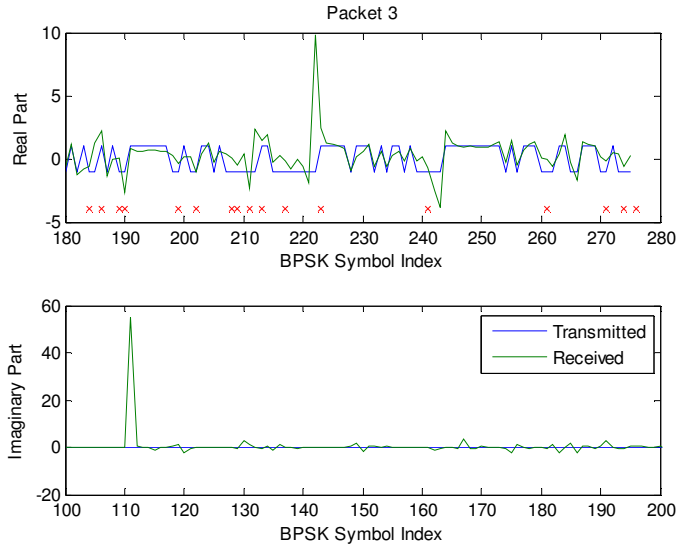

Figure 5.41. Packet 3 obtained by using the expansion/contraction Doppler correction technique.

Table 5-2. Estimates obtained from the expansion/contraction method.

Packet #	a (Doppler shift)	Velocity (m/s)	Frequency Shift (Hz) at 5 kHz
1	-0.00080	-0.2722	-4.003
2	0.0012	0.4187	6.158
3	-0.0019	-0.6490	-9.544
4	0.00080	0.2722	4.003

Table 5-3. BER comparison (for a total of 1104 bits transmitted; 276 bits per packet) for the two Doppler correction techniques under consideration, applied to the same received burst.

Packet #	BER with Expansion/Contraction	BER with Time warp based method
1	0.351	0.011
2	0.047	0.000
3	0.304	0.000
4	0.341	0.000

The results in Table 5-3 are based on a single burst, consisting of 4 packets, with 276 data bits per packet. Each BER value given is thus based on 276 bits. These results illustrate the variability of the environment, even within the time span of a single burst, and are illustrative of a typical execution of this experiment with manual microphone movement. Without an accurate replication of the microphone movement, statistical averaging over a large number of runs would produce an average BER but not clearly illustrate the BER variation across packets.

The major improvement in BER obtained by using the time warp based Doppler correction technique stems from the fact that the relative velocity between the speaker and the microphone actually changed within a packet. While the expansion/contraction technique only accounts for the average Doppler shift over a packet, the time warp based correction method takes the Doppler rate into account as well. This can be observed in Figures 5.42 shown below. The

average Doppler shift estimated using the uniform expansion/contraction based method does not accurately correspond to the average of the linear change estimated using the time warp based method. However, bear in mind that the time warp based method was not designed to correct for the average Doppler shift; rather it was designed to model expansion/contraction which occurred in a non-uniform manner.

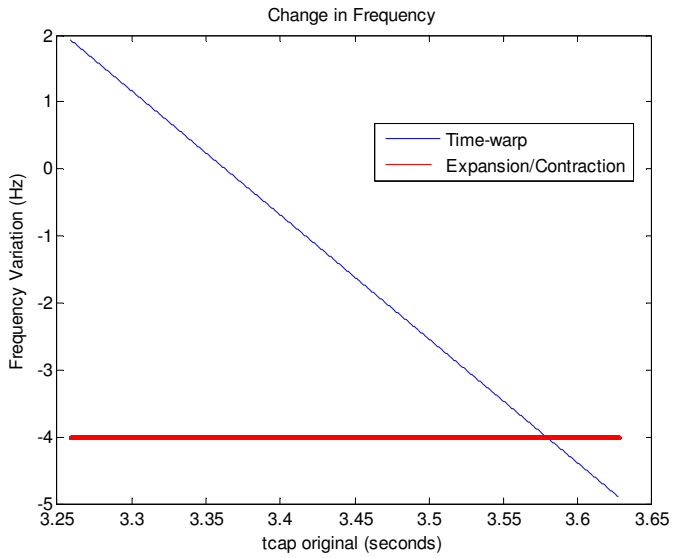

(a)

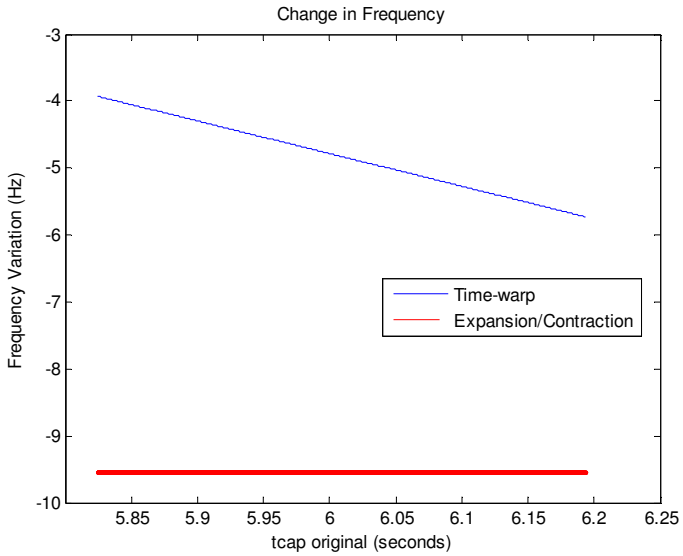

(b)

Figure 5.42. Model estimate of the frequency variation over (a) packet 1 (b) packet 3.

A comparison of the time warps estimated, for packet 1, using the two Doppler correction techniques is shown in Figure 5.43. Even though both warps look almost like a straight line, the

effect of β can be clearly seen by looking at the difference between the warps corresponding to packet 1.

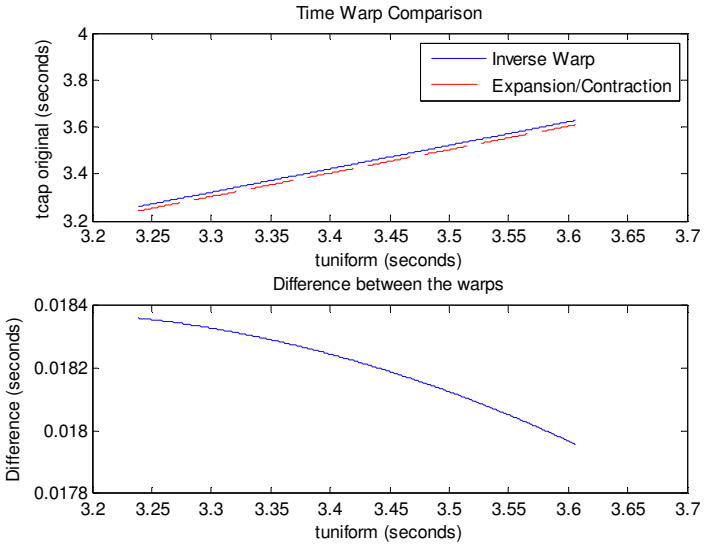

(a)

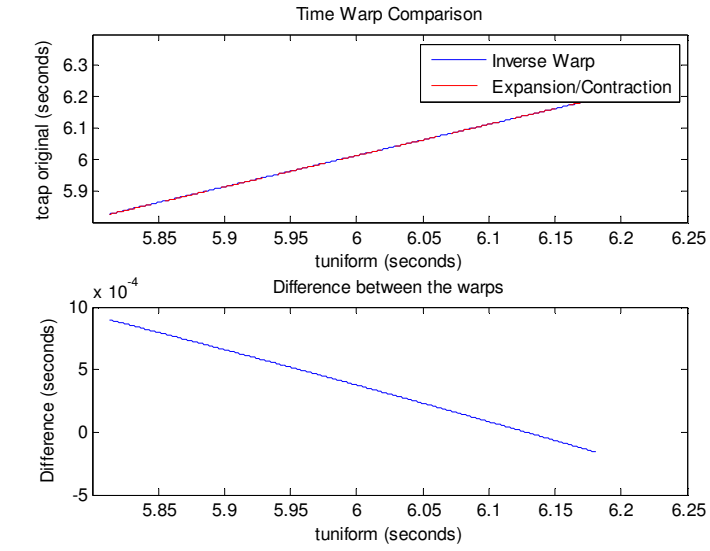

(b)

Figure 5.43. Comparison of the time warps (a) Packet 1 (b) Packet 3.

5.4.2 Circular Movement

This section describes the results obtained by moving the microphone along the arc of a semi-circle while the transmission of the burst (same as that used in the previous section) was in progress. It was observed that the performance of several portions of the receiver degraded due to the circular motion. The time synchronization performed using the matched filter approach did not produce distinct correlation peaks for all the packets. Figures 5.44 (a) and (b) show the output of the correlation for the packets which could not be synchronized.

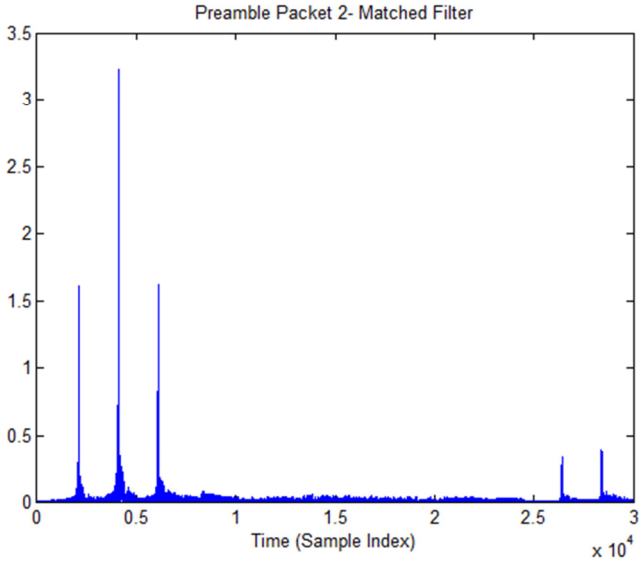

(a)

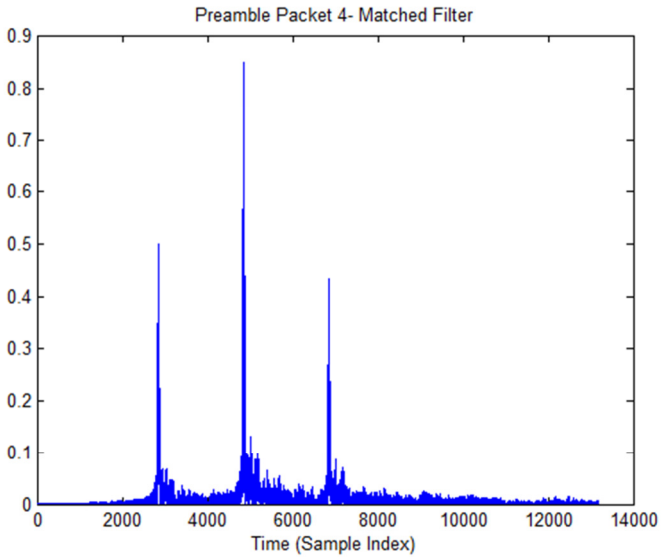

(b)

Figure 5.44. Output of the matched filter for packets (a) 2 and (b) 4.

The packets which could not be synchronized using the matched filter correlator were synchronized manually by observing the received burst in the time domain. The estimated values for α and β for each packet are shown in Table 5-4, and a comparison of the BERs obtained by applying the two Doppler correction techniques under consideration is shown in Table 5-5.

Table 5-4. Estimated values of α and β for each packet.

Packet #	α	β (sec^{-1})
1	0.0041	-0.00072
2	-0.0170	0.0018
3	0.0190	-0.0016
4	0.0290	-0.0020

Table 5-5. BER Comparison based on 276 bits transmitted per packet.

Packet #	Time warp	Expansion/Contraction
1	0.044	0.145
2	0.138	0.417
3	0.145	0.254
4	0.062	0.449

Even though the BERs observed in this case are worse than the BERs seen for the case of radial motion, the improvement that is obtained by using the time warp based method is distinctly observable.

In summary this chapter introduced a time-warp based Doppler correction technique which, unlike the uniform expansion/contraction based technique, corrects for within-packet variation of

the relative Doppler shift. These results support that improvement is obtained over the simple expansion/contraction approach, and suggests further improvement maybe realized by even higher order Doppler modeling.

6 Conclusion and Future Work

In this work two different Doppler correction techniques, both based on modeling of the wideband Doppler effect as a change in the time scale, were discussed and compared. In the first method the average expansion/contraction over a packet was corrected for by resampling the received packet so as to make its length equal to that of the transmitted packet. The second method involved using a time-warp to model Doppler shifts which varied within a packet, and a correction method which aims to invert the effect of the time warp. Both techniques were shown to work in MATLAB based simulations as well as in over-the-air experiments. Although the resampling based correction technique worked pretty well when the microphone motion was relatively slow and uniform, the time warp based correction technique worked better even for much faster and more varied kinds of motion. The better over-the-air channel results, in terms of lower bit-error-rates with OFDM packet transmission, obtained from the time warp based correction method, provide sufficient indication to hypothesize that the time-warp based Doppler correction method would most likely work better than the resampling based method in an UWA channel, especially when the transceivers are attached to accelerating platforms.

The results presented in this work were obtained under relatively low-noise conditions. The received signal had a SNR on the order of 40 dB. The next step in this research would be to analyze the performance of the proposed Doppler correction technique in the presence of non-negligible noise (possibly modeled as non-Gaussian). This work modeled the time warp using two parameters namely α and β. Future work could extend this idea to model the time warp using a larger number of parameters, and analyze the optimal number of parameters to be used to

model the practically observable time warp most accurately. Future work could also involve implementing the OFDM receiver (with the time warp based Doppler correction method built in) on hardware so as to be able to conduct experiments in an underwater channel. Performing such experiments would require the usage of two transducers (one at the transmit and one at the receive end) connected to the hardware which implements the transceiver. A key assumption that was made while developing the Doppler correction model was that the Doppler rate was the same for each multipath component. This assumption need not be true always, and the performance of the receiver could degrade significantly when this assumption does not hold. Hence future work could also involve using MIMO based techniques to correct for Doppler rates which are different for different multipath components.

7 Bibliography

[1] A. Goldsmith, “Wireless Communications” *Cambridge: Cambridge University Press*, 2005.

[2] Y. S. Cho, “MIMO-OFDM Wireless Communication with MATLAB”, Singapore:IEEE Press, 2010.

[3] S. Weinstein and P. Ebert, "Data Transmission by Frequency-Division Multiplexing Using the Discrete Fourier Transform," *IEEE Transactions on Communication Technology,* , Vol. 19, No. 5, pp. 628-634, October 1971.

[4] A. Peled and A. Ruiz, “Frequency domain data transmission using reduced computational complexity algorithms", *Proc. of the IEEE Int. Conf. Acoustics, Speech and Signal Processing*, Denver, CO, pp. 964-967, 1980.

[5] B. Muquet, Z. Wang, and G. Giannakis, "Cyclic prefix or zero padding for wireless multicarrier transmissions?", *IEEE Trans. Commun.*, Vol. 50, No. 12, pp. 2136-2148, Dec. 2002.

[6] R. Van Nee and R. Prasad, “OFDM for Wireless Multimedia Communications”*, Artech House Publishers, 2000.*

[7] H. Sari, G. Karam, and I. Jeanclaude, “Transmission Techniques for digital terrestial TV broadcasting”, *IEEE Communications Magazine*, Vol. 33, No. 2, pp. 100-109, February 1995.

[8] T. Pollet, M. van Bladel, and M. Moeneclaey, “BER Sensitivity of OFDM Systems to Carrier Frequency Offset and Wiener Phase Noise”, *IEEE Trans. on Comm.*, Vol. 43, No. 2/3/4, pp.191-193, Feb.-Apr. 1995.

[9] J. Heiskala and J. Terry, “OFDM Wireless LANS: A Theoretical and Practical Guide”*, Sams Publishers, 2001.*

[10] T. M. Schmidl and D. C. Cox, "Low-overhead, low-complexity [burst] synchronization for OFDM," *IEEE International Conference on Communications, ICC 96, Conference Record, Converging Technologies for Tomorrow's Applications,* , Vol. 3, pp. 1301-1306, 23-27 Jun 1996.

[11] H. Minn, M. Zeng, and V. K. Bhargava, "On timing offset estimation for OFDM systems." , *IEEE Trans. Commun.*, Vol. 4, No. 5, pp. 242–244, 2000.

[12] J.-J. van de Beek, M. Sandell, M. Isaksson, and P. Ola Borjesson, "Low-complex frame synchronization in OFDM systems," *Fourth IEEE International Conference on Universal Personal Communications,* pp. 982-986, 6-10 Nov 1995.

[13] K. Taura, M. Tsujishta, and M. Takeda, "A digital audio broadcasting (DAB) receiver", *IEEE Trans. Consumer Electronics*, Vol. 42, No. 3, pp. 322–326, 1996.

[14] M. Hsieh and C. Wei, "A Low-Complexity Frame Synchronization and Frequency Offset Compensation Scheme for OFDM Systems over Fading Channels," *in IEEE Transactions on Vehicular Technology*, Vol. 48, No. 5, September 1999.

[15] C. Tellambura, "Computation of the Continuous–Time PAR of an OFDM Signal with BPSK Subcarriers," *IEEE Commun. Lett.*, Vol. 5, No. 5, pp. 185–87, May 2001.

[16] X. Li and L. J. Cimini, Jr., "Effect of Clipping and Filtering on the Performance of OFDM," *IEEE Commun. Lett.*, Vol. 2, No. 5, pp. 131– 33, May 1998.

[17] R. van Nee and A. de Wild, "Reducing the peak-to-average power ratio of OFDM," *48th IEEE Vehicular Technology Conference* (VTC 98), Vol. 3, pp. 2072-2076, 18-21 May 1998.

[18] A. E. Jones, T. A. Wilkinson, and S. K. Barton, "Block Coding Scheme for Reduction of Peak to Mean Envelope Power Ratio of Multicarrier Transmission Scheme," *Elect. Lett.*, Vol. 30, No. 22, pp. 2098–99, Dec. 1994.

[19] A. E. Jones and T. A. Wilkinson, “Combined Coding for Error Control and Increased Robustness to System Nonlinearities in OFDM,” *Proc. IEEE VTC '96*, Atlanta, GA, pp. 904–08, Apr.–May 1996.

[20] S. H. Müller and J. B. Huber, “OFDM with Reduced Peak–to–Average Power Ratio by Optimum Combination of Partial Transmit Sequences,” *Elect. Lett.*, Vol. 33, No. 5, pp. 368–69, Feb. 1997.

[21] R. W. Bäuml, R. F. H. Fisher, and J. B. Huber, “Reducing the Peak-to-Average Power Ratio of Multicarrier Modulation by Selected Mapping,” *Elect. Lett.*, Vol. 32, No. 22, pp. 2056–57, Oct. 1996.

[22] J. Tellado, “Multicarrier Modulation with Low Par: Applications to DSL and Wireless.” , Boston, Mass: *Kluwer Academic Publishers,* 2000.

[23] R. Coates, Underwater Acoustic Systems, New York: Wiley, 1989.

[24] M. Stojanovic, "Recent advances in high-speed underwater acoustic communications" *IEEE Journal of Oceanic Engineering,* Vol. 21, No. 2, pp. 125-136, Apr 1996.

[25] M. Stojanovic and J. Presig, ”Underwater Acoustic Communication Channels: Propagation Models and Statistical Characterization,” IEEE Communications Magazine, pp. 84-89, January 2009.

[26] A. F. Harris III and M. Zorzi, “Modeling the Underwater Acoustic Channel in ns2”, NSTools '07, Nantes, France, October 22, 2007.

[27] P. King, R. Venkatesan, and C. Li, “An Improved Communications Model for Underwater Sensor Networks” IEEE "GLOBECOM" 2008, pp. 1-6, Nov. 30 2008-Dec. 4 2008.

[28] X. Che and I. Wells, “A Static Multihop Underwater Wireless Sensor Network Using RF Electromagnetic Communications,” *29 IEEE International Conference on distributed computing system workshop*, Swansea metropolitan university UK, pp. 460-463, 2009.

[29] P. C. Etter, Underwater Acoustic Modeling: Principle, Techniques And Applications. Elsevier Science Publishers, 1991.

[30] M. C. Domingo and R. Prior, Energy Analysis Of Routing Protocol For Underwater Wireless Sensor Networks, Computer Communications, Vol. 31, Issue 6, Pages 1227-1238, 18 April 2008.

[31] L. Liu, S. Zhou, and J. Cui, ”Prospects and Problems of Wireless Communication for Underwater Sensor Networks”, Wiley WCMC Special Issue on Underwater Sensor Networks.

[32] R. J. Urick, Principles of Underwater Sound, New York: McGraw-Hill, 1983.

[33] S. A. Kassam**,** "Signal detection in non-Gaussian noise," New York: Springer-Verlag, 1988.

[34] M. Chitre, J. Potter, and O. S. Heng, "Underwater acoustic channel characterisation for medium-range shallow water communications," *OCEANS '04. MTTS/IEEE TECHNO-OCEAN '04* , Vol. No. 1, pp. 40- 45, 9-12 Nov. 2004.

[35] M. Stojanovic, J. Catipovic, and J. G. Proakis, "Adaptive multichannel combining and equalization for underwater acoustic communications," *The Journal of the Acoustical Society of America,* Vol. 94, pp. 1621-1631, 1993.

[36] M. Stojanovic, L. Freitag, and M. Johnson, "Channel-estimation-based adaptive equalization of underwater acoustic signals," in *OCEANS '99 MTS/IEEE*, Vol. 2, pp. 985-990, 1999.

[37] M. J. Lopez and A. C. Singer, "A DFE coefficient placement algorithm for sparse reverberant channels," *IEEE Transactions on Communications,* Vol. 49, pp. 1334-1338, 2001.

[38] L. Weichang and J. C. Preisig, "Estimation of Rapidly Time-Varying Sparse Channels," *IEEE Journal of Oceanic Engineering,* Vol. 32, pp. 927-939, 2007.

[39] S. Roy, T. M. Duman, and V. McDonald, "Error Rate Improvement in Underwater MIMO Communications Using Sparse Partial Response Equalization," in *OCEANS 2006*, pp. 1-6, 2006.

[40] J. Labat, G. Lapierre, and J. Trubuil, "Iterative equalization for underwater acoustic channels potentiality for the TRIDENT system," in *Proceedings OCEANS 2003*, Vol. 3, pp. 1547-1553, 2003.

[41] M. Stojanovic, "Low complexity OFDM detector for underwater channels," in Proc. of MTS/IEEE OCEANS conference, Boston, MA, Sept. 18-21, 2006.

[42] B. Li, S. Zhou, M. Stojanovic, and L. Freitag, "Pilot-tone based ZP-OFDM demodulation for an underwater acoustic channel," in Proc. MTS/IEEE OCEANS conference, Boston, MA, Sept. 18-21, 2006.

[43] P. J. Gendron and T. C. Yang, "Environmental and motion effects on orthogonal frequency division multiplexed on-off keying", *Amer. Inst. Phys. Conf. Ser.*, Vol. 728, pp. 98, 2004.

[44] B. Li, S. Zhou, M. Stojanovic, L. Freitag, and P. Willett, "Non-Uniform Doppler Compensation for Zero-Padded OFDM over Fast-Varying Underwater Acoustic Channels," *OCEANS 2007 - Europe*, pp. 1-6, 18-21 June 2007.

[45] B. S. Sharif, J. Neasham, O. R. Hinton, and A. E. Adams, "A computationally efficient Doppler compensation system for underwater acoustic communications," *IEEE Journal of Oceanic Engineering,* Vol. 25, No. 1, pp. 52-61, Jan 2000.

[46] U. Tureli and H. Liu, "A high-efficiency carrier estimator for OFDM communications," IEEE Communications Letters, Vol. 2, No. 4, pp. 104-106, Apr. 1998.

[47] S. Coleri, M. Ergen, A. Puri, and A. Bahai , "Channel estimation techniques based on pilot arrangement in OFDM systems," *Broadcasting, IEEE Transactions on* , Vol.48, No.3, pp. 223-229, Sep 2002.

[48] Z.-B. Lin, “Wideband ambiguity function of broadband signals,” *J.Acoust. Soc. Amer.*, Vol. 83, No. 6, June 1988.

[49] F. M. Gardner, "Interpolation in digital modems. I. Fundamentals," *IEEE Transactions on Communications*, Vol. 41, No. 3, pp. 501-507, Mar 1993.

[50] L. Erup, F. M. Gardner, and R. A. Harris, "Interpolation in digital modems. II. Implementation and performance," *IEEE Transactions on Communications*, Vol. 41, No. 6, pp. 998-1008, Jun 1993.